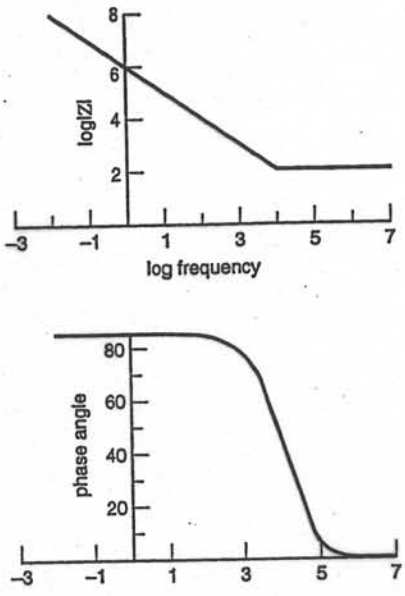

Figure 10.1.8 Bode plots for a series *RC* circuit with $R = 100\ \Omega$ and $C = 1\ \mu$F.

Sometimes it is advantageous to analyze ac circuits in terms of the *admittance*, **Y**, which is the inverse impedance, $1/\mathbf{Z}$, and therefore represents a kind of conductance. The generalized form of Ohm's law, (10.1.10), can then be rewritten as $\dot{I} = \dot{E}\mathbf{Y}$. These concepts are especially useful in the analysis of parallel circuits, because the overall admittance of parallel elements is simply the sum of the individual admittances.

Later we will be interested in the vector relationship between **Z** and **Y**. If **Z** is written in its polar form (Section A.5):

$$\mathbf{Z} = Ze^{j\phi} \tag{10.1.14}$$

then the admittance is

$$\mathbf{Y} = \frac{1}{Z}e^{-j\phi} \tag{10.1.15}$$

Here we see that **Y** is a vector with magnitude 1/Z and a phase angle equal to that of **Z**, but opposite in sign. Figure 10.1.13 is a picture of the arrangement.

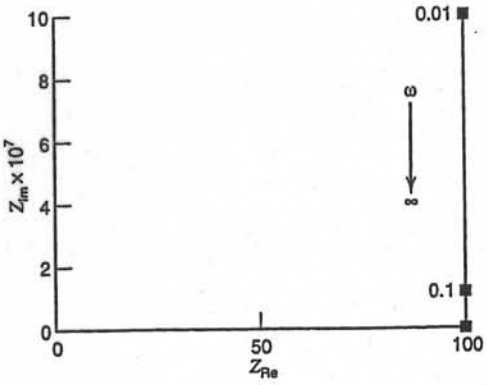

Figure 10.1.9 Nyquist plot for a series *RC* circuit with $R = 100\ \Omega$ and $C = 1\ \mu$F.

CHAPTER

10

TECHNIQUES BASED ON CONCEPTS OF IMPEDANCE

10.1 INTRODUCTION

In previous chapters we have discussed ways of studying electrode reactions through large perturbations on the system. By imposing potential sweeps, potential steps, or current steps, we typically drive the electrode to a condition far from equilibrium, and we observe the response, which is usually a transient signal. Another approach is to perturb the cell with an alternating signal of small magnitude and to observe the way in which the system follows the perturbation at steady state. Many advantages accrue to these techniques. Among the most important are (a) an experimental ability to make high-precision measurements because the response may be indefinitely steady and can therefore be averaged over a long term, (b) an ability to treat the response theoretically by linearized (or otherwise simplified) current-potential characteristics, and (c) measurement over a wide time (or frequency) range (10^4 to 10^{-6} s or 10^{-4} to 10^6 Hz). Since one usually works close to equilibrium, one often does not require detailed knowledge about the behavior of the *i-E* response curve over great ranges of overpotential. This advantage leads to important simplifications in treating kinetics and diffusion.

In deriving the theory below, we will rely frequently on analogies between the electrochemical cell and networks of resistors and capacitors that are thought to behave like the cell. This feature may seem at times to disembody the interpretation from the chemical system, so let us emphasize beforehand that the ideas and the mathematics used in the interpretation are basically simple. We will do our best to tie them to the chemistry at every possible point, and we hope readers will avoid letting the details of interpretation obscure their view of the great power and beauty of these methods.

10.1.1 Types of Techniques (1–12)

The prototypical experiment is the *faradaic impedance* measurement, in which the cell contains a solution with both forms of a redox couple, so that the potential of the working electrode is fixed. For example, one might use 1 m*M* Eu^{2+} and 1 m*M* Eu^{3+} in 1 *M* $NaClO_4$. A mercury drop of fixed area might be employed as the working electrode, and it might be paired with a nonpolarizable reference such as an SCE, which would act also as the counter electrode. It is probably easiest to understand the measurement of impedance by considering the classical approach with an impedance bridge. The cell is inserted as the unknown impedance into one arm of an impedance bridge, and the bridge is balanced by adjusting *R* and *C* in the opposite arm of the bridge, as shown in Figure 10.1.1.

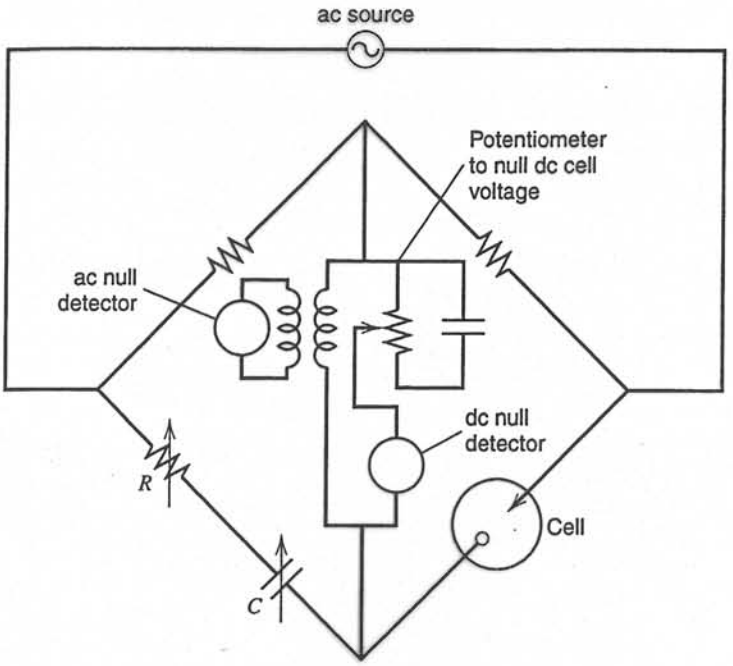

Figure 10.1.1 A bridge circuit for measurements of electrochemical impedance.

This operation determines the values of R and C that, in series, behave as the cell does at the measurement frequency. The impedance is measured as a function of the frequency of the ac source. The technique where the cell or electrode impedance is plotted *vs.* frequency is called *electrochemical impedance spectroscopy* (EIS). In modern practice, the impedance is usually measured with lock-in amplifiers or frequency-response analyzers, which are faster and more convenient than impedance bridges. Such approaches are introduced in Section 10.8. The job of theory is to interpret the equivalent resistance and capacitance values in terms of interfacial phenomena. The mean potential of the working electrode (the "dc potential") is simply the equilibrium potential determined by the ratio of oxidized and reduced forms of the couple. Measurements can be made at other potentials by preparing additional solutions with different concentration ratios. The faradaic impedance method, including EIS, is capable of high precision and is frequently used for the evaluation of heterogeneous charge-transfer parameters and for studies of double-layer structure.

A variation on the faradaic impedance method is *ac voltammetry* (or, with a DME, *ac polarography*). In these experiments, a three-electrode cell is used in the conventional manner, and the potential program imposed on the working electrode is a dc mean value, E_{dc}, which is scanned slowly with time, plus a sinusoidal component, E_{ac}, of perhaps 5-mV peak-to-peak amplitude. The measured responses are the magnitude of the ac component of the current at the frequency of E_{ac} and its phase angle with respect to E_{ac}.[1] A typical experimental arrangement is shown schematically in Figure 10.1.2. As we will see presently, this measurement is equivalent to determining the faradaic impedance. The role of the dc potential is to set the mean surface concentrations of O and R. In general, this potential differs from the true equilibrium value; hence $C_O(0, t)$ and $C_R(0, t)$ differ from C_O^* and C_R^*, and a diffusion layer exists. Note, however, that since E_{dc} is effectively steady, this layer soon becomes so thick that its dimensions greatly exceed those of the diffusion zone affected by the rapid perturbations from E_{ac}. Thus, the mean surface con-

[1]Alternatively, one could measure the current components in phase with E_{ac} and 90° out of phase with E_{ac}. They provide equivalent information.

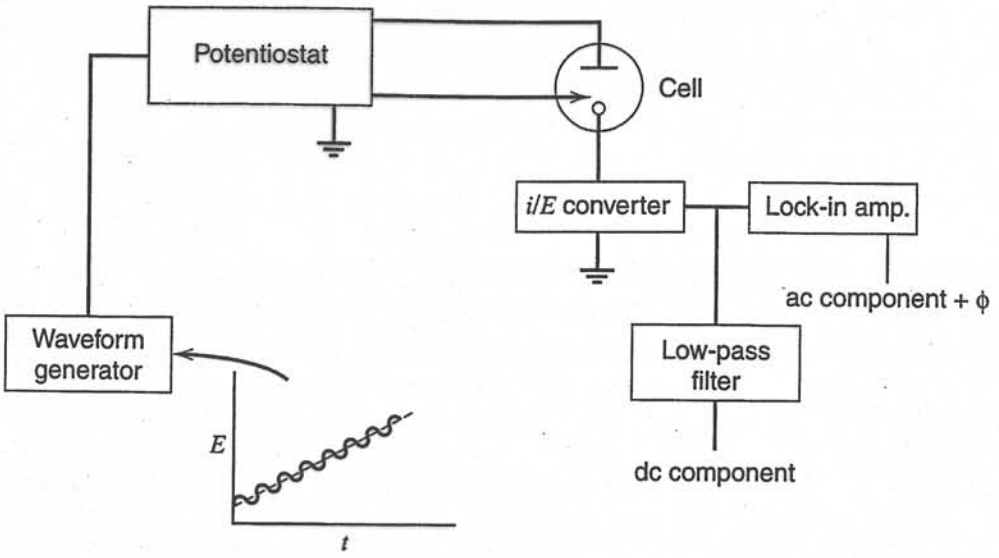

Figure 10.1.2 Schematic diagram of apparatus for an ac voltammetric experiment.

centrations $C_O(0, t)$ and $C_R(0, t)$ look like bulk concentrations to the ac part of the experiment. This same effect is exploited in DPP (see Section 7.3.4). One usually starts with a solution containing only one redox form, for example Eu^{3+}, and obtains continuous plots of the ac current amplitude and the phase angle *vs.* E_{dc}. In effect, these plots represent the faradaic impedance at continuous ratios of $C_O(0, t)$ and $C_R(0, t)$, all recorded without changing the solution. The amplitude plot is also useful for analytical measurements of concentration.

EIS and ac voltammetry normally involve excitation signals, E_{ac}, of very low amplitude, and they depend essentially on the fact that current-overpotential relations are virtually linear at low overpotentials. In a linear system, excitation at frequency ω provides a current also of frequency ω (and only of frequency ω). On the other hand, a nonlinear *i-E* relation gives a distorted response that is not purely sinusoidal; but it is still periodic and can be represented as a superposition (Fourier synthesis) of signals at frequencies ω, 2ω, 3ω, . . . The current-overpotential function for an electrode reaction is nonlinear over moderate ranges of overpotential, and the effects of this nonlinearity can be observed and put to use. For example, consider *second* (and higher) *harmonic ac voltammetry*, which is nearly the same as the first harmonic ac experiment described above. It differs in that one detects an ac component current at 2ω, 3ω, . . . , etc., instead of the component at the excitation frequency ω. *Faradaic rectification* features excitation with a purely sinusoidal source and measurement of the dc component of current flow. *Intermodulation voltammetry* depends on the mixing properties of a nonlinear characteristic. One excites with two superimposed signals at frequencies ω_1 and ω_2 and observes the current at the combination frequencies (sidebands or beat frequencies) $\omega_1 + \omega_2$ and $\omega_1 - \omega_2$. A big advantage common to all techniques based on nonlinearity is comparative freedom from charging currents. The double-layer capacitance is generally much more linear than the faradaic impedance; hence charging currents are largely restricted to the excitation frequencies.

10.1.2 Review of ac Circuits

A purely sinusoidal voltage can be expressed as

$$e = E \sin \omega t \tag{10.1.1}$$

Impedance Techniques Ch. 9 B&F

- method involves treating cell as electrical circuit made of elements R, L, C ⇒ determine values of these & interpret in terms of physical processes

⇒ faradaic impedance measurements —

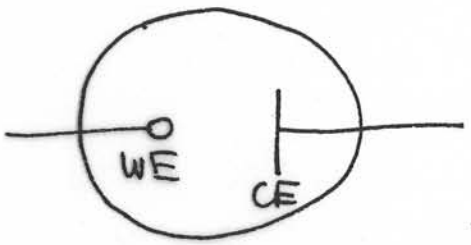

CE is "RE" (nonpolarizable) over small excursions in applied $\mathcal{E}$

⇒ also ac voltammetry — 3-electrode cell —

Review of ac Circuits

- purely sinusoidal voltage $e = \mathcal{E} \sin \omega t$
- represent e as rotating vector, phasor, of length $\mathcal{E}$ and rotational frequency, ω. Denoted $\dot{\mathcal{E}}$

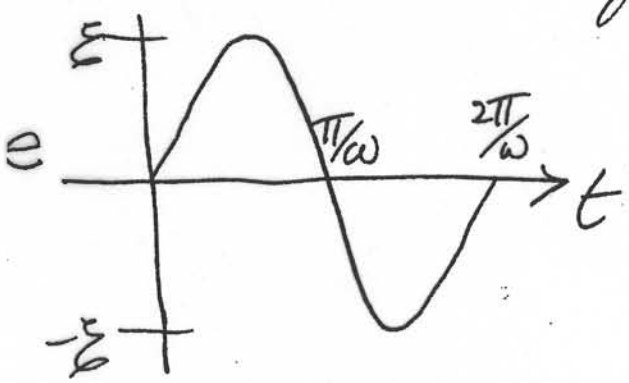

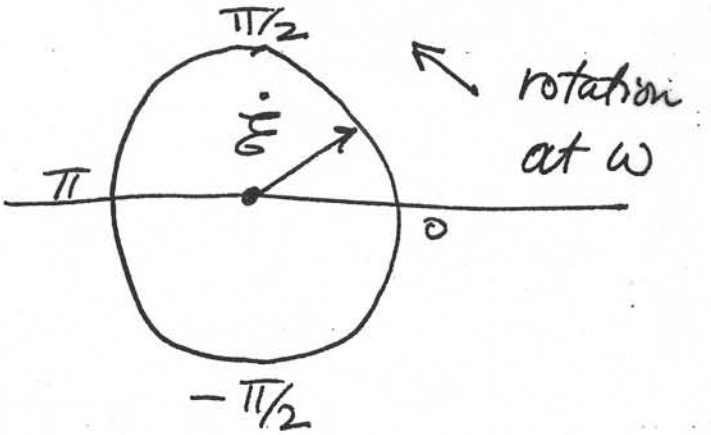

$e = \mathcal{E} \sin \omega t$

- now consider relationship between i & e - represent each as separate phasors, $\dot{I}$ & $\dot{\mathcal{E}}$, rotating at ω

- note - linearity in i-$\mathcal{E}$ characteristic keeps ω invariant; if i-$\mathcal{E}$ nonlinear, ω varies & response is not purely sinusoidal

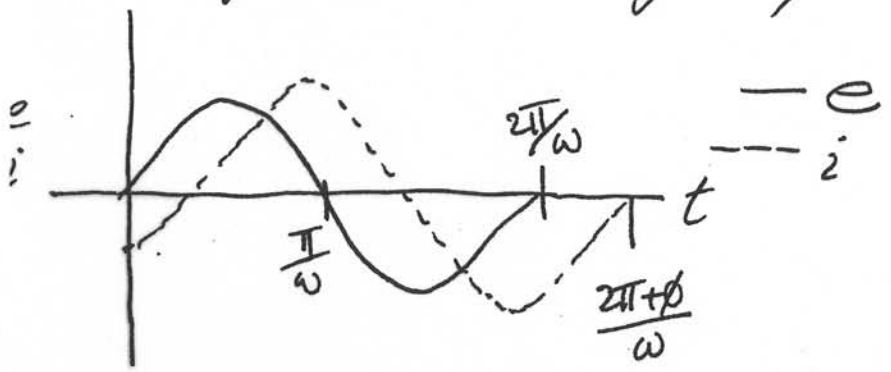

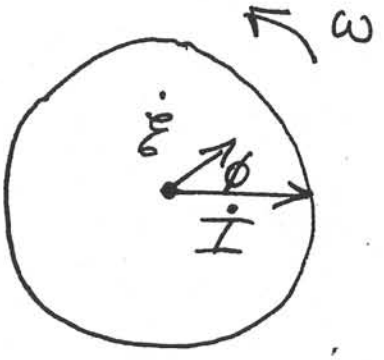

- represent $i = I\sin(\omega t+\phi)$, $\phi < 0$, where $\dot{I}$ lags $\dot{\mathcal{E}}$
- circuit analysis? - common examples useful in a.c. systems: R & C
- apply $e = \mathcal{E}\sin\omega t$ across pure resistor R, i=?
  Ohm gives $I = (\mathcal{E}/R)\sin\omega t \Rightarrow \phi = 0$
  or $\dot{I} = \dot{\mathcal{E}}/R$

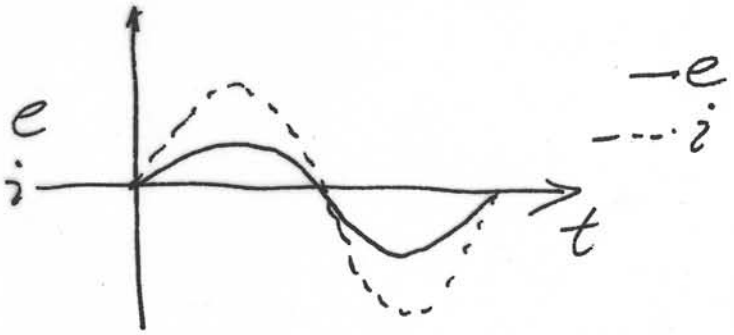

- apply $e = \mathcal{E}\sin\omega t$ across pure capacitor, i=?
  we know $q = Ce$ $\quad i = dq/dt$
  $\therefore i = C\dfrac{de}{dt} = \omega C\mathcal{E}\cos\omega t = \omega C\mathcal{E}\sin\left(\omega t+\pi/2\right)$
  $= \dfrac{\mathcal{E}}{X_C}\sin\left(\omega t+\pi/2\right)$ // $\quad \phi = \pi/2 > 0$ i leads $\mathcal{E}$
  $X_C = \dfrac{1}{\omega C} \equiv$ "capacitive reactance"

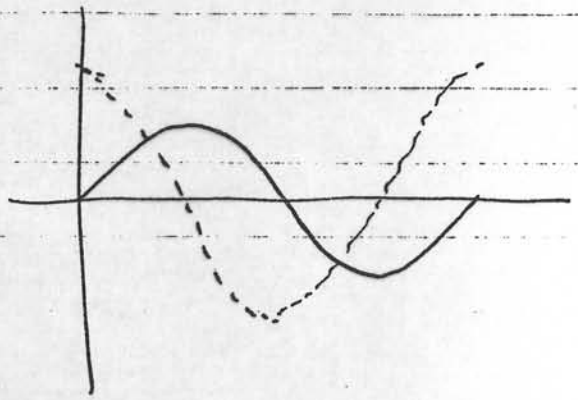

or in phasor notation, plot $\dot{I}$ along abcissa even though we in fact measure ϕ of I wrt $\mathcal{E}$

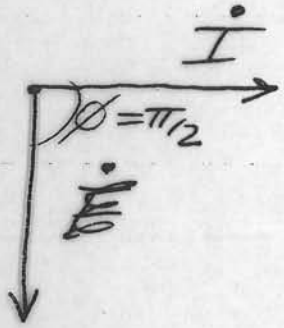

$j = -i$

physics & EE each choose different roots of $\sqrt{-1}$

by convention, ordinate given "unit vector" of $j = \sqrt{-1}$

$\therefore$ $\dot{\mathcal{E}}$ above is, in fact, $\dot{\mathcal{E}} = -j X_C \dot{I}$

X_C has dimensions of resistance but $X_C = X_C(\omega)$

now consider R & C in series — apply voltage

$\dot{\mathcal{E}} = \dot{\mathcal{E}}_R + \dot{\mathcal{E}}_C$ (series circuit)

$= \dot{I}(R - jX_C) = \dot{I}Z$ Ohm's Law

impedance $Z = R - jX_C$

$$|Z| = \left(R^2 + X_C^2\right)^{1/2}$$

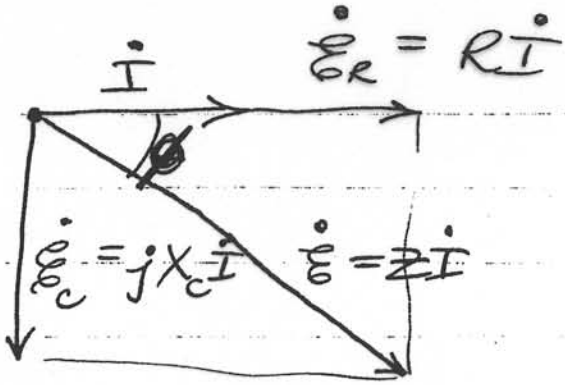

phasor diagram

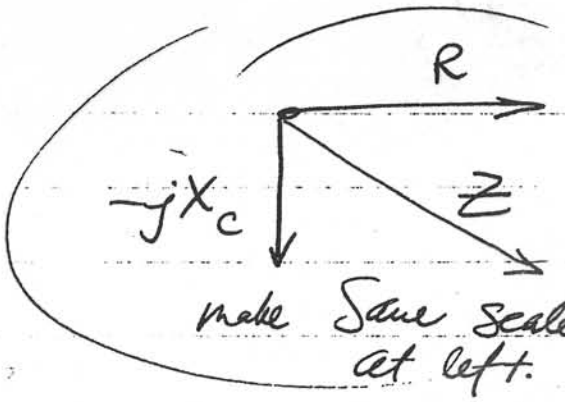

impedance vector diagram

$$\tan\phi = \frac{X_C}{R} = \frac{1}{\omega RC}$$

ϕ expresses balance between purely resistive & capacitive components — $\phi = 0$ "R"
$\phi = \pi/2$ "C"

same rules apply for Z as R ⇒ series — additive; parallel — $\frac{1}{Z}$ additive

— Consider impedance to be "reactive resistance"

— also define admittance, $Y = 1/Z$
"reactive conductance"

Ohm's law $\dot{I} = \dot{E}\vec{Y}$ $\dot{E} = \dot{I}\vec{Z}$

---

also polar form $\vec{Z} = Z e^{j\phi}$

$\vec{Y} = \frac{1}{Z} e^{-j\phi}$

$z = x + jy = r e^{j\theta}$

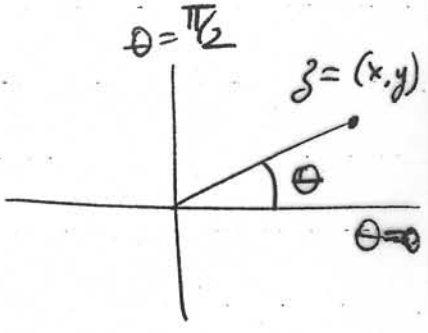

$$r = (x^2 + y^2)^{1/2} \qquad \theta = \tan^{-1}\left(\frac{y}{x}\right)$$

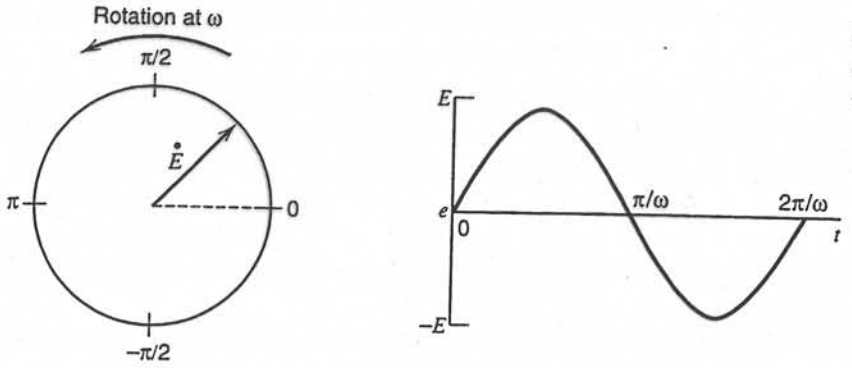

Figure 10.1.3 Phasor diagram for an alternating voltage, $e = E \sin \omega t$.

where ω is the angular frequency, which is 2π times the conventional frequency in Hz. It is convenient to think of this voltage as a rotating vector (or *phasor*) quantity like that pictured in Figure 10.1.3. Its length is the amplitude E and its frequency of rotation is ω. The observed voltage at any time, e, is the component of the phasor projected on some particular axis (normally that at 0°) .

One frequently wishes to consider the relationship between two related sinusoidal signals, such as the current, i, and the voltage, e. Each is then represented as a separate phasor, $\dot{I}$ or $\dot{E}$, rotating at the same frequency. As shown in Figure 10.1.4, they generally will not be in phase; thus their phasors will be separated by a *phase angle*, ϕ. One of the phasors, usually $\dot{E}$, is taken as a reference signal, and ϕ is measured with respect to it. In the figure, the current lags the voltage. It can be expressed generally as

$$i = I \sin(\omega t + \phi) \tag{10.1.2}$$

where ϕ is a signed quantity, which is negative in this case.

The relationship between two phasors at the same frequency remains constant as they rotate; hence the phase angle is constant. Consequently, we can usually drop the references to rotation in the phasor diagrams and study the relationships between phasors simply by plotting them as vectors having a common origin and separated by the appropriate angles.

Let us apply these concepts to the analysis of some simple circuits. Consider first a pure resistance, R, across which a sinusoidal voltage, $e = E \sin \omega t$, is applied. Since Ohm's law always holds, the current is $(E/R)\sin \omega t$ or, in phasor notation,

$$\dot{I} = \frac{\dot{E}}{R} \tag{10.1.3}$$

$$\dot{E} = \dot{I}R \tag{10.1.4}$$

The phase angle is zero, and the vector diagram is that of Figure 10.1.5.

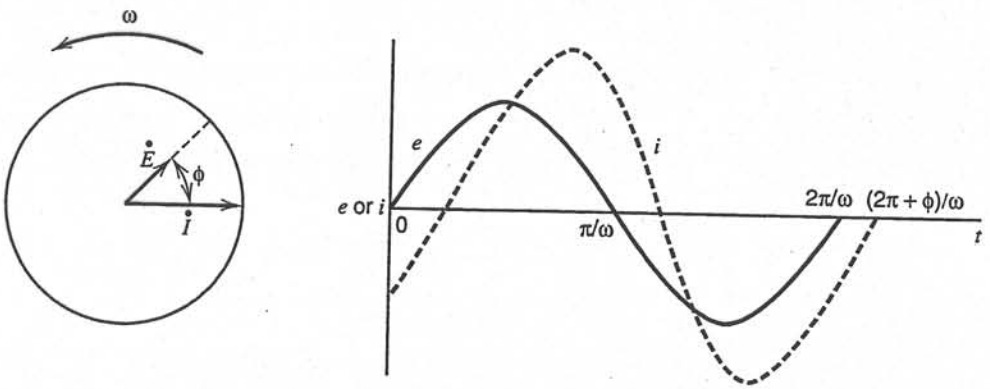

Figure 10.1.4 Phasor diagram showing the relationship between alternating current and voltage signals at frequency ω.

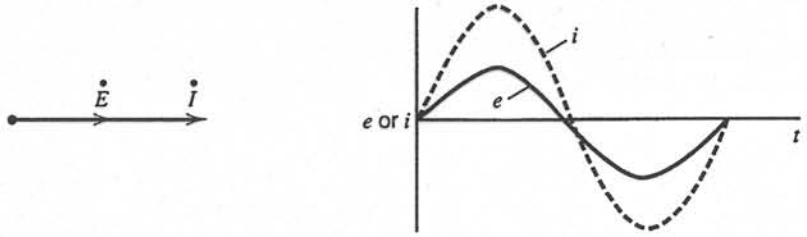

Figure 10.1.5
Relationship between the voltage across a resistor and current through the resistor.

Suppose we now substitute a pure capacitance, C, for the resistor. The fundamental relation of interest is then $q = Ce$, or $i = C(de/dt)$; thus

$$i = \omega CE \cos \omega t \tag{10.1.5}$$

$$i = \frac{E}{X_C} \sin\left(\omega t + \frac{\pi}{2}\right) \tag{10.1.6}$$

where X_C is the *capacitive reactance*, $1/\omega C$.

The phase angle is $\pi/2$, and the current leads the voltage, as shown in Figure 10.1.6. Since the vector diagram has now expanded to a plane, it is convenient to represent phasors in terms of complex notation. Components along the ordinate are assigned as imaginary and are multiplied by $j = \sqrt{-1}$. Components along the abscissa are real. Introducing complex notation here is only a bookkeeping measure to help keep the vector components straight. We handle them mathematically as "real" or "imaginary," but both types are real in the sense of being measurable by phase angle. In circuit analysis, it turns out to be advantageous to plot the current phasor along the abscissa as shown in Figure 10.1.6, even though the current's phase angle is measured experimentally with respect to the voltage. If that is done, it is clear that

$$\dot{E} = -jX_C\dot{I} \tag{10.1.7}$$

Of course, this relation must hold regardless of where $\dot{I}$ is plotted with respect to the abscissa, since only the relationship between $\dot{E}$ and $\dot{I}$ is significant. A comparison of equations 10.1.4 and 10.1.7 shows that X_C must carry dimensions of resistance, but, unlike R, its magnitude falls with increasing frequency.

Now consider a resistance, R, and a capacitance, C, in series. A voltage, $\dot{E}$, is applied across them, and at all times it must equal the sum of the individual voltage drops across the resistor and the capacitor; thus

$$\dot{E} = \dot{E}_R + \dot{E}_C \tag{10.1.8}$$

$$\dot{E} = \dot{I}(R - jX_C) \tag{10.1.9}$$

$$\dot{E} = \dot{I}\mathbf{Z} \tag{10.1.10}$$

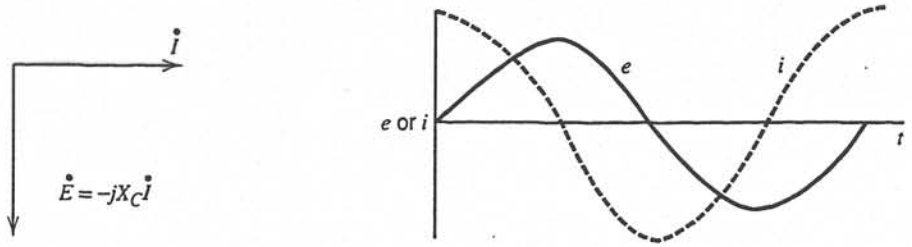

Figure 10.1.6
Relationship between an alternating voltage across a capacitor and the alternating current through the capacitor.

In this way we find that the voltage is linked to the current through a vector $\mathbf{Z} = R - jX_C$ called the *impedance*. Figure 10.1.7 is a display of the relationships between these various quantities. In general the impedance can be represented as[2]

$$\boxed{\mathbf{Z}(\omega) = Z_{Re} - jZ_{Im}} \tag{10.1.11}$$

where Z_{Re} and Z_{Im} are the real and imaginary parts of the impedance. For the example here, $Z_{Re} = R$ and $Z_{Im} = X_C = 1/\omega C$. The magnitude of $\mathbf{Z}$, written $|Z|$ or Z, is given by

$$|Z|^2 = R^2 + X_C^2 = (Z_{Re})^2 + (Z_{Im})^2 \tag{10.1.12}$$

and the phase angle, ϕ, is given by

$$\tan\phi = Z_{Im}/Z_{Re} = X_C/R = 1/\omega RC \tag{10.1.13}$$

The impedance is a kind of generalized resistance, and equation 10.1.10 is a generalized version of Ohm's law. It embodies both (10.1.4) and (10.1.7) as special cases. The phase angle expresses the balance between capacitive and resistive components in the series circuit. For a pure resistance, $\phi = 0$; for a pure capacitance, $\phi = \pi/2$; and for mixtures, intermediate phase angles are observed.

The variation of the impedance with frequency is often of interest and can be displayed in different ways. In a *Bode plot*, $\log|Z|$ and ϕ are both plotted against $\log\omega$. An alternative representation, a *Nyquist plot*, displays Z_{Im} *vs.* Z_{Re} for different values of ω. Plots for the series *RC* circuit are shown in Figures 10.1.8 and 10.1.9. Similar plots for a parallel *RC* circuit are shown in Figures 10.1.10 and 10.1.11.

More complex circuits can be analyzed by combining impedances according to rules analogous to those applicable to resistors. For impedances in series, the overall impedance is the sum of the individual values (expressed as complex vectors). For impedances in parallel, the inverse of the overall impedance is the sum of the reciprocals of the individual vectors. Figure 10.1.12 shows a simple application.

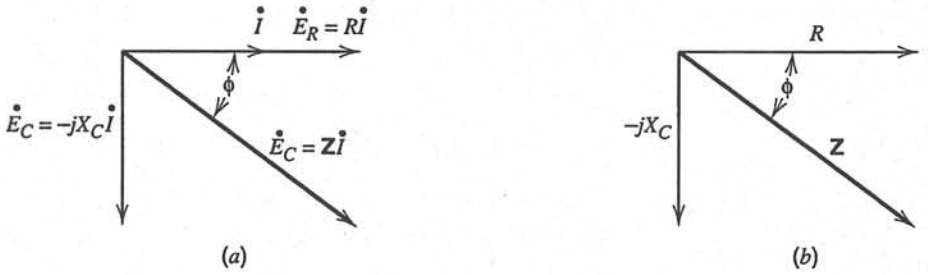

Figure 10.1.7 (*a*) Phasor diagram showing the relationship between the current and the voltages in a series *RC* network. The voltage across the whole network is $\dot{E}$, and $\dot{E}_R$ and $\dot{E}_C$ are its components across the resistance and the capacitance. (*b*) An impedance vector diagram derived from the phasor diagram in (*a*).

[2]In many treatments, the definition of impedance is taken as $\mathbf{Z} = Z_{Re} + jZ_{Im}$, but we can simplify matters with the definition in (10.1.11). In electrochemistry, the imaginary impedance is almost always capacitive and therefore negative. With our definition of $\mathbf{Z}$, we can generally work with positive values and expressions for Z_{Im}, and impedance plots appear naturally in the first quadrant. Our choice is in accord with the general, although sometimes implicit, practice in the field. In reviewing other literature, it is wise to take note of the definition of $\mathbf{Z}$.

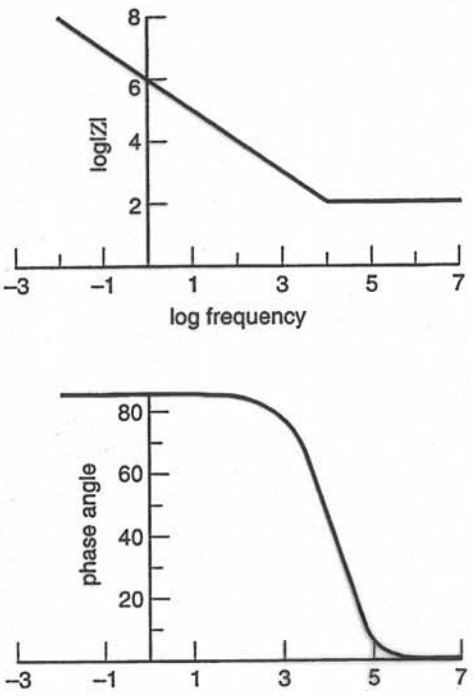

Figure 10.1.8 Bode plots for a series *RC* circuit with $R = 100\ \Omega$ and $C = 1\ \mu$F.

Sometimes it is advantageous to analyze ac circuits in terms of the *admittance*, **Y**, which is the inverse impedance, $1/\mathbf{Z}$, and therefore represents a kind of conductance. The generalized form of Ohm's law, (10.1.10), can then be rewritten as $\dot{I} = \dot{E}\mathbf{Y}$. These concepts are especially useful in the analysis of parallel circuits, because the overall admittance of parallel elements is simply the sum of the individual admittances.

Later we will be interested in the vector relationship between **Z** and **Y**. If **Z** is written in its polar form (Section A.5):

$$\mathbf{Z} = Ze^{j\phi} \tag{10.1.14}$$

then the admittance is

$$\mathbf{Y} = \frac{1}{Z}e^{-j\phi} \tag{10.1.15}$$

Here we see that **Y** is a vector with magnitude $1/Z$ and a phase angle equal to that of **Z**, but opposite in sign. Figure 10.1.13 is a picture of the arrangement.

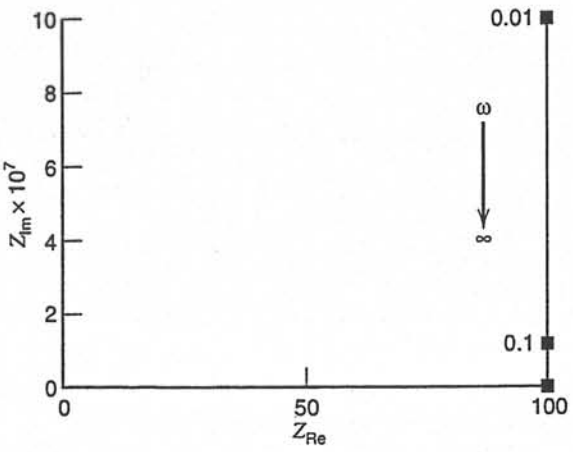

Figure 10.1.9 Nyquist plot for a series *RC* circuit with $R = 100\ \Omega$ and $C = 1\ \mu$F.

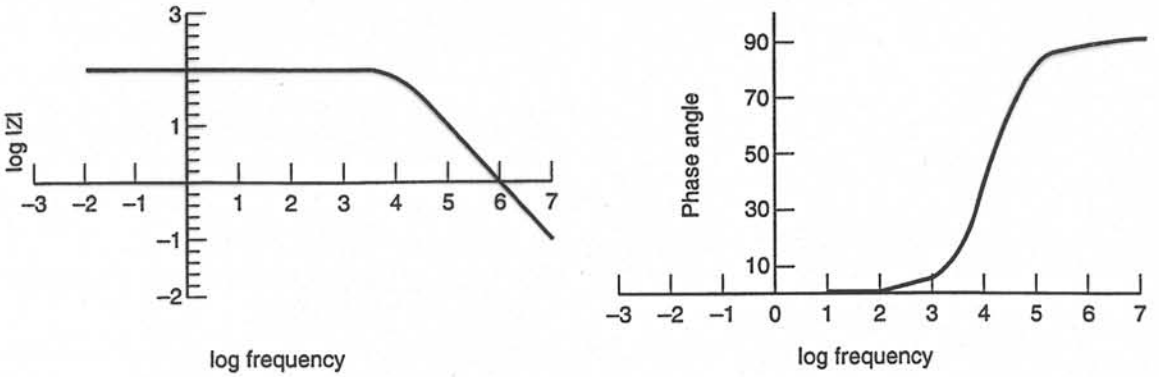

Figure 10.1.10 Bode plots for a parallel RC circuit with $R = 100\ \Omega$ and $C = 1\ \mu$F.

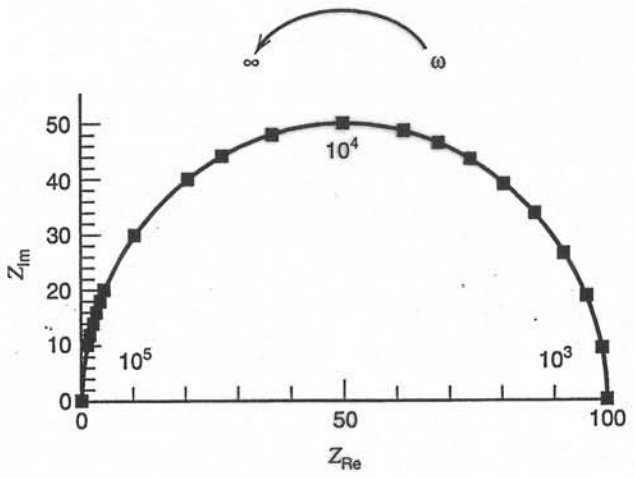

Figure 10.1.11 Nyquist plot for a parallel RC circuit with $R = 100\ \Omega$ and $C = 1\ \mu$F.

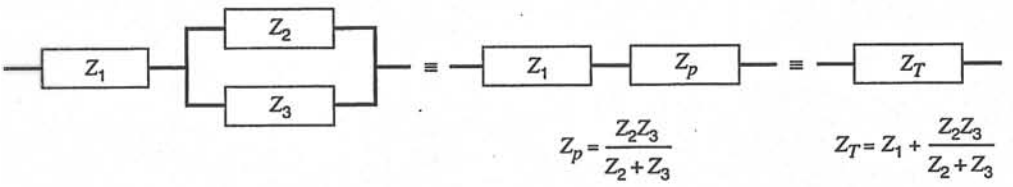

Figure 10.1.12 Calculation of a total impedance from component impedances.

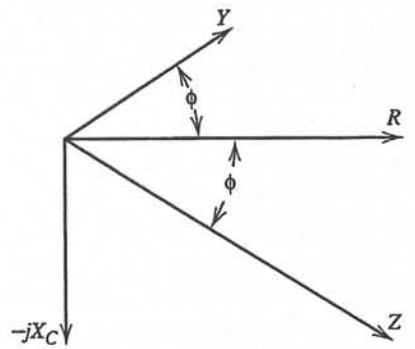

Figure 10.1.13 Relationship between the impedance, **Z**, and the admittance, **Y**.

10.1.3 Equivalent Circuit of a Cell (1, 4, 13, 14)

In a general sense, an electrochemical cell can be considered simply an impedance to a small sinusoidal excitation; hence we ought to be able to represent its performance by an *equivalent circuit* of resistors and capacitors that pass current with the same amplitude and phase angle that the real cell does under a given excitation. A frequently used circuit, called the *Randles equivalent circuit*, is shown in Figure 10.1.14*a*. The parallel elements are introduced because the total current through the working interface is the sum of distinct contributions from the faradaic process, i_f, and double-layer charging, i_c. The double-layer capacitance is nearly a pure capacitance; hence it is represented in the equivalent circuit by the element C_d. The faradaic process cannot be represented by simple linear circuit elements like, R and C, whose values are independent of frequency. It must be considered as a general impedance, Z_f. Of course, all of the current must pass through the solution resistance; therefore R_Ω is inserted as a series element to represent this effect in the equivalent circuit.[3]

The faradaic impedance has been considered in the literature in various ways. Figure 10.1.14*b* shows two equivalences that have been made. The simplest representation is to take the faradaic impedance as a series combination comprising the *series resistance*, R_s, and the *pseudocapacity*, C_s.[4] An alternative is to separate a pure resistance, R_{ct}, the *charge-transfer resistance* (Sections 1.3 and 3.4.3), from another general impedance, Z_w, the *Warburg impedance*, which represents a kind of resistance to mass transfer. In contrast to R_Ω and C_d, which are nearly ideal circuit elements, the components of the faradaic impedance are not ideal, because they change with frequency, ω. A given equivalent circuit represents cell performance at a given frequency, but not at other frequencies. In fact, a chief objective of a faradaic impedance experiment is to discover the frequency dependencies of R_s and C_s. Theory is then applied to transform these functions into chemical information.

The circuits considered here are based on the simplest electrode processes. Many others have been devised in order to account for more complex situations, for example, those involving adsorption of electroreactants, multistep charge transfer, or homogeneous

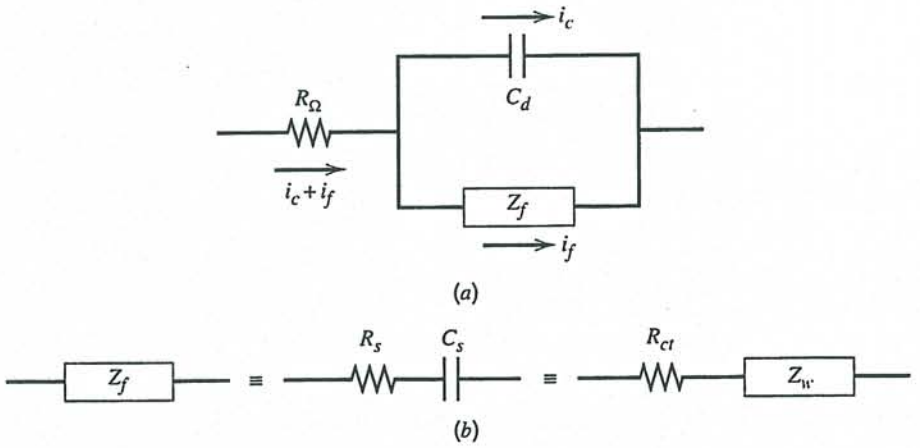

Figure 10.1.14
(*a*) Equivalent circuit of an electrochemical cell. (*b*) Subdivision of Z_f into R_s and C_s, or into R_{ct} and Z_w.

[3]In the faradaic impedance measurements described above (Section 10.1.1), the impedance determined by the bridge is a whole-cell impedance and includes contributions from the counter electrode's interface. Processes at the counter electrode are not usually of interest; hence the impedance at that interface is intentionally reduced to insignificance by employing a counter electrode of large area.

[4]In some treatments, R_s is called the *polarization resistance*. However, that name is applied to other variables in electrochemistry, so we avoid it here.

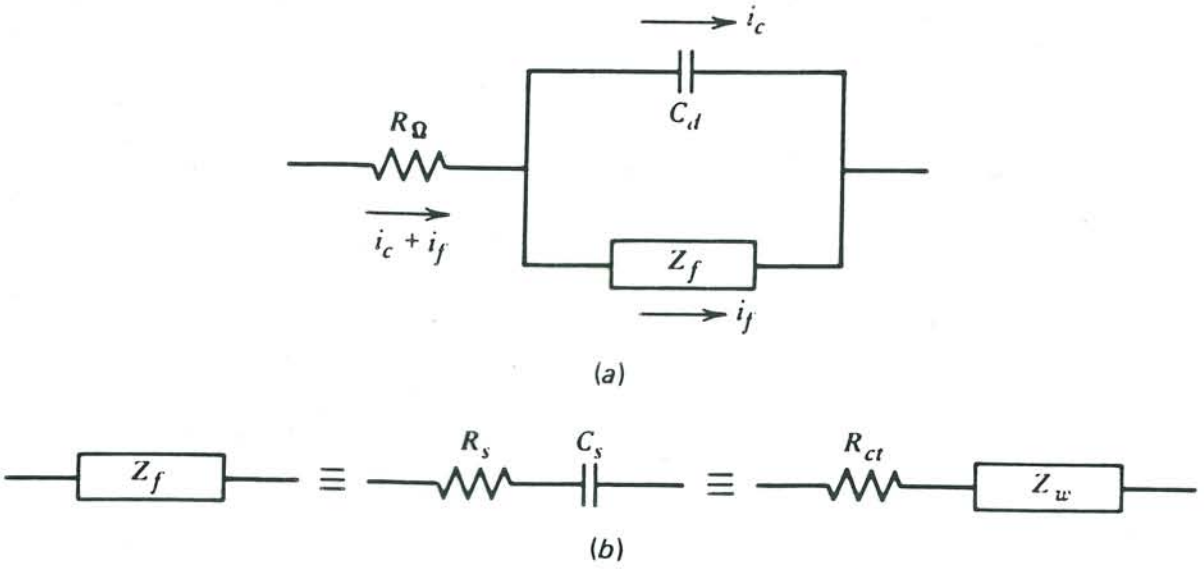

Figure ~~9.1.13~~ 10.1.14

t) Equivalent circuit of an electrochemical cell. (*b*) Subdivision of Z_f into R_s and C_s or into R_{ct} and Z_w.

$$\mathcal{E} = \mathcal{E}\left[i, C_O(0,t), C_R(0,t)\right]$$

$$\Rightarrow \frac{d\mathcal{E}}{dt} = R_{ct}\frac{di}{dt} + \beta_O \frac{dC_O(0,t)}{dt} + \beta_R \frac{dC_R(0,t)}{dt}$$

chemistry. It is important to understand that equivalent circuits drawn for electrochemical cells are not unique. Moreover, only in the simplest cases can one identify individual circuit elements with processes that occur in the electrochemical cell. This is especially true for equivalent circuits that represent more complicated processes, such as, coupled homogeneous reactions or the behavior of adsorbed intermediates. In fact even the simple $R_\Omega C_d$ circuit in the absence of a faradaic process at low electrolyte concentration shows *frequency dispersion* (i.e., variation of R_Ω and C_d with frequency) (15). For specific information, the original or review literature should be consulted (1, 4, 8–14, 16).

▶ 10.2 INTERPRETATION OF THE FARADAIC IMPEDANCE

10.2.1 Characteristics of the Equivalent Circuit

The measurement of the cell characteristics in a bridge yields values of R_B and C_B that in series are equivalent to the whole cell impedance, including the contributions from R_Ω and C_d, which are often not of interest in studies focused on the faradaic process. In general, one desires to separate the faradaic impedance from R_Ω and C_d. It is possible to do so by considering the frequency dependencies of R_B and C_B, or by evaluating R_Ω and C_d from separate experiments in the absence of the electroactive couple.[5] Techniques for making such determinations are considered in Section 10.4. For the moment, let us assume that the faradaic impedance, expressed as the series combination R_s and C_s, is evaluable from the total impedance (see Figure 10.1.14).

Now consider the behavior of this impedance as a sinusoidal current is forced through it. The total voltage drop is

$$E = iR_s + \frac{q}{C_s} \tag{10.2.1}$$

hence

$$\frac{dE}{dt} = R_s \frac{di}{dt} + \frac{i}{C_s} \tag{10.2.2}$$

If the current is

$$i = I \sin \omega t \tag{10.2.3}$$

then

$$\frac{dE}{dt} = (R_s I\omega) \cos\ \omega t + \left(\frac{I}{C_s}\right) \sin\ \omega t \tag{10.2.4}$$

This equation is the link we will use to identify R_s and C_s in electrochemical terms. We will find that the response of the electrode process to the current stimulus, (10.2.3), will also give dE/dt having the form of (10.2.4). That is, sine and cosine terms will appear; thus R_s and C_s can be identified by equating the coefficients of those terms in the electrical and chemical equations.

10.2.2 Properties of the Chemical System (1, 4, 13, 14)

For our standard system, $O + ne \rightleftarrows R$, with both O and R soluble, we can write

$$E = E[i, C_O(0, t), C_R(0, t)] \tag{10.2.5}$$

[5]However, O and R must not affect R_Ω and C_d appreciably if separate experiments are used.

hence,

$$\frac{dE}{dt} = \left(\frac{\partial E}{\partial i}\right)\frac{di}{dt} + \left[\frac{\partial E}{\partial C_O(0,t)}\right]\frac{dC_O(0,t)}{dt} + \left[\frac{\partial E}{\partial C_R(0,t)}\right]\frac{dC_R(0,t)}{dt} \tag{10.2.6}$$

or

$$\frac{dE}{dt} = R_{ct}\frac{di}{dt} + \beta_O\frac{dC_O(0,t)}{dt} + \beta_R\frac{dC_R(0,t)}{dt} \tag{10.2.7}$$

where

$$R_{ct} = \left(\frac{\partial E}{\partial i}\right)_{C_O(0,t),C_R(0,t)} \tag{10.2.8}$$

$$\beta_O = \left[\frac{\partial E}{\partial C_O(0,t)}\right]_{i,C_R(0,t)} \tag{10.2.9}$$

$$\beta_R = \left[\frac{\partial E}{\partial C_R(0,t)}\right]_{i,C_O(0,t)} \tag{10.2.10}$$

Obtaining an expression for dE/dt depends on our ability to evaluate the six factors on the right of (10.2.7). The three parameters R_{ct}, β_O, and β_R depend specifically on the kinetic properties of the electrode reaction. Special cases will be considered later. The remaining three factors [the derivatives of i, C_O^* and C_R^*] can be evaluated generally for current flow according to (10.2.3). One of them is trivial:

$$\frac{di}{dt} = I\omega\cos\omega t \tag{10.2.11}$$

The others are evaluated by considering mass transfer.[6]

Assuming semi-infinite linear diffusion with initial conditions $C_O(x, 0) = C_O^*$ and $C_R(x, 0) = C_R^*$, we can write from our experience in Section 8.2.1 that

$$\bar{C}_O(0,s) = \frac{C_O^*}{s} + \frac{\bar{i}(s)}{nFAD_O^{1/2}s^{1/2}} \tag{10.2.12}$$

$$\bar{C}_R(0,s) = \frac{C_R^*}{s} - \frac{\bar{i}(s)}{nFAD_R^{1/2}s^{1/2}} \tag{10.2.13}$$

Inversion by convolution gives

$$C_O(0,t) = C_O^* + \frac{1}{nFAD_O^{1/2}\pi^{1/2}}\int_0^t \frac{i(t-u)}{u^{1/2}}\,du \tag{10.2.14}$$

$$C_R(0,t) = C_R^* - \frac{1}{nFAD_R^{1/2}\pi^{1/2}}\int_0^t \frac{i(t-u)}{u^{1/2}}\,du \tag{10.2.15}$$

[6]Note that the equivalent impedance was analyzed just above in terms of current as it is usually defined for circuit analysis. That is, a positive change in E causes a positive change in i. On the other hand, the electrochemical current convention followed elsewhere in this book denotes cathodic currents as positive; hence a *negative* change in E causes a positive change in i. If we adhere to this convention now, confusion will reign when we try to make comparisons between the electrical equivalents and the chemical systems. We must have a common basis for the current. Since the interpretations of the measurements are closely linked to electronic circuit analysis, it is advantageous to adopt the electronic convention. *For this chapter, then, we take an anodic current as positive.*

This expedient will turn out not to cause much trouble, because we never really follow the instantaneous sign of the current in ac experiments. Instead, we measure the amplitude of the sinusoidal component and its phase angle with respect to the sinusoidal potential. Of course the phase angle would depend on our choice of current convention, but it is advantageous even here to take the electronic custom, because the electronic devices used to measure phase angle are based on it.

From (10.2.3), we can substitute for $i(t-u)$; hence the problem becomes one of evaluating the integral common to both of these relations.

We begin with the trigonometric identity:

$$\sin \omega(t-u) = \sin \omega t \cos \omega u - \cos \omega t \sin \omega u \tag{10.2.16}$$

which implies that

$$\int_0^t \frac{I \sin \omega(t-u)}{u^{1/2}}\,du = I \sin \omega t \int_0^t \frac{\cos \omega u}{u^{1/2}}\,du - I \cos \omega t \int_0^t \frac{\sin \omega u}{u^{1/2}}\,du \tag{10.2.17}$$

Now let us consider the range of times in which we are interested. Before the current is turned on, the surface concentrations are C_O^* and C_R^*, and after a few cycles we can expect them to reach a *steady state* in which they cycle repeatedly through constant patterns. We can be sure of this point because no net electrolysis takes place in any full cycle of current flow. Our interest is not in the transition from initial conditions to steady state, but in the steady state itself. The two integrals on the right side of (10.2.17) embody the transition period. Because $u^{1/2}$ appears in their denominators, the integrands are appreciable only at short times. After a few cycles, each integral must reach a constant value characteristic of the steady state. We can obtain it by letting the integration limits go to infinity:

$$\int_{\substack{\text{Steady}\\ \text{state}}} \frac{I \sin \omega(t-u)}{u^{1/2}}\,du = I \sin \omega t \int_0^\infty \frac{\cos \omega u}{u^{1/2}}\,du - I \cos \omega t \int_0^\infty \frac{\sin \omega u}{u^{1/2}}\,du \tag{10.2.18}$$

It is easy to show that both integrals on the right side of (10.2.18) are equal to $(\pi/2\omega)^{1/2}$; hence we have by substitution into (10.2.14) and (10.2.15)

Solution to Fick's 2nd Law

$$C_O(0,t) = C_O^* + \frac{I}{nFA(2D_O\omega)^{1/2}}(\sin \omega t - \cos \omega t) \tag{10.2.19}$$

$$C_R(0,t) = C_R^* - \frac{I}{nFA(2D_R\omega)^{1/2}}(\sin \omega t - \cos \omega t) \tag{10.2.20}$$

Now we can evaluate the derivatives of the surface concentrations as required above:[7]

$$\frac{dC_O(0,t)}{dt} = \frac{I}{nFA}\left(\frac{\omega}{2D_O}\right)^{1/2}(\sin \omega t + \cos \omega t) \tag{10.2.21}$$

$$\frac{dC_R(0,t)}{dt} = -\frac{I}{nFA}\left(\frac{\omega}{2D_R}\right)^{1/2}(\sin \omega t + \cos \omega t) \tag{10.2.22}$$

10.2.3 Identification of R_s and C_s

By substitution of (10.2.11), (10.2.21), and (10.2.22) into (10.2.7), we obtain

$$\frac{dE}{dt} = \left(R_{ct} + \frac{\sigma}{\omega^{1/2}}\right) I\omega \cos \omega t + I\sigma\omega^{1/2} \sin \omega t \tag{10.2.23}$$

[7] In general, we ought to consider the current as $i = i_{dc} + I \sin \omega t$, where i_{dc} is steady or varies only slowly with time. However, we are interested now in derivatives of surface concentrations, and they will be dominated by the higher-frequency ac signal. Relations (10.2.21) and (10.2.22) will still apply to a very high approximation. This is a mathematical manifestation of the way in which the ac part of the experiment can usually be uncoupled from the dc part.

where

$$\sigma = \frac{1}{nFA\sqrt{2}}\left(\frac{\beta_O}{D_O^{1/2}} - \frac{\beta_R}{D_R^{1/2}}\right) \tag{10.2.24}$$

It is easy to identify R_s and C_s by comparison with (10.2.4):

$$R_s = R_{ct} + \sigma/\omega^{1/2} \tag{10.2.25}$$

$$C_s = \frac{1}{\sigma\omega^{1/2}} \tag{10.2.26}$$

The complete evaluation of R_s and C_s depends on finding relations for R_{ct}, β_O, and β_R.

We will see below that R_{ct} is primarily determined by the heterogeneous charge-transfer kinetics, and we have already observed above that the terms $\sigma/\omega^{1/2}$ and $1/\sigma\omega^{1/2}$ come from mass-transfer effects. Recognition of this situation has led to a division of the faradaic impedance into the charge-transfer resistance, R_{ct}, and the Warburg impedance, Z_w, as shown in Figure 10.1.14*b*. Equations 10.2.25 and 10.2.26 demonstrate that this latter impedance can be regarded as a frequency-dependent resistance, $R_w = \sigma/\omega^{1/2}$, in series with the pseudocapacitance, $C_w = C_s = 1/\sigma\omega^{1/2}$. Thus the total faradaic impedance, $\mathbf{Z}_f$, can be written

$$\mathbf{Z}_f = R_{ct} + R_w - j/(\omega C_w) = R_{ct} + [\sigma\omega^{-1/2} - j(\sigma\omega^{-1/2})] \tag{10.2.27}$$

with the term in brackets representing the Warburg impedance.

▶ 10.3 KINETIC PARAMETERS FROM IMPEDANCE MEASUREMENTS (1, 4, 6, 8–14, 16)

From the description of the faradaic impedance experiment given in Section 10.1, it is clear that measurements are made with the working electrode's mean potential at equilibrium. Since the amplitude of the sinusoidal perturbation is small, we can use the linearized i-η characteristic to describe the electrical response to the departure from equilibrium. For a one-step, one-electron process, $O + e \underset{k_b}{\overset{k_f}{\rightleftarrows}} R$, the linearized relationship is (3.4.30), which can be rewritten in terms of the electronic current convention as

$$\eta = \frac{RT}{F}\left[\frac{C_O(0,t)}{C_O^*} - \frac{C_R(0,t)}{C_R^*} + \frac{i}{i_0}\right] \tag{10.3.1}$$

hence

$$R_{ct} = \frac{RT}{Fi_0} \tag{10.3.2}$$

$$\beta_O = \frac{RT}{FC_O^*} \tag{10.3.3}$$

$$\beta_R = -\frac{RT}{FC_R^*} \tag{10.3.4}$$

Now we see that

$$R_s - \frac{1}{\omega C_s} = R_{ct} = \frac{RT}{Fi_0} \tag{10.3.5}$$

so that the exchange current, and therefore k^0, can be evaluated easily when R_s and C_s are known. The bridge method allows a precise definition of these electrical equivalents; thus it can yield kinetic data of very high quality.

Equation 10.3.5 shows that one can, in principle, evaluate i_0 from data taken at a single frequency. However, doing so is not really wise, because one has no experimental assurance that the equivalent circuit actually mirrors the performance of the system. The best way to check for agreement is to examine the frequency dependence of the impedance. For example, (10.2.25) and (10.2.26) predict that R_s and $1/\omega C_s$ should both be linear with $\omega^{-1/2}$ and should have a common slope, σ, which is quantitatively predictable from the constants of the experiment; that is,

$$\boxed{\sigma = \frac{RT}{F^2 A\sqrt{2}}\left(\frac{1}{D_O^{1/2}C_O^*} + \frac{1}{D_R^{1/2}C_R^*}\right)} \tag{10.3.6}$$

Figure 10.3.1 is a display of these relationships.

The plot of R_s should have an intercept, R_{ct}, from which i_0 can be evaluated. Extrapolation to the intercept is equivalent to estimating the system's performance at infinite frequency. The Warburg impedance drops out at high frequencies, because the time scale is so short that diffusion cannot manifest itself as a factor influencing the current. Since the surface concentrations never change significantly from the mean values [see (10.2.19) and (10.2.20)], charge-transfer kinetics alone dictate the current.

If the linear behavior typified in Figure 10.3.1 is not observed, then the electrode process is not as simple as we assume here, and a more complex situation must be considered. The availability of this kind of check for internal consistency is an extremely important asset of the impedance technique. See Section 10.4 for more details.

The conclusions of the foregoing discussion are also applicable to a quasireversible multistep mechanism, for which R_{ct} is defined as

$$R_{ct} = \frac{RT}{nFi_0} \tag{10.3.7}$$

See Section 3.5.4(d) for more about the interpretation of i_0 in such a system.

Let us now consider the general impedance properties of a reversible system, which is an important limiting case. When charge-transfer kinetics are very facile, $i_0 \to \infty$; hence $R_{ct} \to 0$. Thus $R_s \to \sigma/\omega^{1/2}$. The corresponding impedance plot is shown in Figure 10.3.2*a*.

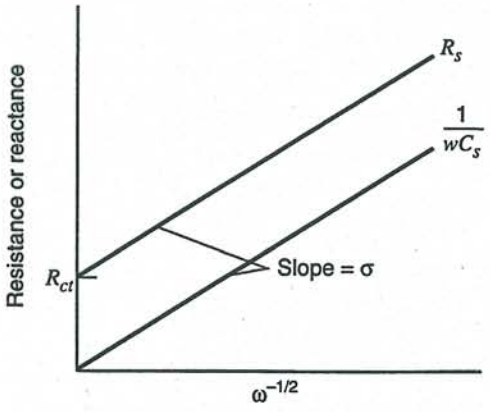

Figure 10.3.1 Dependence of R_s and $1/\omega C_s$ on frequency.

$$R_s = R_{ct} + \frac{\sigma}{\omega^{1/2}}$$

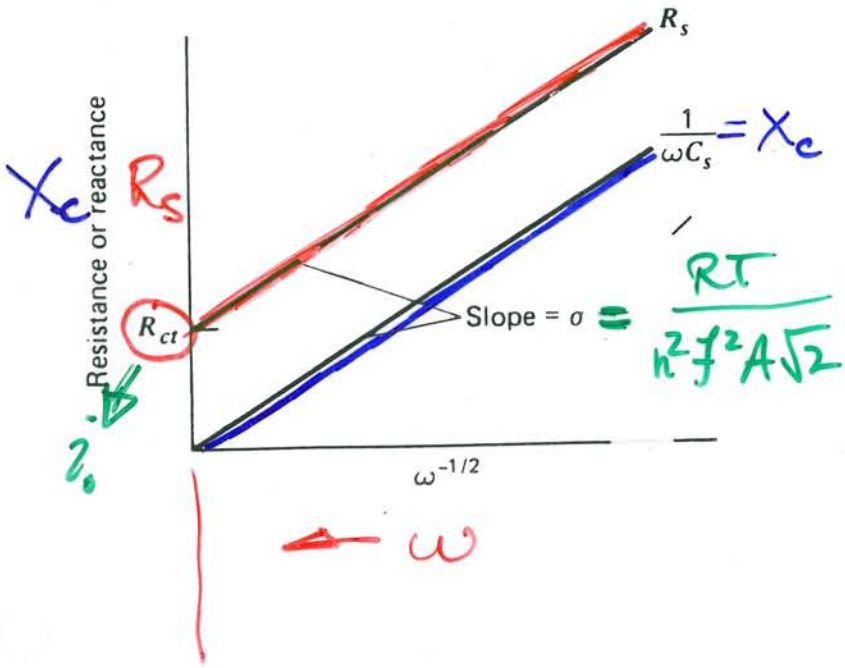

$$= \frac{RT}{n^2 f^2 A \sqrt{2}} \left(\frac{1}{D_O^{1/2} C_O^*} + \frac{1}{D_R^{1/2} C_R^*} \right)$$

Figure 10.3.1
Dependence of R_s and $1/\omega C_s$ on frequency

$\omega = \infty$
$\therefore$ no mt effects

$\omega = \infty$
$\therefore$ zero capacitance

$$X_c = \frac{1}{\omega C_s} \; ; \; C_s = \frac{1}{\sigma \omega^{1/2}}$$

$$\therefore X_c = \frac{\sigma}{\omega^{1/2}}$$

Reversible system: $i_0 \to \infty$, $R_{ct} \to 0$,

$R_s \to \frac{\sigma}{\omega^{1/2}} = X_c \quad \therefore Z_f = \left(\frac{2}{\omega}\right)^{1/2} \sigma$ (9.3.7)

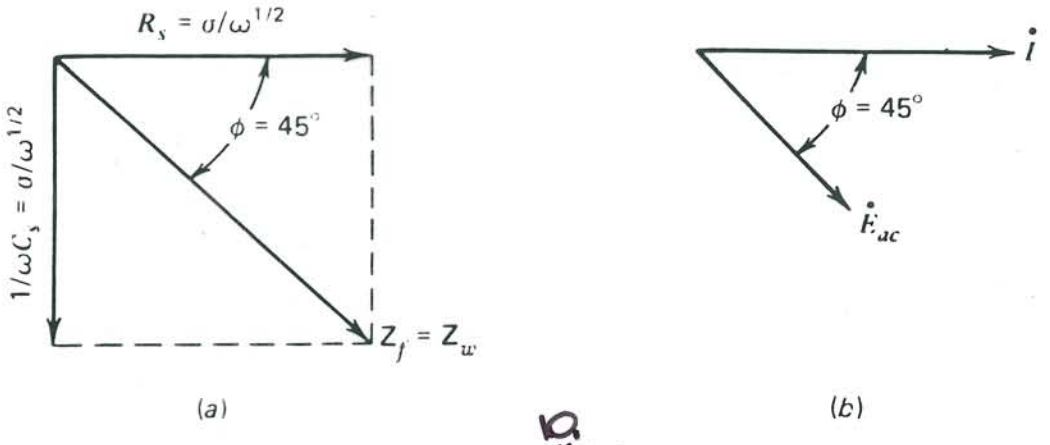

Figure 9.3.2

(*a*) Vector diagram showing the components of the faradaic impedance for a reversible system. (*b*) Phase relationship between ac current and the ac component of potential.

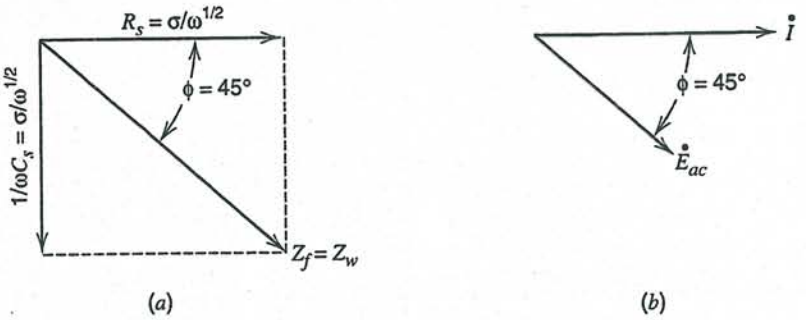

Figure 10.3.2 (*a*) Vector diagram showing the components of the faradaic impedance for a reversible system. (*b*) Phase relationship between the ac current and the ac component of potential.

Since the resistance and the capacitive reactance are exactly equal, the magnitude of the faradaic impedance is

$$Z_f = \left(\frac{2}{\omega}\right)^{1/2} \sigma \tag{10.3.8}$$

which is the magnitude of the Warburg impedance alone.

Since this is a mass-transfer impedance that applies to any electrode reaction, it is a minimum impedance. If kinetics are observable, another factor, R_{ct}, contributes, and Z_f must be greater, as Figure 10.3.3*a* depicts. Thus the amplitude of the sinusoidal current flowing in response to a given excitation signal, $\dot{E}_{ac}$, is maximal for a reversible system and decreases correspondingly for more sluggish kinetics. If the heterogeneous redox process is very immobile, R_{ct} and Z_f are so large that there is only a very small ac component to the current, and the limit of detection sets the lower bound on rate constants that can be measured by this approach. See Section 10.4.2 for more details about quantitative working ranges.

It is interesting also to examine the effect of concentration, which is manifested through σ. In general, higher concentrations reduce the mass-transfer impedance, as we would expect intuitively. Of greater interest, however, is the effect of the concentration ratio C_O^*/C_R^*. One can change it experimentally in order to vary the equilibrium potential for a series of impedance measurements. Both large and small ratios imply that one of the concentrations is small; hence σ and Z_f must be large. The current response to $\dot{E}_{ac}$ is not very great, because the supply of one reagent is insufficient to permit a high reaction rate for the cyclic, reversible electrode process that causes the ac current. Large rates can be achieved only when both electroreactants are present at comparable concentrations; hence we expect Z_f to be minimal near $E^{0'}$. Impedance measurements are most easily made in that potential region, and they gradually become more difficult as one departs from it ei-

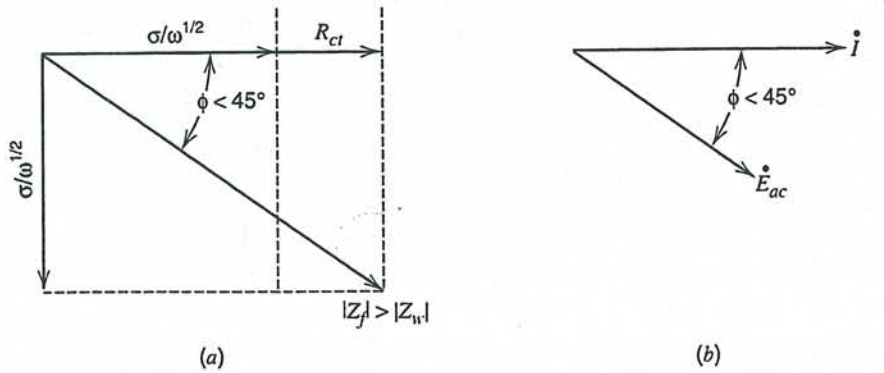

Figure 10.3.3 (*a*) Vector diagram showing the effect of R_{ct} on the impedance. (b) Phase relationship between $\dot{I}$ and $\dot{E}$ for a system with significant R_{ct}.

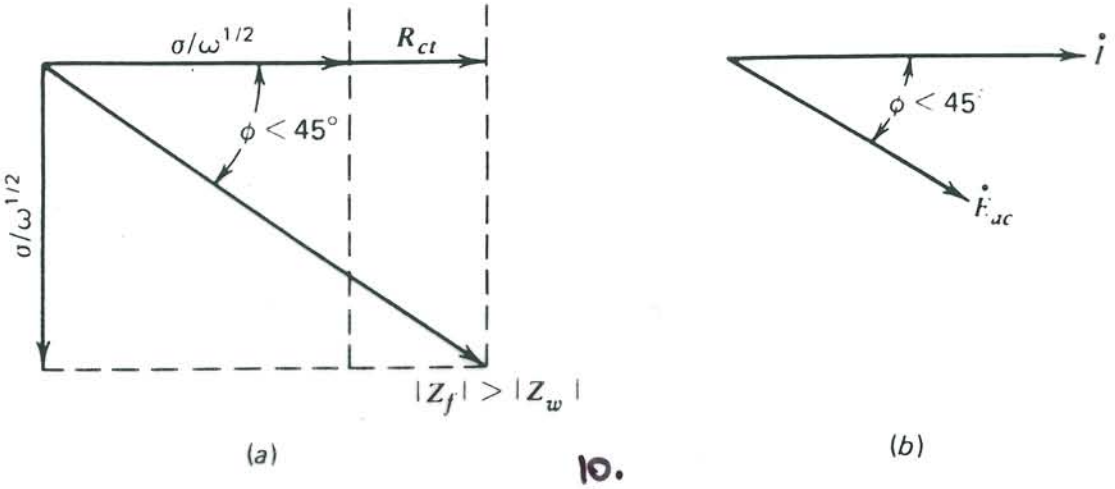

10.

Figure 4.3.3

(*a*) Vector diagram showing the effect of R_{ct} on the impedance. (*b*) Phase relationship between $\dot{I}$ and $\dot{E}_{ac}$ for a system with significant R_{ct}.

in the extreme when $R_{ct} >> Z_w$:

$Z_f \simeq R_{ct}$, $\phi \simeq 0$

ther positively or negatively. This effect presages the shape of the ac voltammetric response, which will be derived in Section 10.5.

A final point of interest is the phase angle between the current phasor, $\dot{I}_{ac}$, and the potential, $\dot{E}_{ac}$. Since $\dot{I}_{ac}$ lies along R_s and $\dot{E}_{ac}$ lies along Z_f, the phase angle is readily calculated as

$$\phi = \tan^{-1}\frac{1}{\omega R_s C_s} = \tan^{-1}\frac{\sigma/\omega^{1/2}}{R_{ct} + \sigma/\omega^{1/2}} \tag{10.3.9}$$

For the reversible case, $R_{ct} = 0$; hence $\phi = \pi/4$ or 45°. A quasireversible system shows $R_{ct} > 0$; hence $\phi < \pi/4$. However, ϕ must always be greater than zero, unless $R_{ct} \to \infty$; but then the reaction would be so sluggish that little alternating current would flow anyway in a conventional impedance measurement. This sensitivity of ϕ to kinetics suggests that R_{ct} might be extracted from the phase angle. It can be, and often it is, by ac voltammetric experiments. Before we proceed to a discussion of them, let us note that since $0 \le \phi \le 45°$, there is always a component of i_{ac} that is in-phase (0°) with $\dot{E}_{ac}$, and it can be measured with a phase-sensitive detector (e.g., a lock-in amplifier) referenced to $\dot{E}_{ac}$. This feature is extremely useful as a basis for discriminating against charging current in ac voltammetry.

Even though this section has been developed with the assumption that the electrode reaction is a one-step, one-electron process, many of the conclusions apply generally for chemically reversible multi-electron mechanisms. The nernstian limit is still described by (10.3.8) and Figure 10.3.2, but with σ given by

$$\boxed{\sigma = \frac{RT}{n^2F^2A\sqrt{2}}\left(\frac{1}{D_O^{1/2}C_O^*} + \frac{1}{D_R^{1/2}C_R^*}\right)} \tag{10.3.10}$$

When charge-transfer kinetics manifest themselves in a chemically reversible n-electron system, they do so in the manner discussed in relation to Figure 10.3.3. The kinetic effects can be expressed in terms of a charge-transfer resistance R_{ct} defined operationally as in (10.2.8). Further analysis of R_{ct}, such as to obtain the rate constant of the RDS, requires knowledge of the i-E characteristic for the mechanism, which can, however, be difficult to develop (see Section 3.5.4).

10.4 ELECTROCHEMICAL IMPEDANCE SPECTROSCOPY

In Section 10.3, we concentrated on the components of the faradaic impedance, R_s and C_s. We assumed that they can be extracted readily from direct measurements of the total impedance, which also includes the solution resistance, R_Ω, and the double-layer capacitance, C_d. In this section we will consider measurements of the total cell or electrode impedance as a function of ω and methods of extracting the faradaic impedance, R_Ω, and C_d from the results.

At a given frequency, the equivalent circuit of the cell can be taken as in Figure 10.1.14, but we measure its impedance as a resistance value R_B and the capacitance value C_B in series [or equivalently as $Z_{Re} = R_B$ and $Z_{Im} = 1/\omega C_B$]. One approach to obtaining the faradaic impedance from these values is to measure the cell impedance in a separate experiment under identical conditions, but in the absence of the electroactive couple. This measurement should yield the values of R_Ω and C_d (assuming they are not changed by the presence of the electroactive species), since the faradaic path is inactive. One can then subtract these graphically or analytically from the R_B and C_B values. This approach is

often used when impedance bridge measurements are made and was discussed in some detail in the first edition.[8] A more direct approach involves a study of the way in which the total impedance $\mathbf{Z} = R_B - j/(\omega C_B) = Z_{Re} - jZ_{Im}$ varies with frequency. From this variation, one can extract R_Ω, C_d, R_s, and C_s directly. This method circumvents the need for separate measurements without the electroactive species, and it eliminates the need to assume that the electroactive species has no effect on the nonfaradaic impedance.

10.4.1 Variation of Total Impedance (4, 16)

The electrochemical impedance spectroscopic approach, which is largely based on similar methods used to analyze circuits in electrical engineering practice, was developed by Sluyters and coworkers (4) and later extended by others (8–12). It deals with the variation of total impedance in the complex plane [as represented in Nyquist plots (Section 10.1.2)]. Let us consider this approach for our standard system.

The measured total impedance of the cell, $\mathbf{Z}$, is expressed as the series combination of R_B and C_B. These two elements provide the real and imaginary components of $\mathbf{Z}$, that is, $Z_{Re} = R_B$ and $Z_{Im} = 1/\omega C_B$. The electrochemical system is described theoretically in terms of an equivalent circuit such as that in Figure 10.1.14. Its impedance is readily written down according to the methods of Section 10.1.2. The real part, which must equal the measured Z_{Re}, is

$$Z_{Re} = R_B = R_\Omega + \frac{R_s}{A^2 + B^2} \tag{10.4.1}$$

where $A = (C_d/C_s) + 1$ and $B = \omega R_s C_d$. Similarly,

$$Z_{Im} = -\frac{1}{\omega C_B} = \frac{B^2/\omega C_d + A/\omega C_s}{A^2 + B^2} \tag{10.4.2}$$

Substitution for R_s and C_s by (10.2.25) and (10.2.26) provides

$$Z_{Re} = R_\Omega + \frac{R_{ct} + \sigma\omega^{-1/2}}{(C_d\sigma\omega^{1/2} + 1)^2 + \omega^2 C_d^2 (R_{ct} + \sigma\omega^{-1/2})^2} \tag{10.4.3}$$

$$Z_{Im} = \frac{\omega C_d (R_{ct} + \sigma\omega^{-1/2})^2 + \sigma\omega^{-1/2}(\omega^{1/2} C_d \sigma + 1)}{(C_d\sigma\omega^{1/2} + 1)^2 + \omega^2 C_d^2 (R_{ct} + \sigma\omega^{-1/2})^2} \tag{10.4.4}$$

Chemical information can be extracted by plotting Z_{Im} *vs.* Z_{Re} for different ω. For simplicity let us first consider the limiting behavior at high and low ω.

(a) Low-Frequency Limit

As $\omega \to 0$, the functions (10.4.3) and (10.4.4) approach the limiting forms:

$$Z_{Re} = R_\Omega + R_{ct} + \sigma\omega^{-1/2} \tag{10.4.5}$$

$$Z_{Im} = \sigma\omega^{-1/2} + 2\sigma^2 C_d \tag{10.4.6}$$

Elimination of ω between these two gives

$$\boxed{Z_{Im} = Z_{Re} - R_\Omega - R_{ct} + 2\sigma^2 C_d} \tag{10.4.7}$$

Thus, the plot of Z_{Im} *vs.* Z_{Re} should be linear and have unit slope, as shown in Figure 10.4.1. The extrapolated line intersects the real axis at $R_\Omega + R_{ct} - 2\sigma^2 C_d$. One can see

[8] First edition, pp. 347–349.

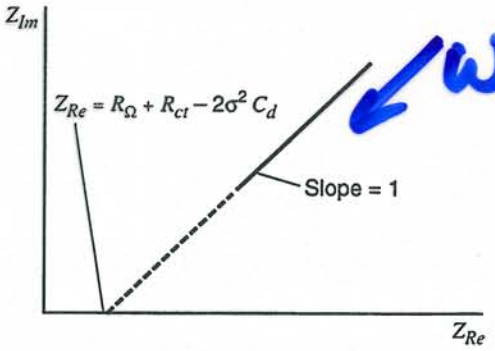

Figure 10.4.1 Impedance plane plot for low frequencies.

from (10.4.5) and (10.4.6) that the frequency dependence in this regime comes only from Warburg impedance terms; thus the linear correlation of Z_{Re} and Z_{Im} is characteristic of a diffusion-controlled electrode process. As the frequency rises, the charge-transfer resistance, R_{ct}, and the double-layer capacitance become more important elements, and we can expect a departure from (10.4.7).

(b) High-Frequency Limit

At very high frequencies, the Warburg impedance becomes unimportant in relation to R_{ct}, and the equivalent circuit converges to that of Figure 10.4.2. The impedance is

$$\mathbf{Z} = R_\Omega - j\left(\frac{R_{ct}}{R_{ct}C_d\omega - j}\right) \tag{10.4.8}$$

which has the components

$$Z_{Re} = R_\Omega + \frac{R_{ct}}{1 + \omega^2 C_d^2 R_{ct}^2} \tag{10.4.9}$$

$$Z_{Im} = \frac{\omega C_d R_{ct}^2}{1 + \omega^2 C_d^2 R_{ct}^2} \tag{10.4.10}$$

Elimination of ω from this pair of equations yields

$$\boxed{\left(Z_{Re} - R_\Omega - \frac{R_{ct}}{2}\right)^2 + Z_{Im}^2 = \left(\frac{R_{ct}}{2}\right)^2} \tag{10.4.11}$$

Hence Z_{Im} *vs.* Z_{Re} should give a circular plot centered at $Z_{Re} = R_\Omega + R_{ct}/2$ and $Z_{Im} = 0$ and having a radius of $R_{ct}/2$. Figure 10.4.3 depicts the result.

The general features of the plot are readily grasped intuitively. The imaginary component to the impedance in the circuit of Figure 10.4.2 comes solely from C_d. Its contribution falls to zero at high frequencies, because it offers no impedance. All of the current is charging current, and the only impedance it sees is the ohmic resistance. As the frequency drops, the finite impedance of C_d manifests itself as a significant Z_{Im}. At very low frequencies, the capacitance C_d offers a high impedance; hence current flow passes mostly

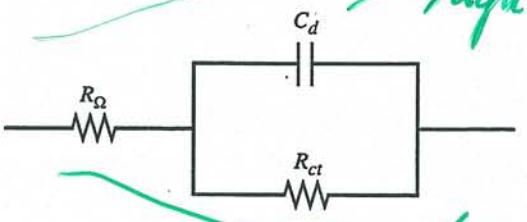

Figure 10.4.2 Equivalent circuit for a system in which the Warburg impedance is unimportant.

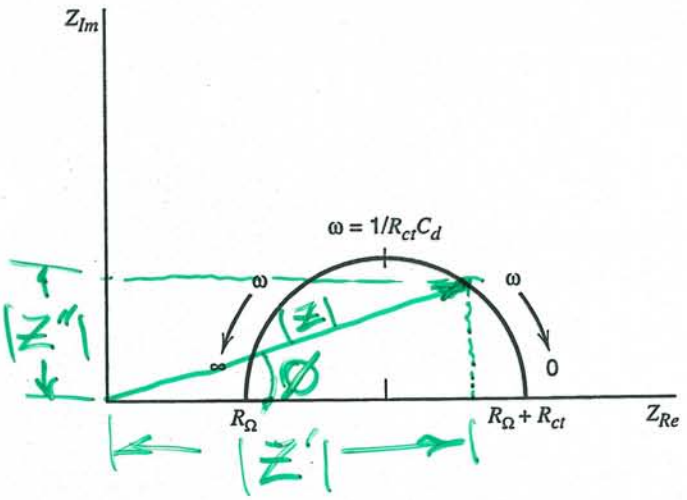

Figure 10.4.3 Impedance plane plot for the equivalent circuit of Figure 10.4.2.

through R_{ct} and R_Ω. Thus the imaginary impedance component falls off again. In general, we can expect to see a departure from this plot in this lower-frequency regime, because the Warburg impedance will become important.

(c) Application to Real Systems

An actual plot of impedance in the complex plane will combine the features of our two limiting cases as in Figure 10.4.4. However, both regions may not be well defined for any given system. The determining feature is the charge-transfer resistance, R_{ct}, and its relation to the Warburg impedance, which is controlled by σ. If the chemical system is kinetically sluggish, it will show a large R_{ct}, and may display only a very limited-frequency region where mass transfer is a significant factor. This case is shown in Figure 10.4.5*a*. At the other extreme, R_{ct} might be inconsequentially small by comparison to the ohmic resistance and the Warburg impedance over nearly the whole available range of σ. Then the system is so kinetically facile that mass transfer always plays a role, and the semicircular region is not well defined. An example is shown in Figure 10.4.5*b*.

10.4.2 Limits to Measurable k^0 by the Faradaic Impedance Method (1–6, 9–12)

The foregoing paragraphs highlight the limitations in interpreting impedance data, and they lead naturally to the idea that k^0 must fall in some fairly well-defined range in

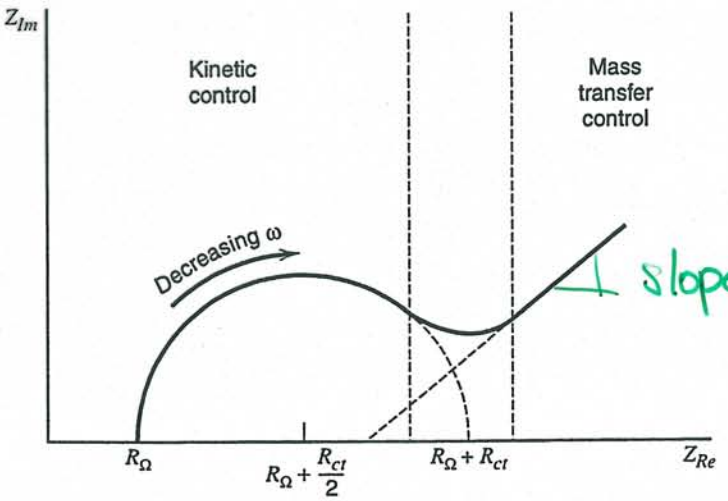

Figure 10.4.4 Impedance plot for an electrochemical system. Regions of mass-transfer and kinetic control are found at low and high frequencies, respectively.

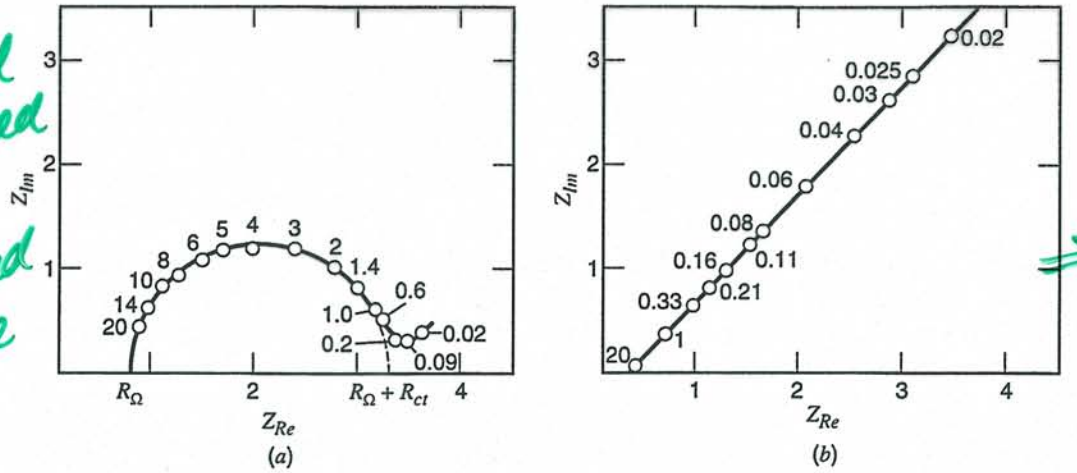

Figure 10.4.5 Impedance plane plots for actual chemical systems. Numbers by points are frequencies in kHz. (*a*) For the electrode reaction $Zn^{2+} + 2e \rightleftarrows Zn(Hg)$. $C^*_{Zn^{2+}} = C^*_{Zn(Hg)} = 8 \times 10^{-3}\ M$. Electrolyte was 1 M $NaClO_4$ plus $10^{-3}\ M$ $HClO_4$. (b) For the electrode reaction $Hg_2^{2+} + 2e \rightleftarrows Hg$ in 1 M $HClO_4$. $C_{Hg_2^{2+}} = 2 \times 10^{-3}\ M$. [From J. H. Sluyters and J. J. C. Oomen, *Rec. Trav. Chim. Pays-Bas*, **79**, 1101 (1960), with permission.]

order to be reliably measured by an impedance method. We can define the range semiquantitatively.

(a) Upper Limit

The parameter R_{ct} must make a significant contribution to R_s hence $R_{ct} \geq \sigma/\omega^{1/2}$. Substituting from (10.3.2), (10.3.6), and (3.4.7) and assuming $D_O = D_R$ and $C^*_O = C^*_R$, we obtain the condition that $k^0 \leq (D\omega/2)^{1/2}$. The highest practical value of ω is determined by the cell time constant, $R_u C_d$, which must remain much smaller than the cycle period of the applied ac stimulus. With a UME, one can do useful work at several MHz, so that $\omega \leq 10^7\ s^{-1}$, and with $D \sim 10^{-5}\ cm^2/s$, we have $k^0 \leq 7$ cm/s.[9] In addition, there are requirements that $C_s \geq C_d$ and $R_s \geq R_\Omega$.

(b) Lower Limit

For very large R_{ct}, the Warburg impedance is negligible, and the equivalent circuit of Figure 10.4.2 can be applied. One problem here is that R_{ct} cannot be so large that all the current takes the path through C_d. That is, $R_{ct} \leq 1/\omega C_d$ or $k^0 \geq RTC_d\omega/F^2C^*A$. If we choose the most favorable conditions of $C^* = 10^{-2}\ M$ and $\omega = 2\pi \times 1$ Hz,[10] then at $T = 298$ K and with $C_d/A = 20\ \mu F/cm^2$, we obtain $k^0 \geq 3 \times 10^{-6}$ cm/s.

[9]The reductions and oxidations of aromatic species to anion and cation radicals in aprotic solvents are generally among the fastest known heterogeneous charge-transfer reactions. The values of k^0 can exceed 1 cm/s. See references 17 and 18 for measurements of such systems by impedance methods.

[10]It is also essential that the period of the ac stimulus not be so long that convection becomes a factor within a few cycles. The lower frequency limit was set here at 1 Hz because convection would become a problem in the range of several seconds in most liquid systems with water-like viscosity. Current equipment for EIS can operate at much lower frequencies (as low as 10 μHz) and can be usefully applied in the low-frequency (long-time) regime when the processes being examined are not controlled by convection. Examples include transport or reaction at a solid–solid interfaces or diffusion and reaction in extremely viscous media, such as glasses or polymers.

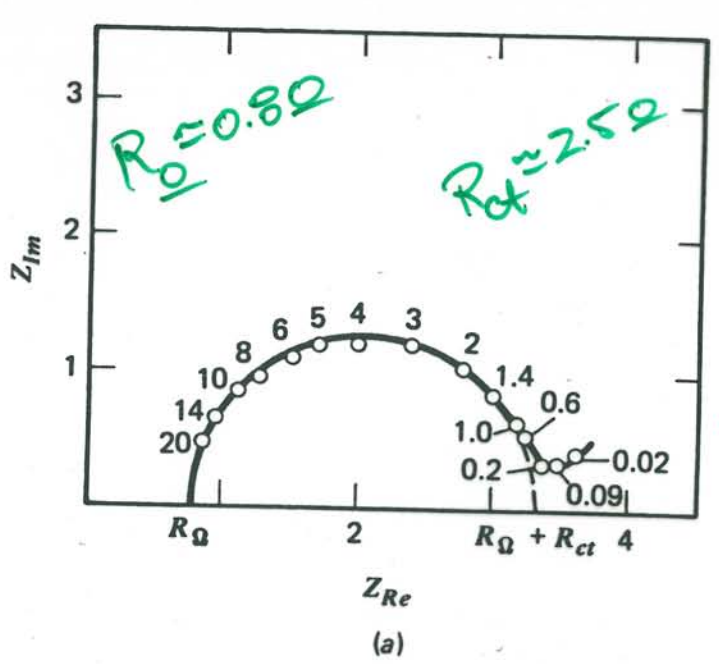

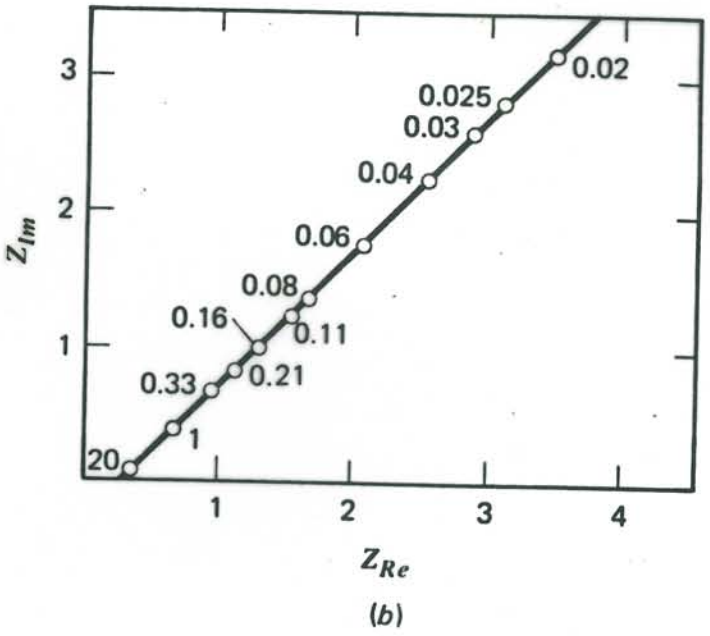

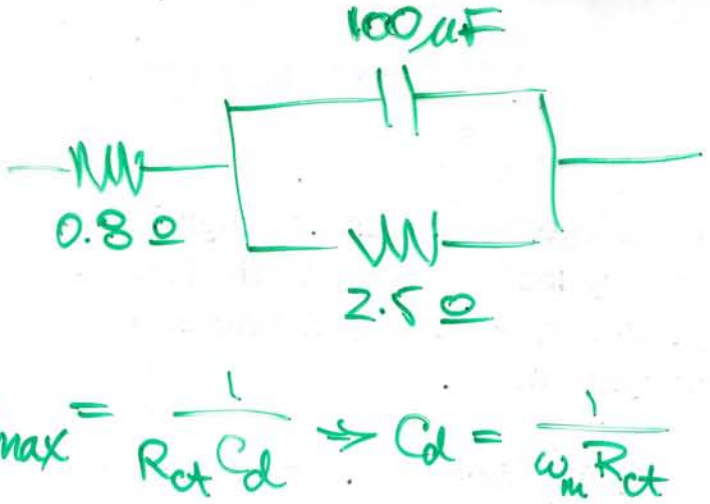

$$\omega_{max} = \frac{1}{R_{ct} C_d} \Rightarrow C_d = \frac{1}{\omega_m R_{ct}}$$

Figure 9.5.8
Impedance plane plots for actual chemical systems. Numbers by points are frequencies in kilohertz. (*a*) For the electrode reaction $Zn^{2+} + 2e \rightleftharpoons Zn(Hg)$. $C^*_{Zn^{2+}} = C^*_{Zn(Hg)} = 8 \times 10^{-3}\ M$. Electrolyte was $1\ M\ NaClO_4$ plus $10^{-3}\ M\ HClO_4$. (*b*) For the electrode reaction $Hg_2^{2+} + 2e \rightleftharpoons Hg$ in $1\ M\ HClO_4$. $C^{2+}_{Hg_2} = 2 \times 10^{-3}\ M$. [From J. H. Sluyters and J. J. C. Oomen, *Rec. Trav. Chim.*, **79**, 1101 (1960), with permission.]

9.5.4 Matched Cells

In ac polarographic measurements, one can often employ a dual cell configuration in which one cell contains the electroactive species of interest and the other holds only the supporting electrolyte. If the DMEs are synchronized and matched in m values, and if both are controlled at the same potential, then their difference current represents the faradaic current of interest at every point in time.† The difference current is readily recorded directly by electronic means; hence this technique is essentially a method for compensating charging current in real time. It is most useful in kinetic studies involving sufficiently high concentrations of electroactive substances that the faradaic currents are relatively large. Of course, the fundamental assumption behind this scheme is that the electroactive substance of interest does not alter the interfacial capacitance.

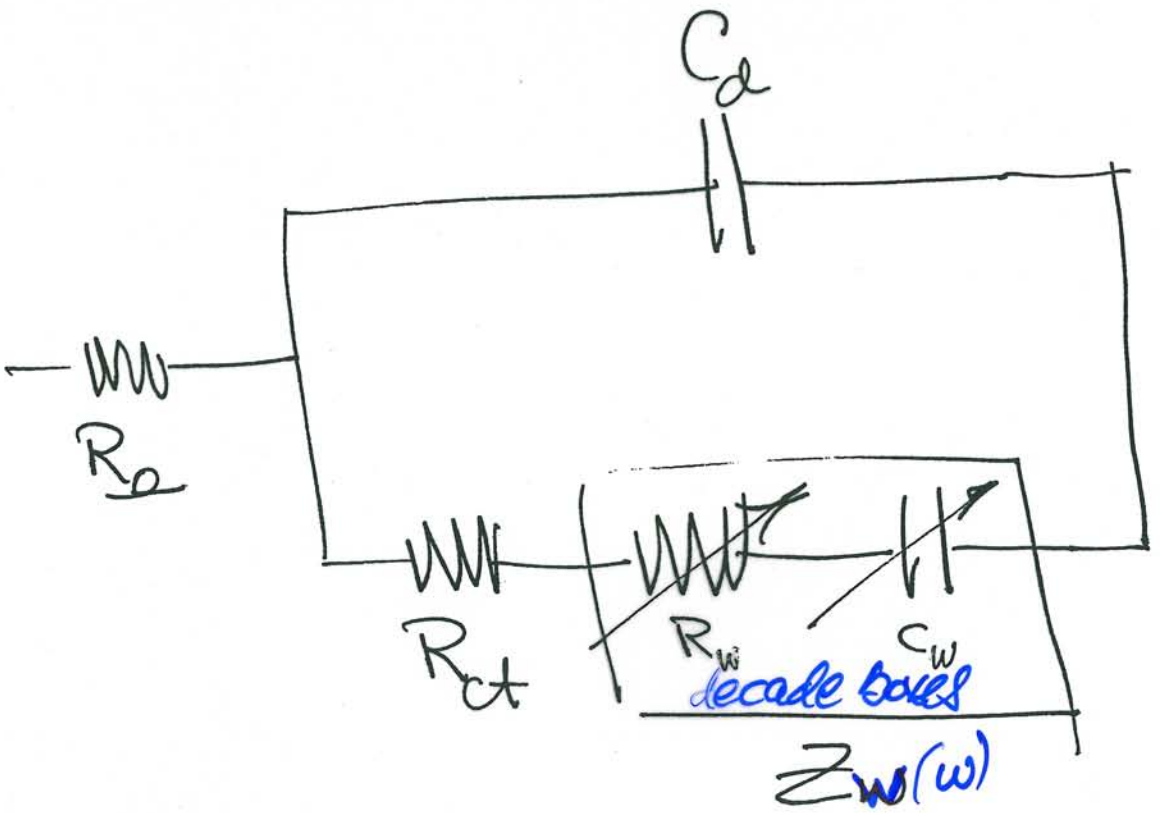

$R_o = 5 \ \Omega$

$C_d = 100 \mu F$

$R_{ct} = 5 \ \Omega$

$$R_w = \frac{100}{\omega^{1/2}}$$

$$C_w = \frac{1}{100\,\omega^{1/2}}$$

ω (Hz)	R_w (Ω)	~~X_C~~ (Ω)	C_w (μF)
25	20	20	2000
400	5	5	500
2500	2	2	200
10,000	1	1	100
65,000	0.39	0.39	39

10.4.3 Other Applications of Electrochemical Impedance Spectroscopy

The approach discussed above for EIS of a simple heterogeneous electron-transfer reaction of solution components can be applied to more complicated electrochemical systems, like those with coupled homogeneous reactions or with adsorbed intermediates. In such cases Nyquist plots can be obtained and compared to theoretical models based on the appropriate equations representing the rates of the various processes and their contributions to the current. It may be useful in these cases to represent the system by an equivalent circuit involving different components (resistors, capacitors, inductors). However, such equivalent circuits are not unique and one cannot easily guess the form or structure of the equivalent circuit from the processes involved in the reaction scheme (19). Electrode surface roughness and heterogeneity can also be significant factors in the ac response in EIS. Indeed, even for simple electron-transfer reactions, measurements that can be made usefully with a smooth and homogeneous mercury electrode are often not possible with solid electrodes.

EIS has been applied to a variety of electrochemical systems, including those involved in corrosion, electrodeposition, polymer films, and semiconductor electrodes. Representative studies can be found in EIS symposia proceedings (20–22).

▶ 10.5 AC VOLTAMMETRY

We noted in Section 10.1 that ac voltammetry is basically a faradaic impedance technique in which the mean potential, E_{dc}, is imposed potentiostatically at arbitrary values that usually differ from the equilibrium value. Ordinarily, E_{dc} is varied systematically (e.g., linearly) on a long time scale compared to that of the superimposed ac variation, E_{ac} (10 Hz to 100 kHz). The output is a plot of the magnitude of the ac component of the current *vs.* E_{dc}. The phase angle between the alternating current and E_{ac} is also of interest.

Treatments of this problem are greatly simplified by uncoupling the long-term diffusion due to E_{dc} from the rapid diffusional fluctuations due to E_{ac}. We do that by recognizing that E_{dc} sets up mean surface concentrations that look like bulk values to the ac perturbation because of the difference in time scale. In Section 10.3, we defined the faradaic impedance in terms of bulk concentrations; thus the current response in ac voltammetry as a function of E_{dc} is readily obtained by substituting the surface concentrations imposed by E_{dc} directly into these impedance relations. Since this strategy is simple and intuitive, we will pursue it. More rigorous treatments are available in the literature for the interested reader (2, 3, 5). The results are the same by either approach.

The mean surface concentrations enforced by E_{dc} depend on many factors: (a) the way in which E_{dc} is varied; (b) whether or not there is periodic renewal of the diffusion layer; (c) the applicable current-potential characteristic; and (d) homogeneous or heterogeneous chemical complications associated with the overall electrode reaction. For example, one could vary E_{dc} in a sequential potentiostatic manner with periodic renewal of the diffusion layer, as in sampled-current voltammetry. This is the technique that is actually used in *ac polarography*, which features a DME and effectively constant E_{dc} during the lifetime of each drop. Alternatively one could use a stationary electrode and a fairly fast sweep without renewal of the diffusion layer. Both techniques have been developed and are considered below. The effects of different kinds of charge-transfer kinetics will also be examined here, but the effects of homogeneous complications are deferred to Chapter 12. Throughout the discussion, one should keep in mind that the chief strength of ac

voltammetry is the access it gives to exceptionally precise quantitative information about electrode processes. Diagnostic aspects certainly exist, but they are more subtle than with other methods.

10.5.1 ac Polarography in a Reversible System

Let us consider the ac response at a renewable stationary mercury drop electrode immersed in a solution containing initially only species O in the nernstian process $O + ne \rightleftarrows R$. The dc potential starts at a value considerably more positive than $E^{0'}$ and is scanned slowly in a negative direction. During the lifetime of a single drop, E_{dc} is effectively constant; hence the dc part of the experiment is conventional polarography and is treated as a series of individual step experiments (see Sections 7.1 and 7.2).

Since the charge-transfer resistance is completely negligible, (10.3.10) always applies where

$$\sigma = \frac{RT}{n^2F^2A\sqrt{2}}\left[\frac{1}{D_O^{1/2}C_O(0,t)_m} + \frac{1}{D_R^{1/2}C_R(0,t)_m}\right] \tag{10.5.1}$$

and the mean concentrations $C_O(0,t)_m$ and $C_R(0,t)_m$ are determined by the nernstian relation:

$$\frac{C_O(0,t)_m}{C_R(0,t)_m} = \theta_m = \exp\left[\frac{nF}{RT}(E_{dc} - E^{0'})\right] \tag{10.5.2}$$

The arguments that led to (5.4.29) and (5.4.30) apply equally to the dc part of this experiment; hence we write

$$C_O(0,t)_m = C_O^*\left(\frac{\xi\theta_m}{1+\xi\theta_m}\right) \tag{10.5.3}$$

$$C_R(0,t)_m = C_O^*\left(\frac{\xi}{1+\xi\theta_m}\right) \tag{10.5.4}$$

where ξ is $D_O^{1/2}/D_R^{1/2}$, as usual. Thus the faradaic impedance is obtained by substitution into (10.5.1) and then into (10.3.8):

$$Z_f = \frac{RT}{n^2F^2A\omega^{1/2}D_O^{1/2}C_O^*}\left(\frac{1}{\xi\theta_m} + 2 + \xi\theta_m\right) \tag{10.5.5}$$

Let us note now that $\xi\theta_m$ can be written

$$\xi\theta_m = e^a \tag{10.5.6}$$

where

$$a = \frac{nF}{RT}(E_{dc} - E_{1/2}) \tag{10.5.7}$$

and $E_{1/2}$ is the reversible half-wave potential defined in (5.4.21):

$$E_{1/2} = E^{0'} + \frac{RT}{nF}\ln\frac{D_R^{1/2}}{D_O^{1/2}} \tag{10.5.8}$$

By substitution from (10.5.6), we find that the term in parentheses in (10.5.5) is $e^{-a} + 2 + e^a$, which is also $4\cosh^2(a/2)$. Thus we have

$$Z_f = \frac{4RT}{n^2F^2A\omega^{1/2}D_O^{1/2}C_O^*}\cosh^2\left(\frac{a}{2}\right) \tag{10.5.9}$$

In Section 10.3 we saw that the faradaic current for a reversible system leads $\dot{E}_{ac}$ by exactly 45°. If $\dot{E}_{ac} = \Delta E \sin \omega t$, then

$$i_{ac} = \frac{\Delta E}{Z_f} \sin\left(\omega t + \frac{\pi}{4}\right) \tag{10.5.10}$$

and the amplitude of this current, which is the chief observable, is simply

$$I = \frac{\Delta E}{Z_f} = \frac{n^2F^2A\omega^{1/2}D_O^{1/2}C_O^* \Delta E}{4RT \cosh^2(a/2)} \tag{10.5.11}$$

Figure 10.5.1 is a display of the ac polarogram defined by this equation. The bell shape derives from the factor $\cosh^{-2}(a/2)$, and it reflects the potential dependence of the impedance, Z_f. The maximum in the current occurs at $a/2 = 0$ or at $E_{dc} = E_{1/2}$, which is near E^0. As one moves away from that potential, either positively or negatively, the impedance rises sharply and the current falls off. The physical basis for this behavior was outlined in Section 10.3. In effect, the current is controlled by the limiting reagent, that is, the smaller of the two surface concentrations. At potentials far from $E^{0'}$, where only small amounts of one reagent can exist at the surface, only small currents can flow.

The peak current at $E_{dc} = E_{1/2}$ comes easily from (10.5.11). Since $\cosh(0) = 1$,

$$I_p = \frac{n^2F^2A\omega^{1/2}D_O^{1/2}C_O^* \Delta E}{4RT} \tag{10.5.12}$$

From this relation and (10.5.11) one can show straightforwardly that the shape of the ac polarogram adheres to

$$E_{dc} = E_{1/2} + \frac{2RT}{nF} \ln\left[\left(\frac{I_p}{I}\right)^{1/2} - \left(\frac{I_p - I}{I}\right)^{1/2}\right] \tag{10.5.13}$$

(See Problem 10.1.)

The same results hold for the DME, where one must account for the effect of drop growth on the polarogram. The use of linear diffusion relations for the dc part of the

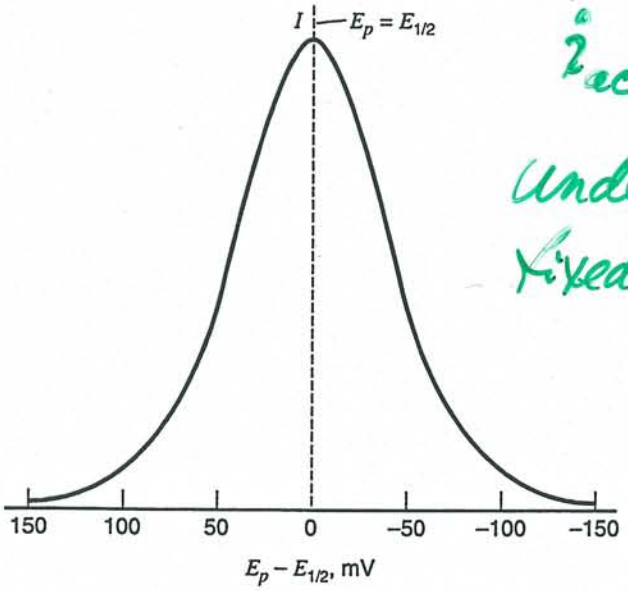

Figure 10.5.1 Shape of a reversible ac voltammetric peak for $n = 1$.

experiment has already been justified (see Section 7.1.2), and that justification is even more valid for the ac part because of its shorter time scale. Thus the peculiarities of the expanding sphere are felt only in the changing area A with time, and that factor is directly accountable by substitution of (7.1.3) into (10.5.11). Since A grows as $t^{2/3}$ as the drop ages, the current also shows the same dependence. Thus we can expect the current to oscillate as successive drops grow and fall. Maxima should be observed at the end of each drop's life. Experimental results in Figure 10.5.2 bear out these expectations. Measurements carried out on the envelope of the ac polarogram can be treated by all relations derived above, provided that A is defined as the area just before drop fall.

A number of important properties of the reversible ac voltammogram can be deduced from (10.5.11)–(10.5.13). Among them are the direct proportionalities between I_p and n^2, $\omega^{1/2}$, and C_O^*. There is also a proportionality to ΔE; however, this relation is a limited one, because the linearized i-E characteristic underlying the derivation of Z_f becomes invalid if ΔE is too large. For linearity within a few percent, ΔE must be less than about $10/n$ mV. Not surprisingly, the width of the peak at half height also depends on ΔE if large values are used. If it is kept below $10/n$ mV, there is a constant width of $90.4/n$ mV at 25°C. At larger ΔE the peaks are broader.

10.5.2 Voltammetric ac Response to Quasireversible and Irreversible Systems

When heterogeneous kinetics become sluggish enough to be visible, one requires a more elaborate theory to predict the voltammetric ac response. Even for a one-step, one-electron process, the general case in which k^0 can adopt any value is very complex. The reader is referred to the literature for complete discussions (2, 3, 5). Here we examine

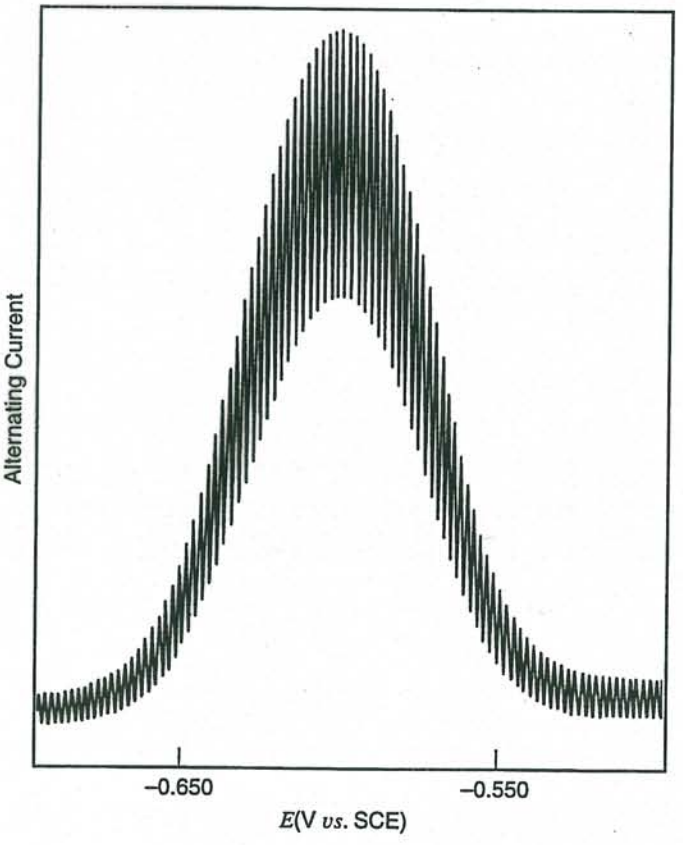

Figure 10.5.2 An ac polarogram for 3×10^{-3} M Cd^{2+} in 1.0 M Na_2SO_4. $\Delta E = 5$ mV, $\omega/2\pi = 320$ Hz. [Reprinted with permission from D. E. Smith, *Anal Chem.*, **35**, 1811 (1963). Copyright 1963, American Chemical Society.]

an important special case in detail, and it will provide us with a good intuitive understanding of the kinetic effects of interest.

That special case is the situation in which the dc response from a one-step, one-electron system is effectively nernstian, whereas the ac response is not. This situation is frequently seen in real systems because the time scales of the two aspects can differ so greatly. That is, k^0 can be sufficiently large that the mean surface concentrations are kept in the ratio dictated in E_{dc} through the nernstian balance, (10.5.2), even though that rate constant is not large enough to assure a negligible charge-transfer resistance to the much faster ac perturbation.

The faradaic impedance in this situation involves both R_{ct} and σ, and the magnitude can be written from (10.2.27):

$$Z_f = \left[\left(R_{ct} + \frac{\sigma}{\omega^{1/2}}\right)^2 + \left(\frac{\sigma}{\omega^{1/2}}\right)^2\right]^{1/2} \tag{10.5.14}$$

The parameters R_{ct} and σ can both be defined through the assumption of dc reversibility, which allows us to use the same mean surface concentrations as in the previous section. They are defined by (10.5.3) and (10.5.4); thus we can develop σ by substitution into (10.5.1). Rearrangements equivalent to those used in obtaining (10.5.9) then yield

$$\sigma = \frac{4RT}{\sqrt{2}F^2AD_O^{1/2}C_O^*}\cosh^2\left(\frac{a}{2}\right) \tag{10.5.15}$$

where we have recognized that $n = 1$.

The charge-transfer resistance, R_{ct}, is given by (10.3.2) in terms of the exchange current, i_0. Normally we speak of i_0 as an equilibrium property defined by bulk concentrations of O and R according to (3.4.6). However, since the mean surface concentrations act like bulk values for the ac process, we can recognize an effective exchange current for ac perturbation that would be given by

$$(i_0)_{eff} = FAk^0[C_O(0, t)_m]^{(1-\alpha)}[C_R(0, t)_m]^{\alpha} \tag{10.5.16}$$

By determining the mean surface concentrations, E_{dc} controls $(i_0)_{eff}$ and, therefore, R_{ct}. A more explicit expression of this dependence is obtained by substitution from (10.5.3), (10.5.4), and (10.5.6), as above:

$$(i_0)_{eff} = FAk^0C_O^*\xi^{\alpha}\left(\frac{e^{\beta a}}{1 + e^a}\right) \tag{10.5.17}$$

where $\beta = (1 - \alpha)$. Since $R_{ct} = RT/F(i_0)_{eff}$, we have

$$R_{ct} = \frac{RT}{F^2Ak^0C_O^*\xi^{\alpha}}\left(\frac{1 + e^a}{e^{\beta a}}\right) \tag{10.5.18}$$

Now that R_{ct} and σ are available, we can write Z_f as a function of E_{dc} by substitution into (10.5.14). That operation is straightforward, but it yields a rather messy expression. Perhaps more instructive is to examine limiting behavior for high and low frequencies, which can be discerned from (10.5.14).

At very low frequencies, R_{ct} is small compared to $\sigma/\omega^{1/2}$; hence the system looks reversible. This is not surprising; after all we are bringing the time domain of the ac process toward that of the dc perturbation, which evokes a reversible response. Everything we found in the previous section about the reversible ac response should also apply to the quasireversible system at the low-frequency limit.

As the frequency is elevated, R_{ct} becomes appreciable in comparison to $\sigma/\omega^{1/2}$; hence reversibility is vitiated. The ac time domain has become shortened enough to strain the

heterogeneous kinetics. Finally, at the high-frequency limit, R_{ct} greatly exceeds $\sigma/\omega^{1/2}$, and Z_f approaches R_{ct} itself. The amplitude of the alternating current is then

$$I = \frac{\Delta E}{R_{ct}} = \frac{F^2 A k^0 C_O^* \Delta E \xi^\alpha}{RT}\left(\frac{e^{\beta a}}{1+e^a}\right) \tag{10.5.19}$$

This equation describes the shape of the ac polarogram. In general, the response as a function of dc potential is bell-shaped, much as in the reversible situation. This point is seen by noting the behavior of the factor in parentheses as a becomes large either positively or negatively. However, positive deviations from $E_{1/2}$ do not evoke the same response as negative deviations; that is, the response is not symmetric and the bell shape is skewed.

The peak is easily found by differentiating (10.5.19) with respect to a. The maximum is reached when $e^a = \beta/\alpha$, or

$$E_{dc} = E_{1/2} + \frac{RT}{F}\ln\frac{\beta}{\alpha} \tag{10.5.20}$$

The peak current amplitude is therefore

$$I_p = \frac{F^2 A k^0 C_O^* \Delta E \xi^\alpha}{RT}\beta^\beta \alpha^\alpha \tag{10.5.21}$$

These equations, together with those describing the reversible, low-frequency limit, give a good picture of the behavior of the system as ω changes. The peak current is at first linear with $\omega^{1/2}$, but with increasing frequency that dependence is reduced until, at the high-frequency limit, I_p becomes independent of ω. It is easy to see from preceding developments that the frequency dependence reflects the mass transport effects manifested in the Warburg impedance. The lack of a frequency dependence in (10.5.19) and (10.5.21) comes about because the current is totally controlled at high ω by heterogeneous kinetics. Mass transfer plays no role. Not surprisingly, then, I_p is proportional to k^0 at high ω, and it is totally insensitive to k^0 at low ω. The proportionalities between I_p and ΔE and C_O^* hold at all frequencies.

Note also that since kinetic control of I at high frequencies implies a faradaic impedance that greatly exceeds the Warburg impedance at those frequencies, the current must be much smaller than that for a truly reversible system, which shows only the Warburg impedance at any frequency. The general reduction in ac response in quasireversible systems is illustrated in Figure 10.5.3. The k^0 values for all curves shown there are sufficiently great that the assumption of dc reversibility holds. It is easy to see the trend in responses with decreasing k^0; hence one recognizes that there will be a rather small ac response if k^0 falls below 10^{-4} to 10^{-5} cm/s. Systems showing totally irreversible dc polarograms can be almost invisible to the ac experiment. This fact is useful for analytical work (see Section 10.7).[11]

[11]The totally irreversible case does yield an ac current, contrary to the impression one might gain from this line of argument. The current arises from the simple modulation of the dc wave (23, 24). Since the shape of that wave is independent of k^0 (Section 5.5), the ac peak height is also independent of k^0. The peak lies near the half-wave potential of the dc wave; hence it is shifted substantially from $E^{0'}$ by an amount related to the size of k^0.

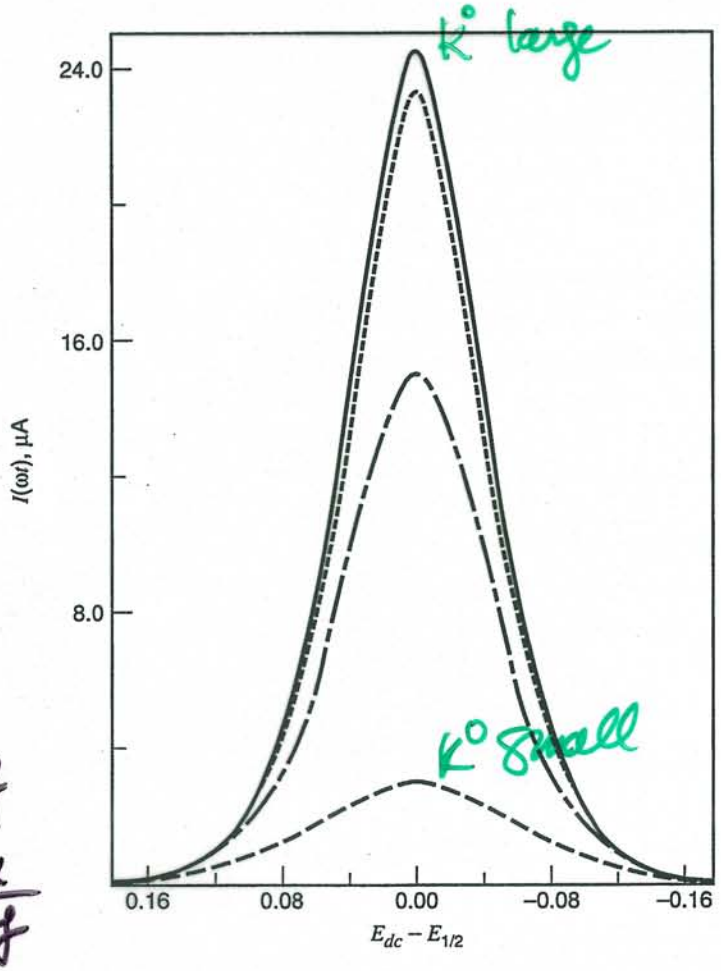

Figure 10.5.3 Calculated ac polarograms for quasireversible one-step, one-electron systems. Curves (from the top) are for $k^0 \to \infty$, $k^0 = 1$, $k^0 = 0.1$, and $k^0 = 0.01$ cm/s. Other parameters are as follows: $\omega = 2500\ s^{-1}$, $\alpha = 0.500$, $D = 9 \times 10^{-6}\ cm^2/s$, $A = 0.035\ cm^2$, $C_O^* = 1.00 \times 10^{-3}\ M$, $T = 298\ K$, $\Delta E = 5.00\ mV$. The curves show the faradaic current at t_{max}. [Reprinted from D. E. Smith, *Electroanal. Chem.*, **1**, 1 (1966), by courtesy of Marcel Dekker, Inc.]

The position of the peak is also of interest. Relations derived above show that there is a slight shift with increasing frequency. At low ω, the peak comes at $E_{dc} = E_{1/2}$, just as for a reversible system at any frequency. As ω becomes greater, the peak potential deviates from this value until it reaches the limiting position defined by (10.5.20). Since α and β are generally comparable, we can expect the extent of this shift, $(RT/F)\ln(\beta/\alpha)$, to be quite small. In other words, the peak potential for an ac polarogram is always near the formal potential for the couple, provided dc reversibility applies.

The phase angle of I_{ac} with respect to E_{ac} is of great interest as a source of kinetic information. This point was suggested in Section 10.3, and it is rooted in equation 10.3.9. We can rewrite that relation as

$$\cot\phi = 1 + \frac{R_{ct}\omega^{1/2}}{\sigma} \tag{10.5.22}$$

Substitution from (10.5.15) and (10.5.18) and rearrangement gives

$$\cot\ \phi = 1 + \frac{(2D_O^{\beta}D_R^{\alpha}\omega)^{1/2}}{k^0}\left[\frac{1}{e^{\beta a}(1 + e^{-a})}\right] \tag{10.5.23}$$

The bracketed factor shows that cot ϕ depends on the dc potential. Large positive and negative values of a force cot ϕ to unity, and hence there must be a maximum in this quantity near the peak of the polarogram. The precise position is easily found by differentiation, and one ascertains that $e^{-a} = \beta/\alpha$ at that point. Thus,

$$E_{dc} = E_{1/2} + \frac{RT}{F}\ln\frac{\alpha}{\beta} \tag{10.5.24}$$

This maximum point is independent of nearly all experimental variables, for example, ΔE, C_O^*, and, most notably, A and ω. The difference between $E_{1/2}$ and the potential of maximum cot ϕ provides access to the transfer coefficient α.

Actual cot ϕ data are shown in Figure 10.5.4 for $TiCl_4$ in oxalic acid solution (25). The electrode reaction is the one-electron reduction of Ti(IV) to Ti(III). Note that the potential of maximum cot ϕ is independent of frequency, as predicted above.

Plots of cot ϕ *vs.* $\omega^{1/2}$ yield k^0, once α is known from the position of $[\cot \phi]_{max}$ and the diffusion coefficients are known from other measurements. This point is easily seen from (10.5.23), which holds for any value of E_{dc}. In practice, these plots are usually made for special values of E_{dc} that give simplified forms of the linear relation.

A convenient procedure is to choose $E_{dc} = E_{1/2}$, for then $a = 0$, and we have

$$[\cot \phi]_{E_{1/2}} = 1 + \left(\frac{D_O^\beta D_R^\alpha}{2}\right)^{1/2} \frac{\omega^{1/2}}{k^0} \tag{10.5.25}$$

If one can take $D_O = D_R = D$, then $D_O^\beta D_R^\alpha = D$, and the slope of this particular plot becomes independent of α. Figure 10.5.5 is an example in which the data from Figure 10.5.4 at $E_{dc} = E_{1/2} = -0.290$ V *vs.* SCE have been plotted *vs.* $\omega^{1/2}$.

Another simplified version of (10.5.23) can be obtained for the potential of maximum cot ϕ. By substituting $e^{-a} = \beta/\alpha$, we obtain

$$[\cot \phi]_{max} = 1 + \frac{(2D_O^\beta D_R^\alpha)^{1/2}}{k^0\left[\left(\frac{\alpha}{\beta}\right)^{-\alpha} + \left(\frac{\alpha}{\beta}\right)^{\beta}\right]} \omega^{1/2} \tag{10.5.26}$$

The product of the diffusion coefficients can usually be simplified as above, but α still must be known for an evaluation of k^0, because of the bracketed factor.

Quantitative information about heterogeneous charge-transfer kinetics obtained from ac polarographic data nearly always comes from the behavior of cot ϕ with po-

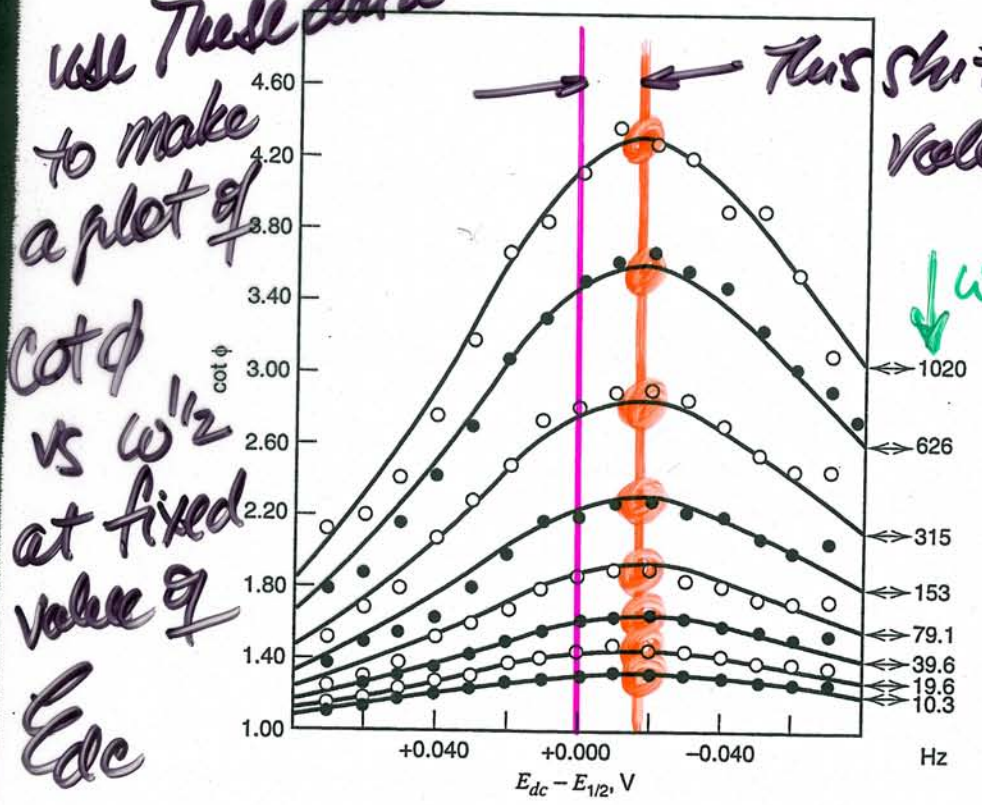

Figure 10.5.4 Dependence of the phase angle on E_{dc}. The system is 3.36 mM $TiCl_4$ in 0.200 M $H_2C_2O_4$. $\Delta E = 5.00$ mV, $T = 25$°C. Points are experimental; curves are predicted from experimental parameters by (10.5.23). [Reprinted with permission from D. E. Smith, *Anal. Chem.*, **35**, 610 (1963). Copyright 1963, American Chemical Society.]

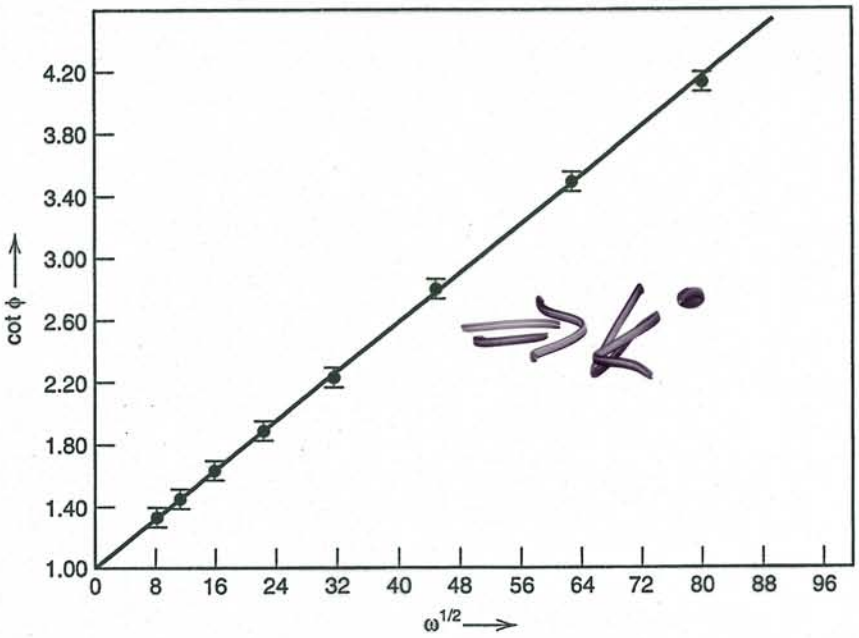

Figure 10.5.5 Plot of cot ϕ *vs.* $\omega^{1/2}$ for 3.36 mM $TiCl_4$ in 0.200 mM $H_2C_2O_4$. $E_{dc} = E_{1/2} = -0.290$ V *vs.* SCE. $\Delta E = 5.00$ mV, $T = 25°C$. [Reprinted with permission from D. E. Smith, *Anal. Chem.*, **35**, 610 (1963). Copyright 1963, American Chemical Society.]

tential and frequency, rather than from the heights, shapes, or positions of the polarograms. One reason for this favor toward cot ϕ is that many experimental variables do not have to be controlled closely or even be known. Among them are C_O^*, ΔE, and A. Freedom from knowing A can be a significant advantage. However, the most important reason for evaluating kinetics through cot ϕ is that relations (10.5.23) to (10.5.26) hold for any quasireversible or irreversible system. We have derived them for the situation in which dc reversibility applies; however, they hold regardless of that condition. Demonstrations of this point are available in the literature (3, 5). Their unconditional validity is a big asset, for it frees the experimenter from having to achieve special limiting conditions.

As in the previous section, we have assumed semi-infinite linear diffusion to a planar electrode throughout the mathematical discussion here. With a reversible dc process, the effects of sphericity and drop growth at the DME are exactly as discussed in Section 10.5.1. In general, the sphericity has a negligible impact and drop growth can be accommodated by using an explicit expression for A as a function of time. If dc reversibility does not apply, these factors influence the ac response in more complex ways (3, 5, 23). The reader is referred to the literature for details.

10.5.3 Linear Sweep ac Voltammetry at Stationary Electrodes (26, 27)

The previous two sections have dealt generally with ac voltammetry as recorded by the application of E_{dc} in successive steps and with a renewal of the diffusion layer between each step. The DME permits the most straightforward application of that technique, but other electrodes can be used if there is a means for stirring the solution between steps so that the diffusion layer is renewed. On the other hand, this requirement for periodic renewal is inconvenient when one wishes to use stationary electrodes, such as metal or carbon disks, or a hanging mercury drop. Then one prefers to apply E_{dc} as a ramp and to renew the diffusion layer only between scans. In this section, we will examine the expected ac voltammograms for reversible and quasireversible systems when E_{dc} is imposed as a linear sweep and we will compare them with the results obtained above for effectively constant E_{dc}.

The strategy is exactly that used before. The time domains associated with variations in E_{dc} and $\dot{E}_{ac}$ are assumed to differ greatly, so that the diffusional aspects of the two parts of the experiment can be uncoupled. This assumption will hold as long as the scan rate, v, is not too large compared to the ac frequency (28). More precisely, $dE_{dc}/dt = v$ should be much smaller than the amplitude of dE/dt, which is $\Delta E\omega$. Then, we can take the mean surface concentrations enforced by E_{dc} as effective bulk values for the ac perturbation, just as we did earlier. The current amplitude and phase angle then follow easily from the impedance properties.

(a) Reversible Systems

Let us consider a completely nernstian system $O + ne \rightleftarrows R$ in which R is initially absent. The starting potential for the linear sweep is rather positive with respect to $E^{0'}$, and the scan direction is negative. Semi-infinite linear diffusion is assumed. The mean surface concentrations, $C_O(0, t)_m$ and $C_R(0, t)_m$, are exactly those obtained in the analogous linear sweep experiment without superposed ac excitation, and they adhere always to the nernstian relation (10.5.2).

The arguments leading to equation 5.4.26 show that it applies without reference to the kinetic properties of the electrode reaction or the nature of the excitation waveform. For the present purpose, we can rewrite it as

$$D_O^{1/2} C_O(0, t)_m + D_R^{1/2} C_R(0, t)_m = C_O^* D_O^{1/2} \qquad (10.5.27)$$

Substitution from (10.5.2) then reveals that the mean surface concentrations are exactly as given in (10.5.3) and (10.5.4). In other words, those relations, which were derived earlier expressly for step excitation, have been shown here to apply regardless of the manner by which E_{dc} is attained.[12]

This conclusion is very important because it implies that all relations and all qualitative conclusions presented in Section 10.5.1 also hold for linear sweep ac voltammetry of reversible systems at a stationary electrode.

(b) Quasireversible Systems

An important special case of quasireversibility is the situation in which a one-step, one-electron process is sufficiently facile to maintain a reversible dc response, but not facile enough to show a negligible charge-transfer resistance, R_{ct}, to the ac perturbation.

If the dc response is nernstian, (10.5.2) and (10.5.27) hold, and the mean surface concentrations are given by (10.5.3) and (10.5.4), which are the same relations used in the treatment of Section 10.5.2. Thus, all of the equations and qualitative conclusions reached there for quasireversible ac polarograms also apply to the corresponding linear sweep ac voltammograms.

These precise parallels between linear sweep voltammetry and ac polarography no longer persist when there is a lack of dc reversibility. Treating such a case is more complex than the situations we have examined above because the mean surface concentrations are affected by the concentration profiles throughout the diffusion layer, and the surface values applicable at any potential generally depend on the waveform used to attain that potential (26, 27).

Linear sweep ac voltammetry allows precise, rapid kinetic measurements at solid electrodes. It can therefore be used to characterize these electrodes themselves, which

[12]Equation 10.5.27 is based on semi-infinite linear diffusion; hence this conclusion applies strictly only to planar electrodes. Work at an SMDE can be affected by sphericity (27).

may be of considerable interest, or to study electrode processes operating outside the working range of mercury or taking place in controlled environments where the DME or SMDE may be inconvenient.

10.5.4 Cyclic ac Voltammetry (26, 27)

Cyclic ac voltammetry is a simple extension of the linear sweep technique; one simply adds the reversal scan in E_{dc}. This technique retains the best features of two powerful, complementary methodologies. Conventional cyclic voltammetry is especially informative about the qualitative aspects of an electrode process. However, the response waveforms lend themselves poorly to quantitative evaluations of parameters. Cyclic ac voltammetry retains the diagnostic utility of conventional cyclic measurements, but it does so with an improved response function that permits quantitative evaluations as precise as those obtainable with the usual ac approaches. Although this technique is not widely employed, it can be a useful adjunct to dc cyclic voltammetry.

Treatments of cyclic ac voltammetry follow the familiar pattern. The ac and dc time scales are independently variable, but are assumed to differ markedly. Then a treatment of the dc aspect yields mean surface concentrations, which are used to calculate faradaic impedances that define the ac response by amplitude and phase angle. The electrode is assumed to be stationary and the solution is regarded as quiescent for the duration of the dc cycle.

(a) Reversible Systems

Cyclic ac voltammograms for completely nernstian systems are easy to predict on the basis of results from the previous section. The mean surface concentrations, $C_O(0, t)_m$ and $C_R(0, t)_m$, adhere to (10.5.3) and (10.5.4) unconditionally; hence at any potential they are the same for both the forward and reverse scans. The cyclic ac voltammogram should therefore show superimposed forward and reverse traces of ac current amplitude *vs.* E_{dc}. We expect a peak-shaped voltammogram that adheres in every way to the conclusions reached in Section 10.5.1 about the general ac voltammetric response to a reversible system at a planar electrode.

Figure 10.5.6 contrasts the responses from the ac and dc versions of cyclic voltammetry for the purely nernstian case. Kinetic reversibility is shown in the dc experiment by a

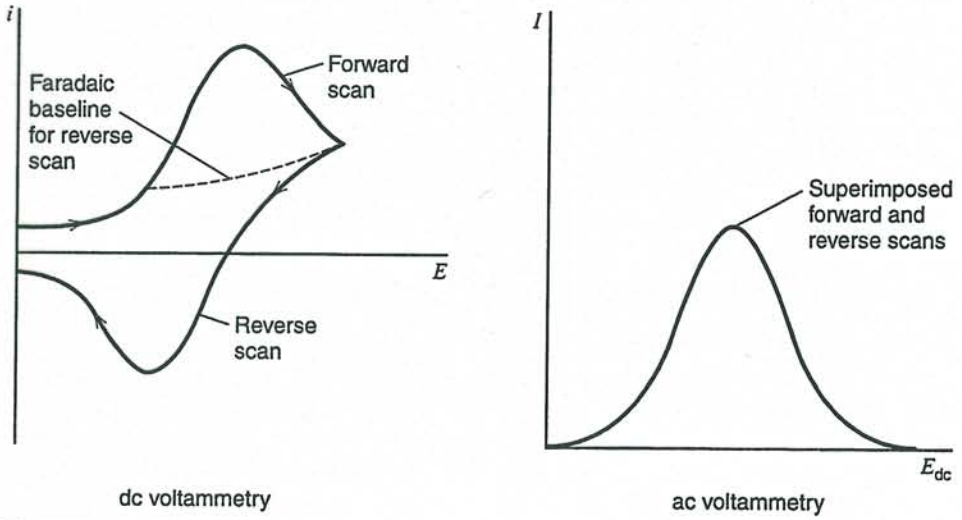

Figure 10.5.6 Comparison of response wave forms for cyclic dc and cyclic ac voltammetry for a reversible system.

peak separation near $60/n$ mV (25°C), regardless of scan rate. In the ac experiment, it is shown by identical forward and reverse peak potentials and by peak widths of $90/n$ mV (25°C), again regardless of scan rate. Chemical stability of the reduced form is demonstrated in the dc experiment by a peak current ratio, $|i_{p,r}/i_{p,f}|$, of unity. Given charge-transfer reversibility, the same thing is shown by the ratio of peak ac current amplitudes, $|I_{p,r}/I_{p,f}|$. The advantage in the ac experiment is that the reversal response has an obvious baseline for quantitative measurements, whereas the baseline for reversal currents in the dc response is more difficult to fix.

(b) Quasireversible Systems

It continues to be helpful to consider two separate cases of quasireversibility in a one-step, one-electron reaction. In both, a significant polarization resistance is manifested in the ac response, but in one instance the dc aspect appears reversible, whereas more generally it is not.

When dc reversibility obtains, a theoretical description is straightforward, because the mean surface concentrations still adhere to (10.5.3) and (10.5.4), regardless of the manner in which the dc potential determining them was established. Thus the forward and the reverse traces again overlap precisely. The shape of the peak and its position adhere to the relations derived in Section 10.5.2, where this kinetic case was considered in detail.

If dc reversibility does not hold, then the situation becomes quite complex. The mean surface concentrations at a given dc potential tend to depend on the way in which that potential is reached. In general, the surface concentrations at any E_{dc} will differ for forward and reverse scans; therefore we can expect the corresponding traces to differ in the voltammogram. In the dc cyclic voltammogram, increasingly sluggish electron transfer causes greater splitting of the forward and reverse peaks, because larger activation overpotentials are needed to motivate charge transfer. This splitting also manifests the fact that the surface concentrations undergo the transition from nearly pure O to virtually pure R in different potential regions for the two scan directions. Since the ac voltammogram shows a response only in the potential regions where such transition takes place, we can expect the cyclic ac voltammogram to show split peaks that are largely aligned with the forward and reverse dc voltammetric peaks. The standard potential $E^{0'}$ will lie between them. Some traces are shown in Figure 10.5.7.

Evidently there is a *crossover potential*, E_{co}, where both scans yield the same response. This potential can be rigorously shown to lie at

$$E_{co} = E_{1/2} + \frac{RT}{F} \ln \frac{\alpha}{1-\alpha} \tag{10.5.28}$$

regardless of the details of dc polarization (26). It serves as a convenient source for the evaluation of α. The amplitude and the phase angle of the ac response at E_{co} are totally independent of the dc process. In this respect E_{co} is a unique potential, and it may be the most convenient point for evaluating k^0 by a plot of cot ϕ *vs.* $\omega^{1/2}$. One can also derive k^0 from the separation of forward and reverse peaks in the ac voltammogram (26, 27).

Figure 10.5.8 is a display of an actual cyclic ac voltammogram for ferric acetylacetonate, $Fe(acac)_3$, in acetone containing 0.1 *M* tetraethylammonium perchlorate. Since this system is very nearly reversible to the dc process, the peak splitting is quite small, but easily detectable. The convenience of the waveform for quantitative work is also readily apparent.

cot ϕ vs $\omega^{1/2}$ at $E = E_{co} \Rightarrow k_0$

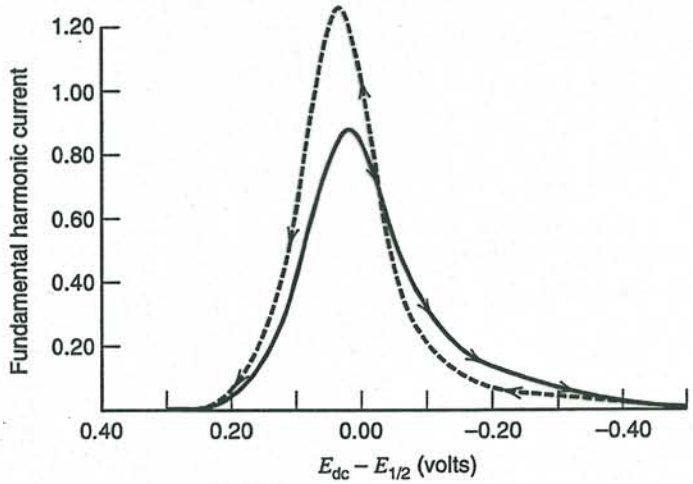

(*a*)

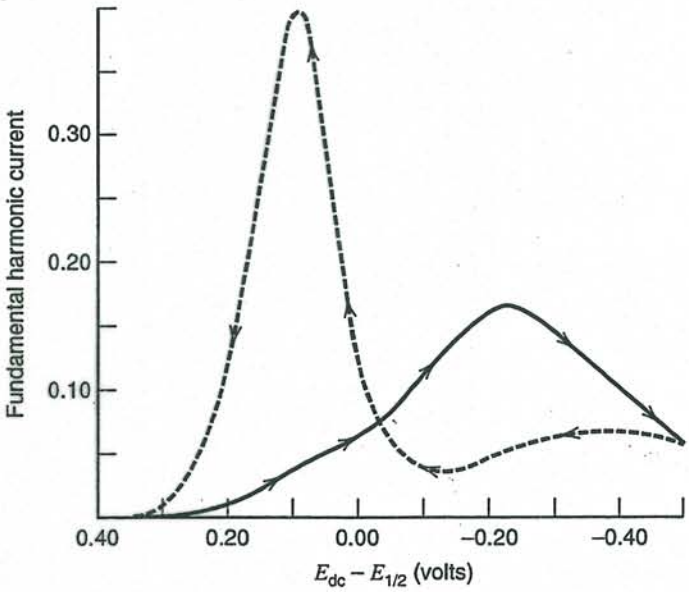

(*b*)

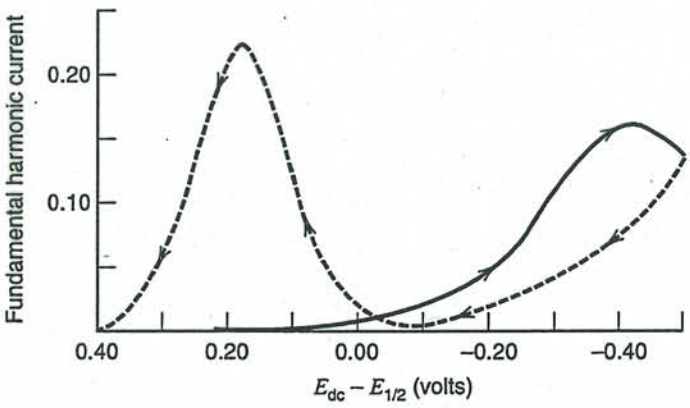

(*c*)

Figure 10.5.7 Predicted cyclic ac voltammograms for systems with non-nernstian dc behavior. (*a*) $k^0 = 4.4 \times 10^{-3}$ cm/s. (*b*) 4.4×10^{-4} cm/s, (*c*) 4.4×10^{-5} cm/s. For $\omega/2\pi = 400$ Hz, $n = 1$, $T = 298$ K, $A = 0.30$ cm^2, $C_O^* = 1.00$ mM, $D_O = D_R = 1.00 \times 10^{-5}$ cm^2/s, $v = 50$ mV/s, $\Delta E = 5.00$ mV, and $\alpha = 0.5$. Ac amplitude given as the normalized function $IRT/n^2F^2A(2\omega D_O)^{1/2}C_O^*\Delta E$. [Reprinted with permission from A. M. Bond et al., *Anal. Chem.*, **48**, 872 (1976). Copyright 1976, American Chemical Society.]

(c) Homogeneous Chemical Complications

Conventional cyclic voltammetry's greatest utility is in the diagnosis of electrode reactions involving chemical complications, and the ac variant is also useful in meeting this kind of problem. The ratio $I_{p,r}/I_{p,f}$ is a sensitive indicator of product stability, just as the dc voltammetric ratio $|i_{p,r}/i_{p,f}|$ is. However, the ac ratio is easier to measure precisely, and it lends itself well to quantitative evaluation of homogeneous rate constants.

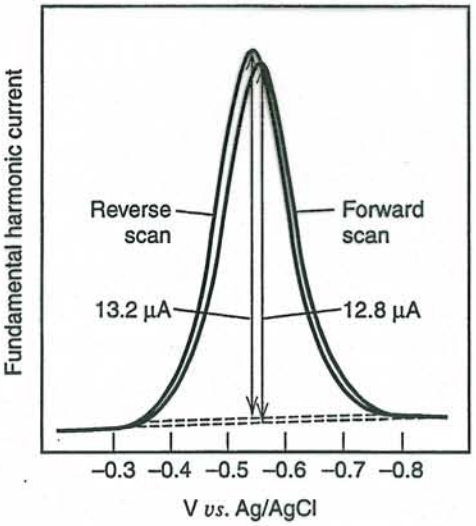

Figure 10.5.8 Cyclic ac voltammogram for 1.0 m*M* tris(acetylacetonate)Fe(III) in acetone containing 0.1 *M* tetraethylammonium perchlorate. Working electrode was a platinum disk. $T = 25°C$, $\Delta E = 5$ mV, $v = 100$ mV/s, $\omega/2\pi = 400$ Hz. (Reprinted with permission from A. M. Bond et al., *Anal. Chem.*, **48,** 872 (1976). Copyright 1976, American Chemical Society.]

Actual results (29) for a complicated case involving two interrelated couples are shown in Figure 10.5.9. The species of interest are the complexes $Mo(CO)_2(DPE)_2$, where DPE is diphenylphosphinoethane. These complexes exist in *cis* and *trans* forms which are oxidized at different potentials. Moreover, the oxidized *cis* form (cis^+) homogeneously converts to the oxidized *trans* form ($trans^+$). That is,

$$trans - e \rightleftarrows trans^+ \tag{10.5.29}$$

$$cis - e \rightleftarrows cis^+ \tag{10.5.30}$$

$$cis^+ \xrightarrow{k} trans^+ \tag{10.5.31}$$

The voltammograms of Figure 10.5.9 were obtained with a solution initially containing only *cis*-$Mo(CO)_2(DPE)_2$. Close study of these curves shows that the diagnostic utility of the dc voltammogram is preserved in the ac traces. In fact, it may be a bit more obvious from the ac curves that cis^+ does not decay completely during the experiment.

▶ 10.6 HIGHER HARMONICS (3, 5, 7)

To this point, we have found that excitation of an electrochemical system by a signal, $E_{ac} = \Delta E \sin \omega t$ produces a sinusoidal current response at the same frequency. That result rests on the fact that only the linearized current-potential relation has been used. The remaining terms in the Taylor expansion of current *vs.* potential were dropped (Section 3.4.6). If we include them, we find that the current response is not purely sinusoidal, but instead comprises a whole series of sinusoidal signals at ω, 2ω, 3ω, . . . , which are summed together. The current component at 2ω is the *second harmonic* response, while that at 3ω is the *third harmonic*, etc.[13] These higher harmonics arise from *curvature* in the *i-E* relation.

Each harmonic is individually detectable by circuits employing tuned amplifiers or lock-in amplifiers. The most common arrangement is a variant of ac voltammetry, as might be implemented according to Figure 10.6.1. The cell is excited exactly as in ac voltammetry, but the lock-in amplifier is tuned to 2ω and detects only that current contribution. The result is a trace of $I(2\omega)$ *vs.* E_{dc}.

[13]This nomenclature differs from that used in electrical engineering, where the signal at ω is the *fundamental* and that at 2ω is the *first harmonic*. We will adhere to the usual electrochemical usage.

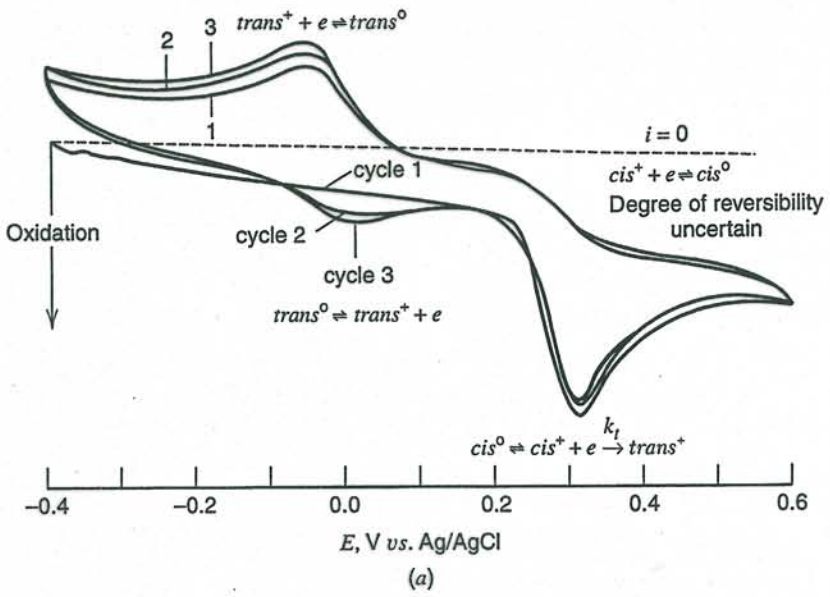

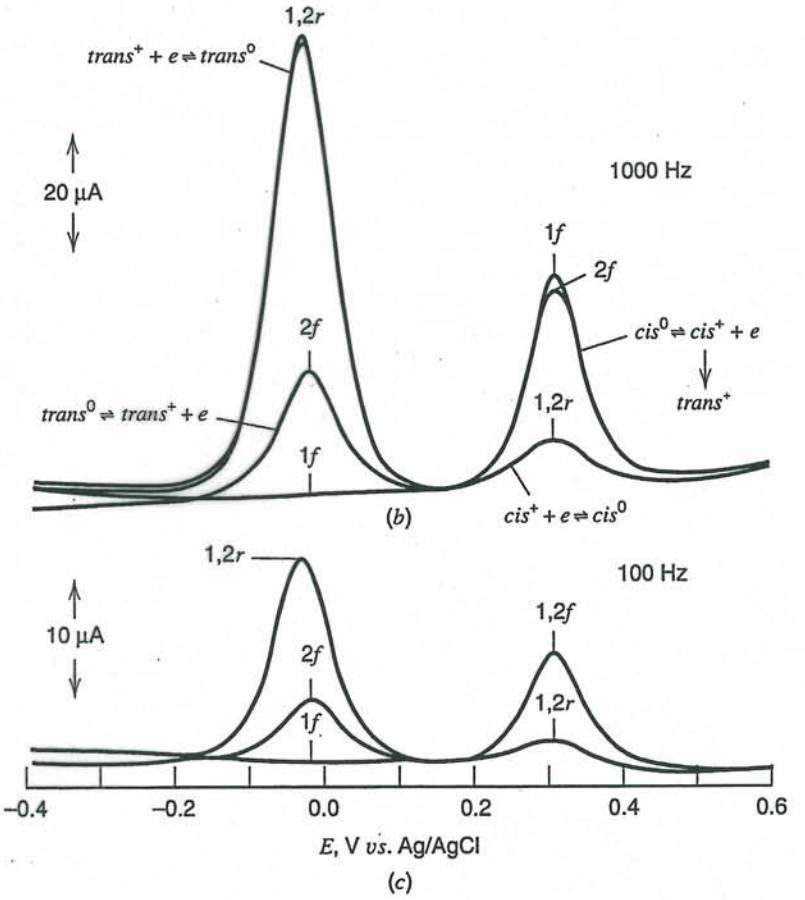

Figure 10.5.9 (*a*) Cyclic dc voltammograms of *cis*-$Mo(CO)_2(DPE)_2$ in acetone containing 0.1 *M* tetraethylammonium perchlorate. Solution was saturated with the molybdenum species. $v = 100$ mV/s. Anodic currents are plotted downward. (*b*, *c*) Cyclic ac voltammograms at the same platinum wire electrode. $v = 100$ mV/s, $\Delta E = 5$ mV. *Notation*: *nf*, scan number *n* in forward direction; *nr*, scan number *n* in reverse direction. [From A. M. Bond, *J. Electroanal. Chem.*, **50**, 285 (1974), with permission.]

An exact treatment of higher harmonic response is straightforward, but it is rather lengthy, so we will leave it to the specialized literature. Instead we will follow an intuitive approach that will reveal most of the distinctive features of second-harmonic ac voltammetry. For simplicity, we consider only a reversible system in which R is initially absent.

The mean surface concentrations, $C_O(0, t)_m$ and $C_R(0, t)_m$, are set by the value of E_{dc} and are given by (10.5.3) and (10.5.4). Figure 10.6.2 is a graphical display of $C_R(0, t)_m$. The ac response is determined by the way in which $\dot{E}_{ac}$ causes small perturbations in the surface concentrations about those mean values. The fundamental (or first-harmonic)

note These are calculated for which $\alpha = 0.5 \Rightarrow E_{co} = E_{1/2}$!

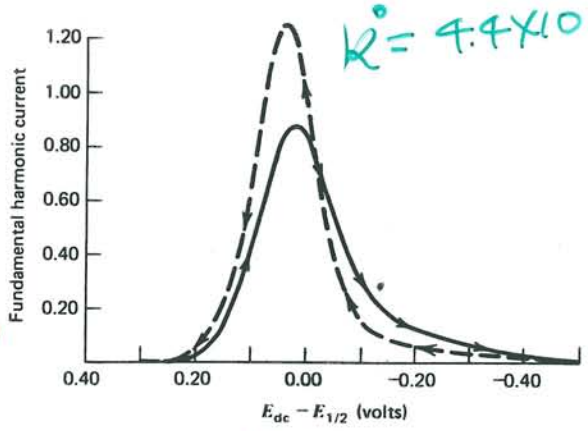

k° decreases

faster kinetics

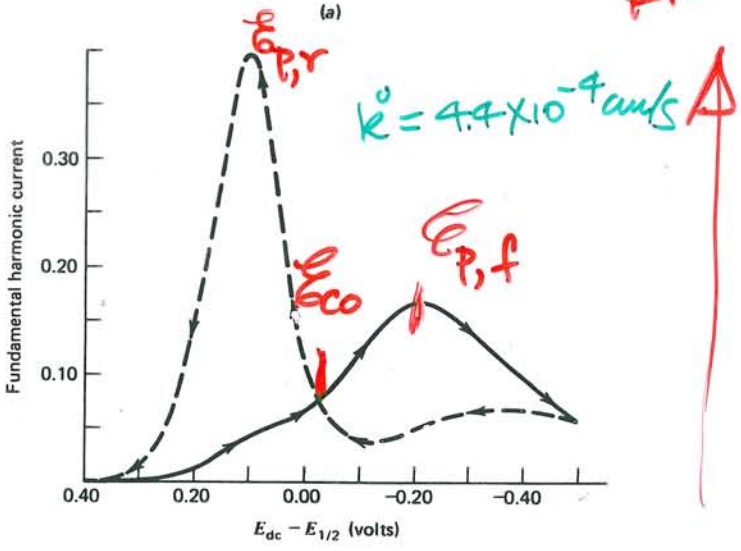

$E_{p,f} < E^{0'} < E_{p,r}$

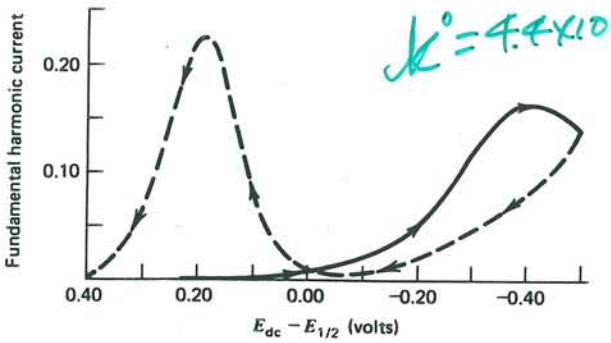

E_{co} crossover potential

$E_{co} = E_{1/2} + \frac{RT}{nF} \ln \frac{\alpha}{1-\alpha}$

rxn or nature of dc polarization

Figure 9.4.7

Predicted cyclic ac voltammograms for systems with nonnernstian dc behavior. (*a*) $k^0 = 4.4 \times 10^{-3}$ cm/sec. (*b*) 4.4×10^{-4} cm/sec, (*c*) 4.4×10^{-5} cm/sec. For $\omega/2\pi = 400$ Hz, $n = 1$, $T = 298$ K, $A = 0.30$ cm^2, $C_O^* = 1.00$ mM, $D_O = D_R = 1.00 \times 10^{-5}$ cm^2/sec, $v = 50$ mV/sec, $\Delta E = 5.00$ mV, and $\alpha = 0.5$. Ac amplitude given as the normalized function $RTI/n^2F^2A(2\omega D_O)^{1/2}C_O^*\Delta E$. [Reprinted with permission from A. M. Bond et al., *Anal. Chem.*, **48**, 872 (1976). Copyright 1976, American Chemical Society.]

$\therefore I_k \phi$ measured at E_{co} also rel. to dc process

$\therefore$ take $(\cot\phi)_{E_{co}}$ vs $\omega^{1/2} \Rightarrow k^\circ$

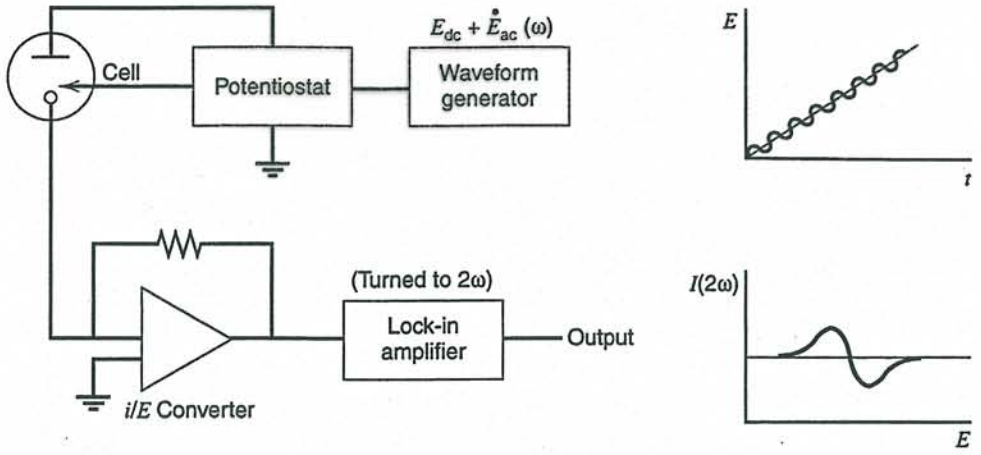

Figure 10.6.1 Block diagram of apparatus for recording a second-harmonic ac voltammogram.

component is controlled essentially by the linear elements of variation, which are the slopes $\partial C_O(0, t)_m/\partial E$ and $\partial C_R(0, t)_m/\partial E$. The higher harmonics reflect curvature; hence they are sensitive to the second and higher derivatives. Comprehension of this point allows us to predict the general shape of the second harmonic response.

Consider potentials E_1, E_3, and E_5 in Figure 10.6.2. Since they have the common feature that the curvature in $C_O(0, t)_m$ and $C_R(0, t)_m$ is zero, there is no second harmonic current. Of course, E_1 and E_5 lie at extreme values where there is also no fundamental response; but E_3 lies at the inflection point $E = E_{1/2}$, where the fundamental response is greatest. The potentials E_2 and E_4 are at points of maximum curvature, hence they should be the potentials of peak second-harmonic current. If we detect only the magnitude $I(2\omega)$, then we can expect a double-peaked voltammogram like that of Figure 10.6.3*a*.

Let us note, though, that the curvature at E_2 is opposite to that at E_4. This difference implies that the second harmonic component undergoes a 180° phase shift when E_{dc} passes through the null point at $E_{1/2}$. Phase-sensitive detection of $I(2\omega)$ at a fixed phase angle will therefore produce a sign inversion at $E_{1/2}$. Figure 10.6.3*b* is an example. In general, a nernstian reaction detected at any phase angle will show positive and negative lobes that are symmetrical around the point of intersection with the potential axis. The dc potential corresponding to this intersection is $E_{1/2}$ at all phase angles (Figure 10.6.4) (30). The responses at a given phase angle compared to the same phase angle plus 90° are symmetrical around the potential axis only at 0° and 180°.

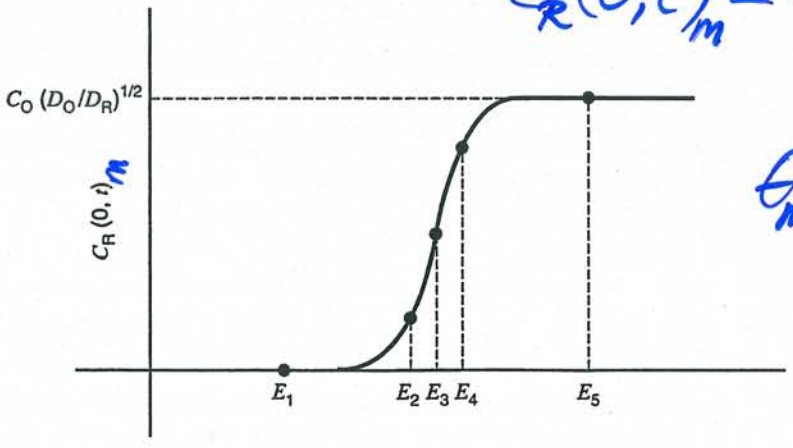

Figure 10.6.2 Dependence of the surface concentration of species R on the electrode potential.

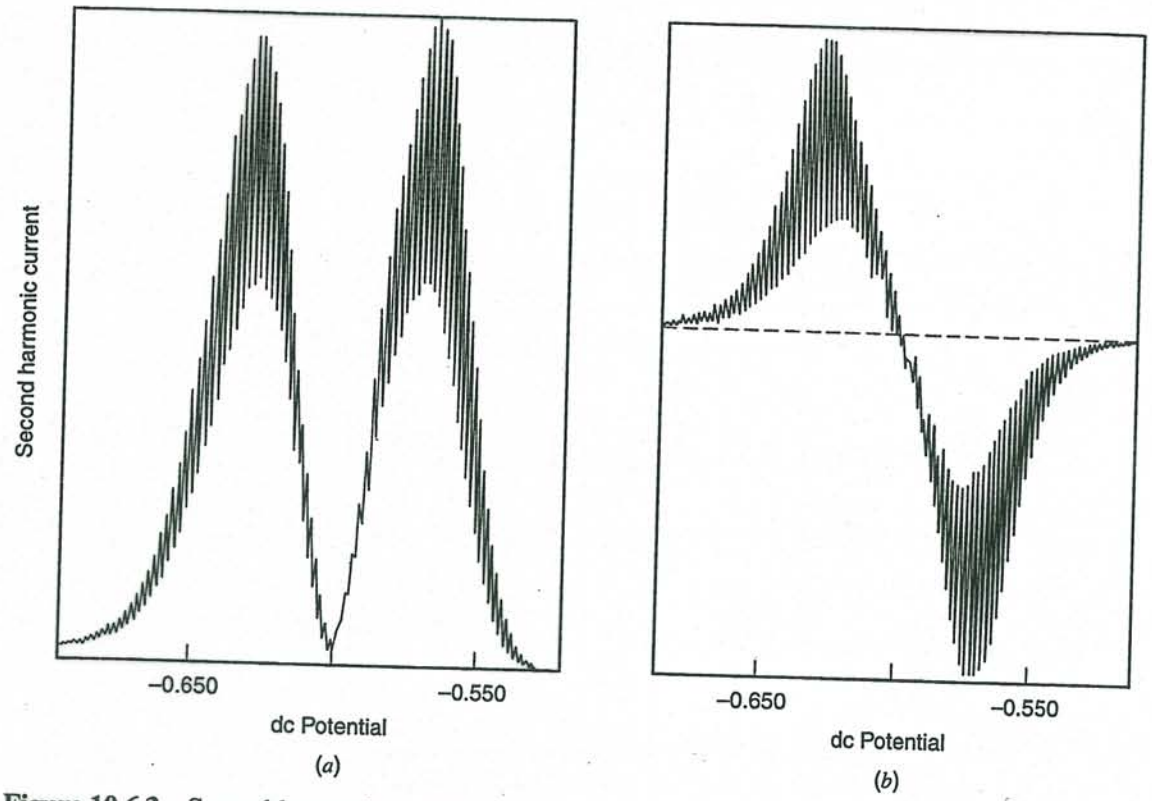

Figure 10.6.3 Second-harmonic ac polarograms for 3 mM Cd^{2+} in 1.0 M Na_2SO_4. $\omega/2\pi = 80$ Hz, $\Delta E = 5$ mV. (*a*) Total ac amplitude *vs.* E_{dc} (*vs.* SCE). (*b*) Phase-selective polarogram showing the ac amplitude at 0° with respect to $\dot{E}_{ac}$. [Reprinted with permission from D. E. Smith, *Anal. Chem.*, **35**, 1811 (1963). Copyright 1963, American Chemical Society.]

$$a = \frac{nf}{RT}(E_{dc} - E_{1/2})$$

The exact solution of this problem is

$$i(2\omega) = \frac{n^3F^3AC_O^*(2\omega D_O)^{1/2}\Delta E^2 \sinh(a/2)}{16R^2T^2\cosh^3(a/2)} \sin\left(2\omega t - \frac{\pi}{4}\right) \qquad (10.6.1)$$

where a is defined in (10.5.7). This equation embodies the proportionalities of C_O^*, $\omega^{1/2}$, and $D_O^{1/2}$ that we have come to expect of diffusion-controlled processes. The phase angle of 45° has the same origin. Note, however, that $i(2\omega)$ is proportional to ΔE^2. This dependence manifests the greater importance of nonlinear effects for perturbations of larger magnitude. The two peak potentials are located at $E_{dc} = E_{1/2} \pm 34/n$ mV at 25°C.

Second-harmonic techniques are useful for analytical purposes and for the quantitative evaluation of heterogeneous kinetic parameters (3, 5, 7, 31). Applications in both areas are attractive, because the double-layer capacitance is a rather linear element and contributes very small second-harmonic currents. Second-harmonic voltammetry has also been used to investigate electrode reactions with coupled homogeneous reactions. In particular, it has been proposed as a method of obtaining the standard potential for a reaction even in the presence of a fast following reaction that consumes the product. However, the fact that a second harmonic response is obtained does not imply that the effects of the following reaction have been eliminated, because one will obtain such a response from simple modulation of the (nonlinear) dc wave. To extract a valid standard potential, one must insure that the observed response shows all of the characteristics of a nernstian process (see Figure 10.6.4) (30). Harmonics above the second have been examined briefly, but have not been applied to any great extent.

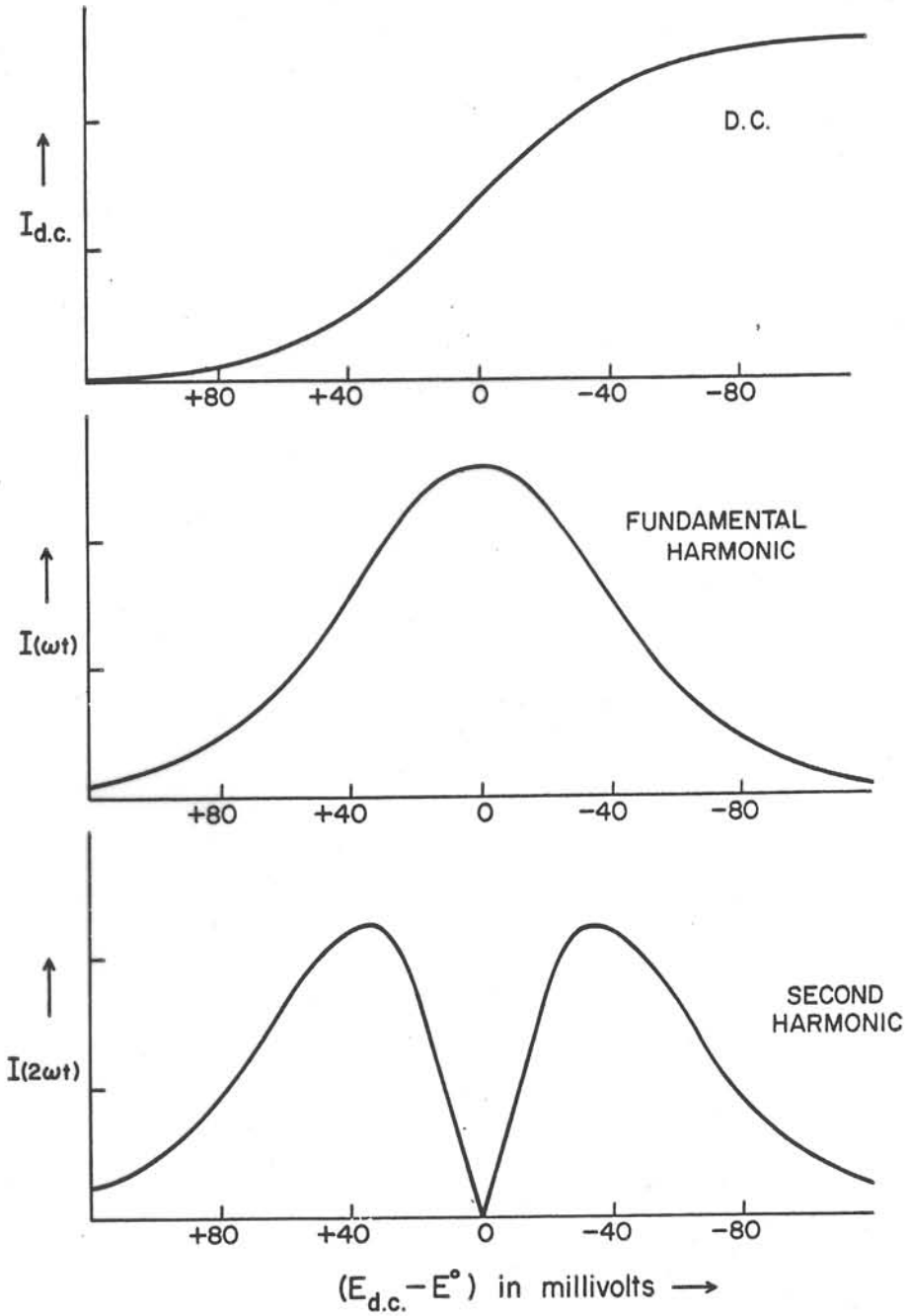

FIGURE 2. Dc, fundamental, and second harmonic ac polarograms with a diffusion-controlled system. (AC polarograms depicted are total current amplitude polarograms–i.e., "conventional" fundamental and second harmonic polarograms. Smooth curves represent currents at the ends of the drop lives–i.e., drop oscillations are not shown). (Reprinted from reference 87 by courtesy of M. Dekker, Inc.)

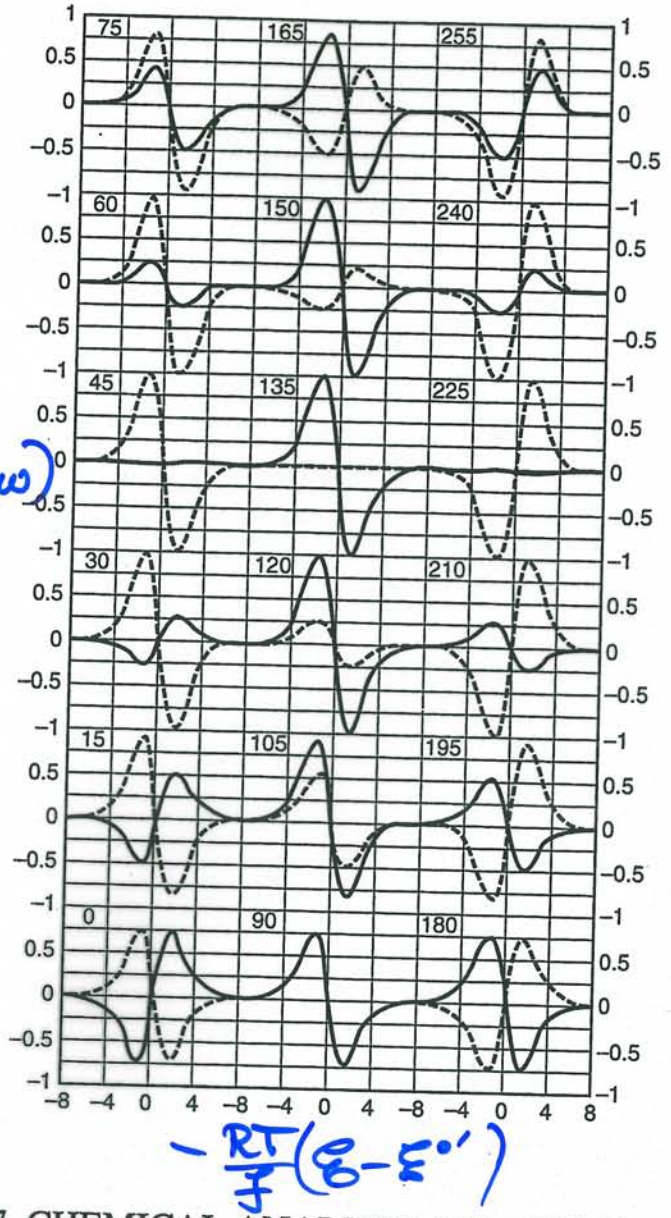

Figure 10.6.4 Theoretical second-harmonic responses for a nernstian reaction as a function of phase angle (solid line) and at that same angle plus 90° (dashed line). The horizontal axis is $-(RT/F)(E - E^{0'})$ and the vertical axis is the second harmonic current normalized to the maximum response. The calculation assumes $D_O = D_R$ and $\Delta E = 25$ mV. [Reprinted with permission from C. P. Andrieux, P. Hapiot, J. Pinson, and J.-M. Savéant, *J. Am. Chem. Soc.*, **115**, 7783 (1993). Copyright 1993, American Chemical Society.]

▶ 10.7 CHEMICAL ANALYSIS BY AC VOLTAMMETRY

Both fundamental and second-harmonic ac voltammetry are attractive as analytical techniques because they offer good sensitivities. Detection limits for the polarographic variants can reach the order of 10^{-7} *M*. Such performance is possible because both methods have ready means for discrimination against capacitive currents (5, 7).

In the fundamental mode, one employs phase-sensitive detection to measure the current component in phase with the excitation signal $\dot{E}_{ac}$. We noted in Section 10.3 that there is generally a faradaic contribution to this current, and Figure 10.7.1 reinforces the idea pictorially. In contrast, the charging current is ideally 90° out of phase with $\dot{E}_{ac}$, since it passes through a purely capacitive element. It therefore has no projection in phase with $\dot{E}_{ac}$. Thus we expect the current in phase to be purely faradaic, whereas the current at 90° (the *quadrature current*) contains a second faradaic component plus the nonfaradaic contribution. By taking the current in phase as the analytical signal, we discriminate effectively against the capacitive interference.

The limitation to this scheme is imposed partially by the uncompensated resistance, R_Ω. Since the charging current passes through R_Ω and C_d in series, this current does not lead $\dot{E}_{ac}$ by exactly 90°, but instead by some smaller angle. Thus the current in phase with

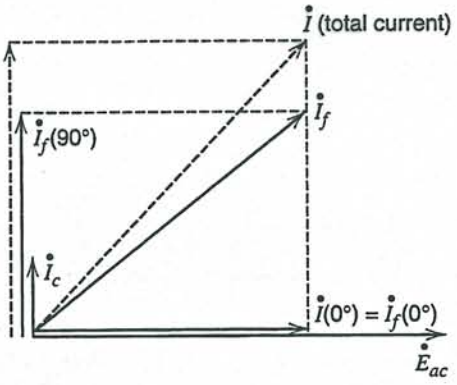

Figure 10.7.1 Phasor diagram showing the relationships between the faradaic ($\dot{I}_f$) and capacitive ($\dot{I}_c$) components to the total current ($\dot{I}$). Note that $\dot{I}_f$ has a component along $\dot{E}_{ac}$, whereas $\dot{I}_c$ does not.

$\dot{E}_{ac}$ must contain a nonfaradaic element, which becomes significant to the measurement as the analyte concentration drops.

Second-harmonic ac voltammetry gains its freedom from nonfaradaic interference from the relative linearity of the double-layer capacitance as a circuit element. There is consequently only a very small second-harmonic capacitive current, although it too can become important at low analyte concentrations.

The shapes of the voltammograms generated in ac measurements are convenient for analysis. Detection of the fundamental current produces a peak whose height is readily measured and is linear with concentration. Phase-selective second-harmonic voltammetry gives the second-derivative waveform of Figure 10.6.3*b*. The peak-to-peak amplitude is linear with concentration and can be read with high precision. It is also relatively unaffected by the background signal (31).

Analytical measurements are usually carried out at excitation frequencies ranging from 10 Hz to 1 kHz, although Bond has noted that frequencies in the upper part of this range allow fuller exploitation of certain aspects of selectivity that are unique to ac methods (32). Their basis is the discrimination against the much smaller response from irreversible systems.

For example, one can effect a significant saving in analysis time by working directly with aerated solutions. Since the reduction of oxygen in most aqueous solutions is irreversible, it does not interfere with determinations made by ac voltammetry. Also, one can often control the medium in order to introduce selectivity toward certain analytes. Transition metals are especially susceptible to such manipulation because their electrode kinetics are often strongly affected by coordination. Thus, one can enhance their ac responses or mask them from the voltammogram by intelligent choice of electrolyte composition. Since many supporting electrolytes show irreversible reductions, there is considerable freedom to manipulate composition without introducing serious interferences.

▶ 10.8 INSTRUMENTATION FOR ELECTROCHEMICAL IMPEDANCE SPECTROSCOPY

Impedance measurements can be made in either the frequency domain with a frequency response analyzer (FRA) or in the time domain using Fourier transformation with a spectrum analyzer. Commercial instrumentation and software is available for these measurements and the analysis of the data.

10.8.1 Frequency Domain Measurements (8, 9, 11)

The basic principles of a FRA in measuring the impedance of an electrochemical cell are shown in the block diagram in Figure 10.8.1. The FRA generates a signal $e(t) =$

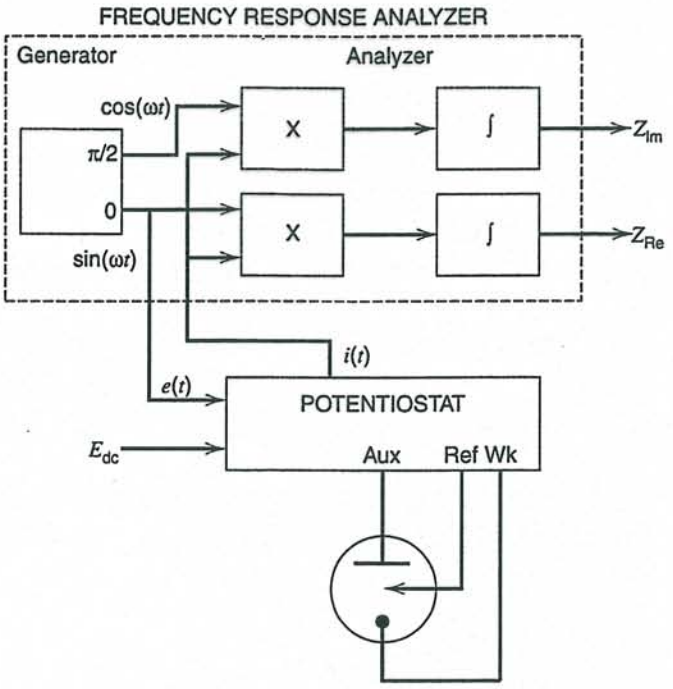

Solartron

Figure 10.8.1 System for measuring the impedance of an electrochemical cell based on a frequency response analyzer (FRA).

$\Delta E \sin(\omega t)$ which is fed to the potentiostat. This is added to E_{dc} and fed to the cell. In practice, care must be taken to avoid phase and amplitude errors that can be introduced by the potentiostat, particularly at higher frequencies. The resulting current, $i(t)$, or more precisely a voltage signal proportional to the current, is fed to the analyzer, mixed with the input signal, and integrated over several signal periods to yield signals that are proportional to the real and imaginary parts of the impedance (or equivalently the magnitude and phase angle of the impedance). Commercial frequency response analyzers are available with a frequency range of 10 μHz to 20 MHz. Means are provided for sweeping the frequency over a given range and storing the resulting impedance data.

10.8.2 Time Domain Measurements and Fourier Transform Analysis

In time domain measurements, the electrochemical system is subjected to a potential variation that is the resultant of many frequencies, like a pulse or white noise signal, and the time-dependent current from the cell is recorded. The stimulus and the response can be converted via Fourier transform methods to spectral representations of amplitude and phase angle *vs.* frequency, from which the desired impedance can be computed as a function of frequency.

Applications of the Fourier transformation to spectroscopy have become widespread and are familiar to most chemists. They are attractive because they allow one to interpret experiments in which several different excitation signals are applied to a chemical system at the same time. The responses to those signals are superimposed on each other, but the Fourier transformation provides a means for resolving them. This capacity for simultaneous measurement is sometimes called the *multiplex advantage* of transform methods, and it is of great importance to applications in electrochemistry (see also Section A.6).

By now it should be clear that fully characterizing an electrochemical process by impedance methods can be a tedious operation, because one requires information at a set of frequencies ranging over 2 to 3 decades and at a set of potentials ranging over $E^{0'} \pm 100$ mV. For example, the data in Figure 10.5.4 alone required eight ac polarograms, each scanned with the tuned circuitry set to a different frequency and each having the in-phase

and quadrature currents separately recorded. Not only does the operation require time and patience, but also there is the danger that the surface properties of the system will change during the procedure.

One can employ an alternative in which excitation signals of all desired frequencies are brought to bear at once (33–37). The idea is outlined in Figure 10.8.2, which shows that the excitation signal, E_{ac}, is actually a noise waveform, rather than a pure sinusoid. As before, E_{ac} is superimposed on a virtually constant level, E_{dc}. Of course E_{ac} will stimulate a current flow showing related "noisy" variations. During a brief period, lasting perhaps 100 ms, the output of the follower and the output of the i/E converter are digitized simultaneously and stored in a computer's memory.

Fourier transformation of these two transients gives the distribution of harmonics that comprise the signals. One therefore knows the amplitude of excitation and the corresponding amplitude and phase angle for current flow at each frequency in the Fourier distributions. In other words, one has the faradaic impedance as a function of ω for the potential E_{dc}. All of this can be obtained with a 100-ms period of data acquisition even on a single drop at a DME; hence it is feasible to repeat the whole procedure, perhaps on subsequent drops, so that more precise ensemble-averaged results are obtained. Changing E_{dc} for each complete set of measurements then provides the potential distribution, that is, $\dot{E}(E_{dc}, \omega)$.

In practice, it is desirable to have a special kind of excitation noise. Smith and his coworkers (34, 36) demonstrated that the best choice is an odd-harmonic, phase-varying pseudorandom white noise of the type displayed in Figure 10.8.3. This noise is the superposition of signals at several frequencies (15 in the example), all of which are odd harmonics of the lowest frequency. The choice of odd harmonics ensures that second-

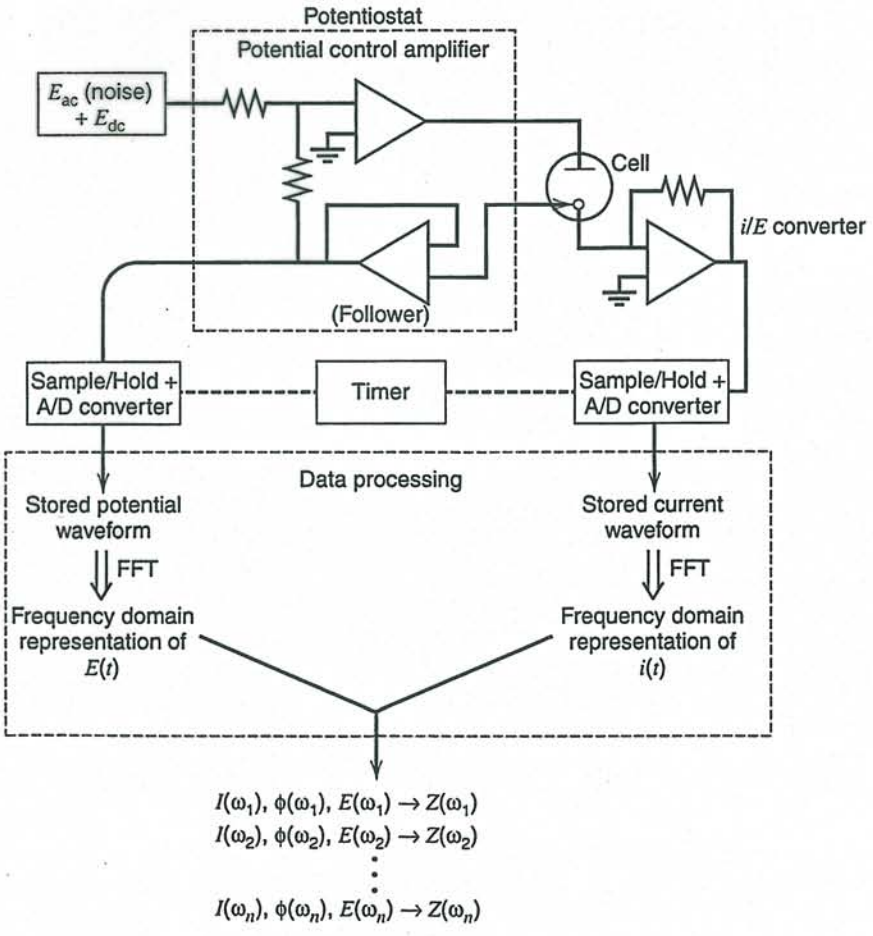

Figure 10.8.2 Schematic diagram showing apparatus and data-processing steps used in on-line Fourier analysis of ac voltammetric data. The steps in the large dashed box are carried out in a computer, usually by the fast Fourier transform (FFT) algorithm (see Section A.6).

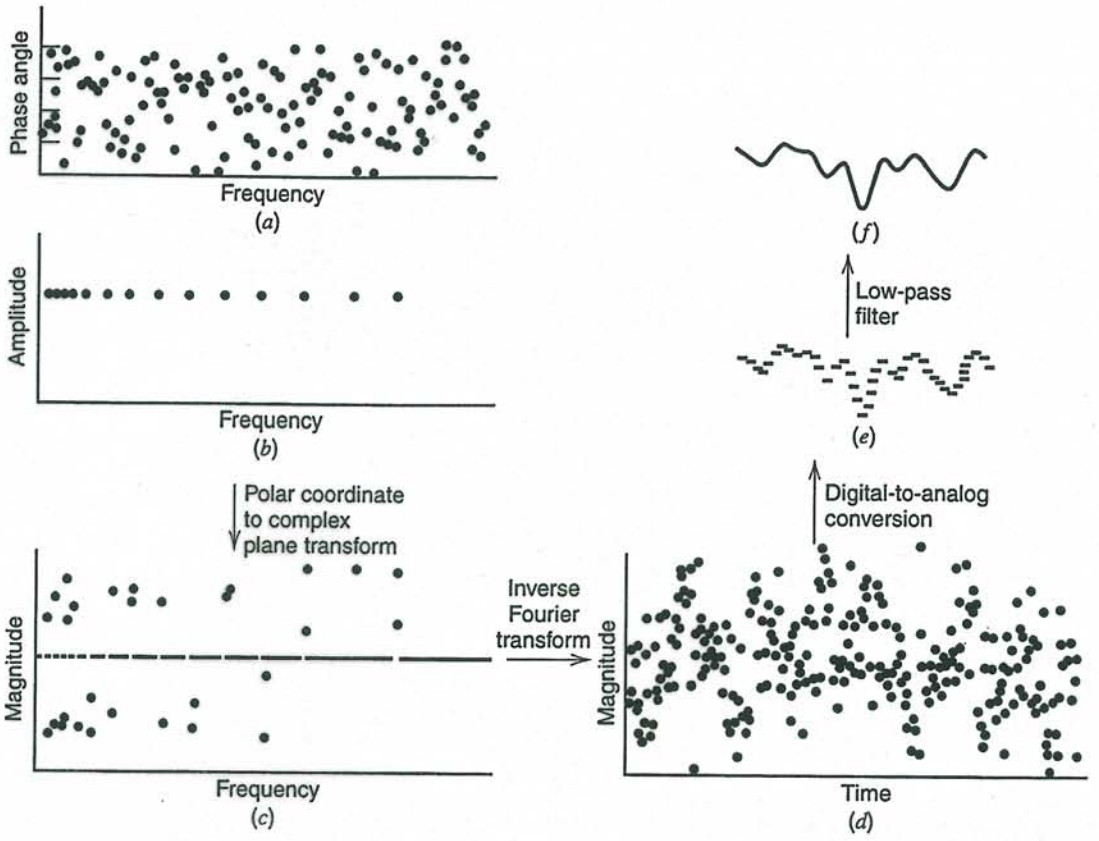

Figure 10.8.3 Procedure for generating a complex excitation waveform. (*b*) Shows the chosen amplitudes for the various frequencies and (*a*) shows randomized phase angles. In (*c*) there is a complex plane representation of the arrays in (*a*) and (*b*). (*d*) The time domain representation, which is subjected to digital/analog conversion to produce (*e*); and in turn, low-pass filtering yields (*f*). Only a small part of the waveform period is shown in (*e*) and (*f*). [From S. C. Creason et al., *J. Electroanal. Chem.*, **47**, 9 (1973), with permission.]

harmonic components will not appear in the currents measured for the 15 fundamental frequencies. The amplitudes of the 15 excitation frequencies are equal ("white" noise) so that each carries equal weight; and their phase angles are randomized, so that the total excitation signal does not show large swings in amplitude.

Despite these demands, it is easy to generate such special noise by inverting the scheme for signal analysis. The method is sketched in Figure 10.8.3. One starts with the amplitude and phase-angle arrays, which have been tailored in the computer according to specifications. These are transformed into the complex plane; then the fast inverse Fourier transform is invoked, so that one obtains a digital representation of the time-domain noise signal. Feeding these numbers sequentially to a digital-to-analog (D/A) converter at the desired rate yields an analog signal, which is filtered and sent to the potentiostat's input. Repeated passage through the D/A conversion and filtering steps yields a repetitive excitation waveform, which is applied continuously until a single measurement pass is completed. A new waveform with different randomized phase angles is generated for the next pass, and so on.

The quality of the results from these experiments is illustrated in Figure 10.8.4 by data for the $Cr(CN)_6^{3-}/Cr(CN)_6^{4-}$ couple. The run represents an average of 64 measurement passes, each taken on one DME drop and each requiring ~2 s for acquisition and reduction of the data. Compare the range of cot ϕ and its precision in this figure with that of the good manual data in Figure 10.5.5.

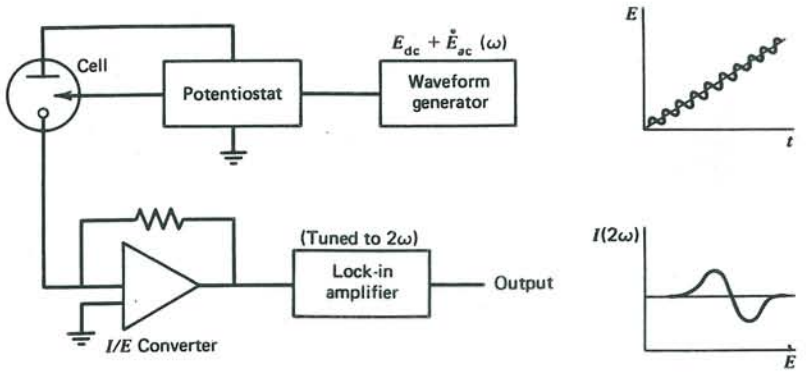

Figure 9.6.1
Block diagram of apparatus for recording a second-harmonic ac voltammogram.

ac voltammetry. For simplicity, we consider only a reversible system in which R is initially absent.

The mean surface concentrations $C_O(0, t)_m$ and $C_R(0, t)_m$ are set by the value of E_{dc} and are given by (9.4.3) and (9.4.4). Figure 9.6.2 is a graphical display of $C_R(0, t)_m$. The ac response is determined by the way in which $\dot{E}_{ac}$ causes small perturbations in the surface concentrations about those mean values. The fundamental (or first harmonic) component is controlled essentially by the linear elements of variation, which are the slopes $\partial C_O(0, t)_m/\partial E$ and $\partial C_R(0, t)_m/\partial E$. The higher harmonics reflect curvature; hence they are sensitive to the second and higher derivatives. Comprehension of this point allows us to predict the general shape of the second harmonic response.

Consider potentials E_1, E_3, and E_5 in Figure 9.6.2. Since they have the common feature that the curvature in $C_O(0, t)_m$ and $C_R(0, t)_m$ is zero, there is no second harmonic current. Of course, E_1 and E_5 lie at extreme values where there is also no fundamental response; but E_3 lies at the inflection point $E = E_{1/2}$, where the fundamental response is greatest. The potentials E_2 and E_4 are at points of maximum curvature, hence they should be the potentials of peak second-harmonic current. If we detect only the magnitude $I(2\omega)$, then we can expect a double-peaked voltammogram like that of Figure 9.6.3*a*.

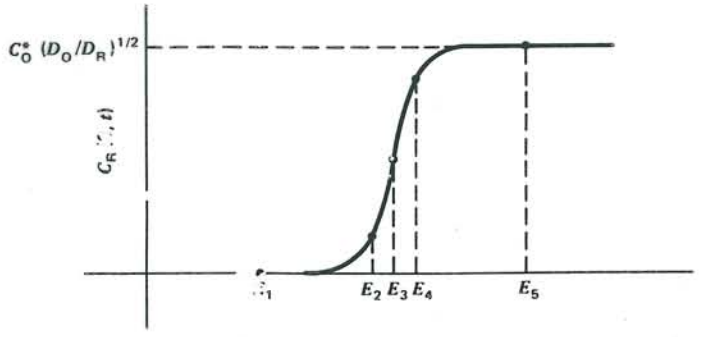

Figure 9.6.2
Dependence of the surface concentration of species R on the electrode potential.

recall $E = E(i, C_O(0,t), C_R(0,t))$

curvature ↔ nonlinearity in i-E characteristic

$cis^{\circ} \rightarrow cis^{+} + e \quad E_1^{\circ\prime}$

$trans^{\circ} \rightarrow trans^{+} + e \quad E_2^{\circ\prime}$

$cis^{+} \rightarrow trans^{+}$

only cis present initially

$\left|\frac{i_{p,r}}{i_{p,f}}\right|$ indicates product Stability

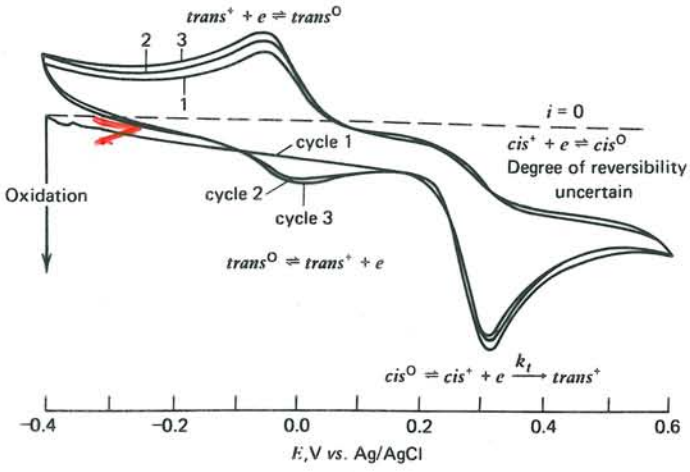

$\frac{I_{p,r}}{I_{p,f}}$ indicates Product Stability

range of $I_p \propto \omega^{1/2}$

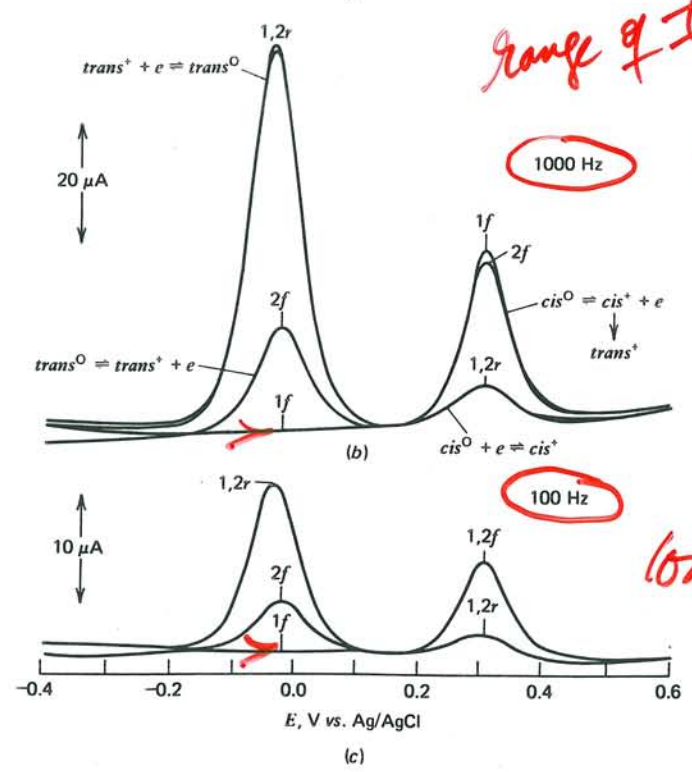

ac gives flatter baseline

Figure 9.4.9

(*a*) Cyclic dc voltammograms of *cis*-$Mo(CO)_2(DPE)_2$ in acetone containing 0.1 *M* tetraethylammonium perchlorate. Solution was saturated with the molybdenum species. v = 100 mV/sec. (*b*, *c*) Cyclic ac voltammograms at the same platinum wire electrode. v = 100 mV/sec, ΔE = 5 mV. *Notation*: *nf*, scan number *n* in forward direction; *nr*, scan number *n* in reverse direction. Anodic currents are plotted downward. [From A. M. Bond, *J. Electroanal. Chem.*, **50**, 285 (1974), with permission.]

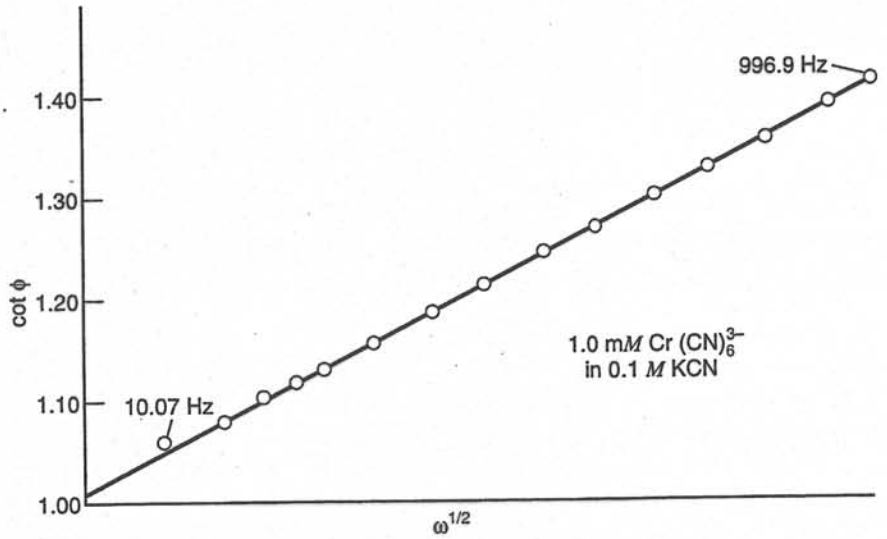

Figure 10.8.4 cot ϕ *vs.* $\omega^{1/2}$ for the chromicyanide system. Data were obtained with a phase-varying, 15-component, odd-harmonic complex waveform. [From S. C. Creason et al., *J. Electroanal. Chem.*, **47**, 9 (1973), with permission.]

The ability of the Fourier transformation to dissect a complex waveform into its components can also be used to obtain higher harmonics (35, 36). In this case, one might excite with a pure sinusoid at frequency ω and examine the transformed current waveform. It will provide the dc current, the current and phase angle at the fundamental frequency ω, as well as amplitudes and phase angles of the higher harmonics. Repeating measurement passes at various values of E_{dc} allows one to trace out all of the corresponding voltammograms from data obtained on a single run.

In addition to its applications as an integral component of the measurement process, the Fourier transformation can be extremely useful for various signal-conditioning operations, such as smoothing, convolution, and correlation. Smith et al. have discussed the possibilities in this area at some length, and the interested reader is urged to pursue their discussions (36, 38).

▶ 10.9 ANALYSIS OF DATA IN THE LAPLACE PLANE

There are many instances in electrochemistry when we find it very difficult to obtain an explicit relationship between current, potential, and time. Either the system itself is intrinsically complex (e.g., a quasireversible charge transfer involving adsorbed and diffusing reactant species) or the experimental conditions are less than ideal (e.g., step experiments carried out on a time domain so short that the rise time of the potentiostat is not negligible). It is usually true in these and other cases that much simpler relationships exist in the Laplace domain between the perturbations and the observables. Thus it can be useful to transform the data and carry out the analysis in transform space (39–42).

As an example, consider the case of potential steps applied to a one-step, one-electron system containing only electroactive species O, which is reduced quasireversibly. In Section 5.5.1, we treated this case conventionally and found that the current-time function was

$$i = FAk_f C_O^* \exp(H^2 t) \operatorname{erfc}(Ht^{1/2}) \tag{10.9.1}$$

where $H = k_f/D_O^{1/2} + k_b/D_R^{1/2}$. The complex time dependence embodied in (10.9.1) is difficult to handle in the analysis of real data; hence various attacks based on linearization or

extrapolation were devised. On the other hand, we could use all of the data without introducing such approximations by considering the transformed current:

$$\bar{i}(s) = \frac{FAk_f C_O^*}{s^{1/2}(H + s^{1/2})} \tag{10.9.2}$$

We might plot, for example, the function $1/\bar{i}(s)s^{1/2}$ *vs.* $s^{1/2}$. The slope and intercept of the resulting linear function would provide k_f and H. In doing this, we have elected to analyze the system in the s domain, rather than the time domain.

To implement such a plan, we must be able to obtain the function $\bar{i}(s)$ from the measured curve $i(t)$. That can be done by considering the definition of the Laplace transformation (Section A.1):

$$\bar{i}(s) = \int_0^\infty i(t)\, e^{-st}\, dt \tag{10.9.3}$$

In a practical situation, $i(t)$ is usually a collection of data points. Thus, $\bar{i}(s)$ is calculated for a given value of s by multiplying each point by e^{-st} and then performing a numeric integration of the resulting curve. Algorithms for carrying out this task on a computer have been published (42). The whole process is repeated for each desired s value, and the final result is a new collection of data points describing $\bar{i}(s)$, just as the original data described $i(t)$. Since s has dimensions of frequency, $\bar{i}(s)$ is sometimes called a representation of the current in the frequency domain.

Many applications of this strategy are based on extensions of the concepts of impedance developed earlier in this chapter (41–43). However, the excitation waveform is usually an impulse in potential (rather than a periodic perturbation), and a transient current is measured. One records both $E(t)$ and $i(t)$ as observed functions. Then both are subjected to transformations, and comparisons are made in the frequency domain between $\bar{E}(s)$ and $\bar{i}(s)$. Ratios of the form $\bar{i}(s)/\bar{E}(s)$ are *transient impedances*, which can be interpreted in terms of equivalent circuits in exactly the fashion we have come to understand. The advantages of this approach are (a) that the analysis of data is often simpler in the frequency domain, (b) that the multiplex advantage applies, and (c) the waveform $E(t)$ does not have to be ideal or even precisely predictable. The last point is especially useful in high-frequency regions, where potentiostat response is far from perfect. Laplace domain analyses have been carried out for frequency components above 10 MHz.

In general, it is useful to regard s as a complex number $s = \sigma + j\omega$ in these analyses (41, 42). Then one can calculate real-axis and imaginary-axis frequency domain representations of a function. For example, the *real-axis transform* of $E(t)$ is

$$\boxed{\bar{E}(\sigma) = \int_0^\infty E(t)\, e^{-\sigma t}\, dt} \tag{10.9.4}$$

and the *imaginary-axis transform* is

$$\boxed{\bar{E}(j\omega) = \int_0^\infty E(t)\, e^{-j\omega t}\, dt = \int_0^\infty E(t)\, \cos\, \omega t\, dt - j \int_0^\infty E(t)\, \sin\, \omega t\, dt} \tag{10.9.5}$$

Note that the real-axis transform of any function is strictly real, but the imaginary-axis transform is complex. It has both real and imaginary components. Since one can transform experimental potential and current transients in this way, one can calculate a *real-axis transient impedance*, $Z(\sigma) = \bar{i}(\sigma)/\bar{E}(\sigma)$, and an *imaginary-axis transient impedance*, $Z(j\omega) = \bar{i}(j\omega)/\bar{E}(j\omega)$. Since $Z(j\omega)$ is complex, we can break it into real and imaginary components $Z(j\omega)_{Re}$ and $Z(j\omega)_{Im}$. One can easily show that $Z(j\omega)$ is the same as the conventional

impedance (comprising resistances and reactances) that we have already discussed. These various functions are useful for the analysis of electrical response in terms of equivalent circuits. In general, all of the various transform functions contain the same chemical information; however, one of them may be more readily applied to data analysis. Since this treatment involves a complex s domain, it is often called *Laplace plane analysis.*

Consider as an example, a double-layer capacitance C_d in series with an uncompensated solution resistance R_u. The overall system obeys

$$E(t) = i(t)\,R_u + \frac{1}{C_d}\int_0^t i(t)\,dt \tag{10.9.6}$$

or, in the frequency domain,

$$\bar{E}(s) = \bar{i}(s)\left(R_u + \frac{1}{C_d s}\right) \tag{10.9.7}$$

Thus the various impedances are[14]

$$Z(\sigma) = R_u + \frac{1}{C_d\sigma} \tag{10.9.8}$$

$$Z(j\omega)_{Re} = R_u \qquad Z(j\omega)_{Im} = \frac{1}{\omega C_d} \tag{10.9.9}$$

and the phase angle ϕ, defined by the real and imaginary components of $Z(j\omega)$, is given by

$$\tan\phi = \frac{1}{\omega R_u C_d} \tag{10.9.10}$$

Thus we have four simple frequency domain relationships that allow the evaluation of R_u and C_d. It is probably most convenient to use $Z(\sigma)$ for that purpose, but the availability of the other functions is useful for cross-checking the validity of one's equivalent circuit as a model for any given chemical system.

An interesting application of Laplace plane analysis comes from the work by Pilla and Margules on ionic transport through biological membranes (43). Their experimental arrangement involved the use of the membrane as a separator between two solutions containing separate electrodes. A small voltage pulse was applied across the membrane and the transient current was measured. Transformation of the voltage and current functions allowed the calculation of the impedances described above.

The equivalent circuits used in the analysis are shown in Figure 10.9.1. The elements correspond to solution resistance, interfacial capacitances, and impedances associated with the transport of ions through the membrane and across the boundary between the solution and the membrane.

Figure 10.9.2 is an illustration of the behavior of $Z(\sigma)$ at high frequencies in an actual system (43). At these frequencies, both of the circuits in Figure 10.9.1 look essentially like a series combination of C_d and R_e, because the impedance of C_d would be much lower than the impedances of the parallel arms involving resistances. Thus $Z(\sigma)$ should adhere to (10.9.8), where R_u is the same as R_e for this example. The intercept and the slope of Figure 10.9.2 therefore allow a determination of R_e and C_d.

Data at lower frequencies contain information about the arms parallel to C_d, but extracting it requires correction for the effects of R_e and C_d. This is accomplished in Figure 10.9.3. The basis for that analysis is left as an exercise in Problem 10.10.

[14]See the footnote concerning the definition of impedance in (10.1.11).

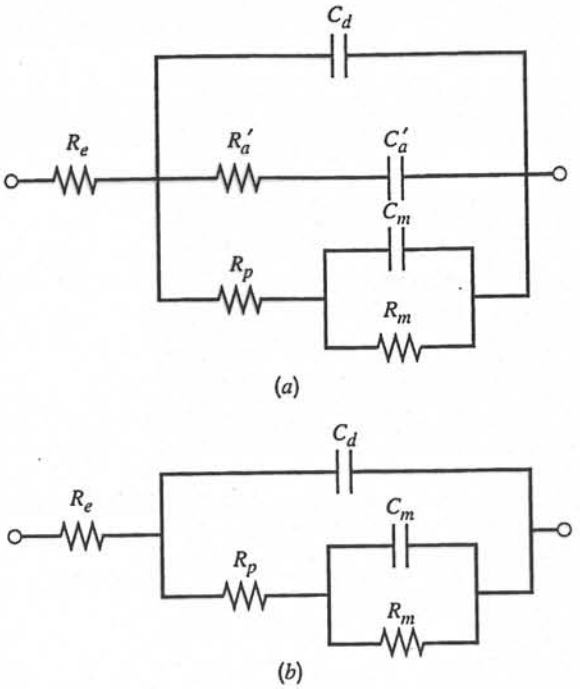

Figure 10.9.1 Equivalent circuits used to analyze the transient behavior of the toad urinary bladder membrane. R_e represents electrolyte resistance and C_d is the dielectric capacitance of the membrane. The branches involving R_p, C_m, and R_m are used to account for the transfer of charge across the membrane boundaries. They are analogous to R_{ct} and Z_w in electrode reactions. In circuit A, R_a' and C_a' model the effects of adsorption. [From A. A. Pilla and G. S. Margules, *J. Electrochem. Soc.*, **124**, 1697 (1977), reprinted by permission of the publisher, The Electrochemical Society, Inc.]

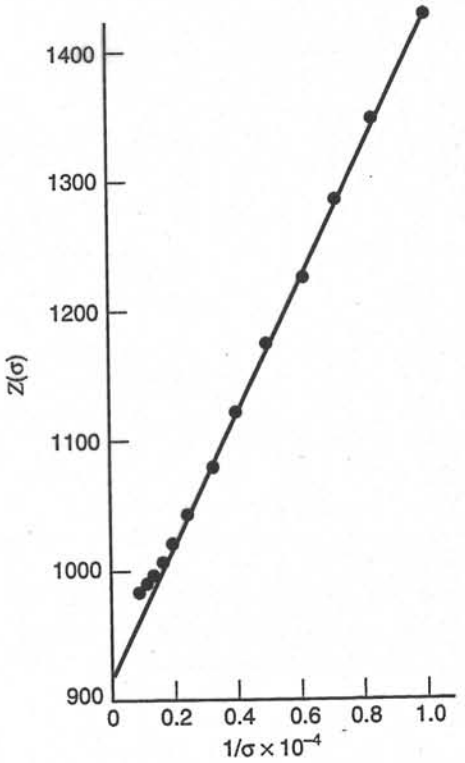

Figure 10.9.2 High-frequency plot of $Z(\sigma)$ *vs.* $1/\sigma$ for the toad urinary bladder membrane. [From A. A. Pilla and G. S. Margules, *J. Electrochem. Soc.*, **124**, 1697 (1977), reprinted by permission of the publisher, The Electrochemical Society, Inc.]

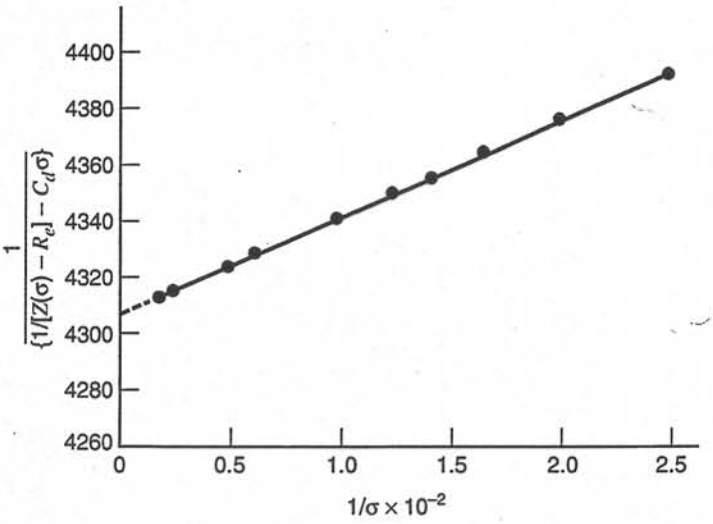

Figure 10.9.3 Intermediate-frequency plot of real-axis impedance data for the toad urinary bladder membrane. [From A. A. Pilla and G. S. Margules, *J. Electrochem. Soc.*, **124**, 1697 (1977), reprinted by permission of the publisher, The Electrochemical Society, Inc.]

▶ 10.10 REFERENCES

1. P. Delahay, "New Instrumental Methods in Electrochemistry," Wiley-Interscience, New York, 1954, Chap. 7.
2. B. Breyer and H. H. Bauer, "Alternating Current Polarography and Tensammetry," Vol. 13 in the series "Chemical Analysis," P. J. Elving and I. M. Kolthoff, Eds., Wiley-Interscience, New York, 1963.
3. D. E. Smith, *Electroanal. Chem.*, **1**, 1 (1966).
4. M. Sluyters-Rehbach and J. H. Sluyters, *Electroanal. Chem.*, **4**, 1 (1970).
5. D. E. Smith, *Crit. Rev. Anal. Chem.*, **2**, 247 (1971).
6. D. D. Macdonald, 'Transient Techniques in Electrochemistry," Plenum, New York, 1977.
7. A. M. Bond, "Modern Polarographic Methods in Analytical Chemistry," Marcel Dekker, New York, 1980.
8. C. Gabrielli, "Identification of Electrochemical Processes by Frequency Response Analysis," Solartron Instrument Group, Solarton-Schlumberger, Farnborough, Hampshire, England, Ref. 004/83, 1980.
9. F. Mansfeld and W. J. Lorenz in "Techniques for Characterization of Electrodes and Electrochemical Processes," R. Varma and J. R. Selman, Eds., Wiley, New York, 1991, Chap. 12.
10. D. D. Macdonald in " Techniques for Characterization of Electrodes and Electrochemical Processes," R. Varma and J. R. Selman, Eds., Wiley, New York, 1991, Chap. 11.
11. C. Gabrielli in "Physical Electrochemistry," I. Rubinstein, Ed., Marcel Dekker, New York, 1995, Chap. 6.
12. A. Lasia, *Mod. Asp. Electrochem.*, **32** (1999), Chap. 2.
13. (a) J. E. B. Randles, *Disc. Faraday Soc.*, **1**, 11 (1947); (b) D. C. Grahame, *J. Electrochem. Soc.*, **99**, C370 (1952).
14. (a) L. Pospisil and R. de Levie, *J. Electroanal. Chem.*, **22**, 227 (1969); (b) H. Moreira and R. de Levie, *ibid.*, **29**, 353 (1971); **35**, 103 (1972).
15. (a) D. C. Grahame, *J. Am. Chem. Soc.*, **68**, 301 (1946); (b) G. C. Barker, *J. Electroanal. Chem.*, **12**, 495 (1966).
16. R. D. Armstrong, M. F. Bell, and A. A. Metcalfe, in "Electrochemistry" (A Specialist Periodical Report), Vol. 6, H. R. Thirsk, Senior Reporter, The Chemical Society, London, 1978.
17. H. Kojima and A. J. Bard, *J. Electroanal. Chem.*, **63**, 117 (1975).
18. H. Kojima and A. J. Bard, *J. Am. Chem. Soc.*, **97**, 6317 (1975).
19. R. de Levie, *Ann. Biomed. Eng.*, **20**, 337 (1992).
20. C. Gabrielli, Ed., "Proceedings of the First International Symposium on Electrochemical Impedance Spectroscopy," *Electrochim. Acta*, **35** (10) (1990).
21. D. D. Macdonald, Ed., "Proceedings of the Second International Symposium on Electrochemical Impedance Spectroscopy," *Electrochim. Acta*, **38** (14) (1993).

22. J. Vareecken, Ed., "Proceedings of the Third International Symposium on Electrochemical Impedance Spectroscopy," *Electrochim. Acta*, **41** (7/8) (1996).
23. B. Timmer, M. Sluyters-Rehbach, and J. H. Sluyters, *J. Electroanal. Chem.*, **14**, 169, 181 (1967).
24. D. E. Smith, and T. G. McCord, *Anal. Chem.*, **40**, 474 (1968).
25. D. E. Smith, *Anal. Chem.*, **35**, 610 (1963).
26. A. M. Bond, R. J. O'Halloran, I. Ruzic, and D. E. Smith, *Anal. Chem.*, **48**, 872 (1976).
27. A. M. Bond, R. J. O'Halloran, I. Ruzic, and D. E. Smith, *Anal. Chem.*, **50**, 216 (1978).
28. W. L. Underkofler and I. Shain, *Anal. Chem.*, **37**, 218 (1965).
29. A. M. Bond, *J. Electroanal. Chem.*, **50**, 285 (1974).
30. C. P. Andrieux, P. Hapiot, J. Pinson, and J.-M. Savéant, *J. Am. Chem. Soc.*, **115**, 7783 (1993).
31. H. Blutstein, A. M. Bond, and A. Norris, *Anal. Chem.*, **46**, 1754 (1974).
32. A. M. Bond, *Anal. Chem.*, **45**, 2026 (1973).
33. H. Kojima and S. Fujiwara, *Bull. Chem. Soc. Jpn.*, **44**, 2158 (1971).
34. S. C. Creason, J. W. Hayes, and D. E. Smith, *J. Electroanal. Chem.*, **47**, 9 (1973).
35. D. E. Glover and D. E. Smith, *Anal. Chem.*, **45**, 1869 (1973).
36. D. E. Smith, *Anal. Chem.*, **48**, 221A, 517A (1976).
37. J. Házì, D. M. Elton, W. A. Czerwinski, J. Schiewe, V. A. Vincente-Beckett, and A. M. Bond, *J. Electroanal. Chem.*, **437**, 1 (1997).
38. J. W. Hayes, D. E. Glover, D. E. Smith, and M. W. Overton, *Anal. Chem.*, **45**, 277 (1973).
39. M. D. Wijnen, *Rec. Trav. Chim.*, **79**, 1203 (1960).
40. E. Levart and E. Poirier d'Ange d'Orsay, *J. Electroanal. Chem.*, **19**, 335 (1968).
41. A. A. Pilla, *J. Electrochem. Soc.*, **117**, 467 (1970).
42. A. A. Pilla in "Computers in Chemistry and Instrumentation," Vol. 2, "Electrochemistry," J. S. Mattson, H. B. Mark, Jr., and H. C. MacDonald, Eds., Marcel Dekker, New York, 1972.
43. A. A. Pilla and G. S. Margules, *J. Electrochem. Soc.*, **124**, 1697 (1977).

▶ 10.11 PROBLEMS

10.1 Derive equation 10.5.13, describing the shape of a reversible polarographic wave, from equation 10.5.11.

10.2 Derive formulas for converting a parallel resistance-capacitance network (R_p and C_p in parallel) to a series equivalent (R_s and C_s in series).

10.3 The faradaic impedance is sometimes represented as a resistance and a capacitance in parallel rather than in series. Find the expressions for the components of the parallel representation of this impedance in terms of R_{ct}, β_O, β_R, and ω. [*Hint.* Use known expressions for series elements and equations for series-to-parallel circuit conversion (Problem 10.2).]

10.4 The faradaic impedance method is employed to study the reaction $O + e \rightleftarrows R$ by imposing a small sinusoidal signal (5 mV) to the cell, and measuring the equivalent series resistance R_B and capacitance C_B of the cell. The following data are obtained for $C_O^* = C_R^* = 1.00$ mM, $T = 25°C$, and $A = 1$ cm^2:

Frequency (ω) (Hz)	R_B (Ω)	C_B (μF)
49	146.1	290.8
100	121.6	158.6
400	63.3	41.4
900	30.2	25.6

In a separate experiment under exactly the same conditions, but in the absence of the electroactive species, the cell resistance R_Ω is found to be 10 Ω, and the double-layer capacity of the electrode C_d is found to be 20.0 μF. (a) From these data calculate at each frequency R_s and C_s and the phase angle ϕ between the components of the faradaic impedance. (b) Calculate i_0 and k^0 for the reaction, and estimate D (assuming $D_O = D_R$).

9.5.2 Analytical Method

Correction for the effects of R_Ω and C_d can also be effected by straightforward methods of circuit analysis through complex algebra. The technique is actually an analytical version of the graphical method that we have just discussed. A rather simple approach, described by Damaskin (19), is based on conversions between equivalent series and parallel *RC* networks.

Suppose we have the series *RC* circuit shown in Figure 9.5.2*a*, and we want to find the unique parallel circuit with the same impedance vector (Figure 9.5.2*b*). For the parallel network, we have

$$\frac{1}{\mathbf{Z}} = \frac{1}{R_p} + j\omega C_p \tag{9.5.1}$$

and, for the series combination,

$$\frac{1}{\mathbf{Z}} = \frac{\omega C}{\omega RC - j} = \frac{\omega C(\omega RC + j)}{(\omega RC)^2 + 1} \tag{9.5.2}$$

which can be simplified by defining $W \equiv (\omega RC)^2$:

$$\frac{1}{\mathbf{Z}} = \frac{W/R}{W+1} + \frac{j\omega C}{W+1} \tag{9.5.3}$$

By equating the real and imaginary components of (9.5.1) and (9.5.3), we obtain the useful conversion formulas:

$$\boxed{R_p = R\left(\frac{W+1}{W}\right) \qquad C_p = \frac{C}{W+1}} \tag{9.5.4}$$

Now suppose the problem is reversed, and we have a parallel circuit (Figure 9.5.2*b*) whose series equivalent (Figure 9.5.2*a*) is desired. The conversion formulas turn out to be

$$\boxed{R = \frac{R_p}{W_p + 1} \qquad C = \left(\frac{W_p + 1}{W_p}\right) C_p} \tag{9.5.5}$$

where $W_p = (\omega R_p C_p)^2$. The derivation is left to Problem 9.2.

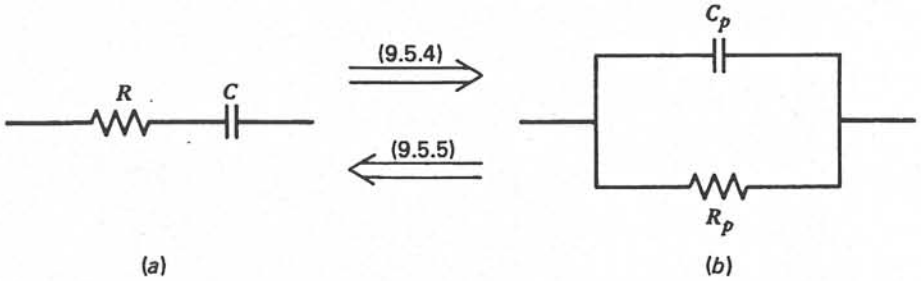

Figure 9.5.2
Interconversion of series and parallel equivalent circuits.

With (9.5.4) and (9.5.5) in hand, we are ready to face the problem of converting the measured electrochemical impedance parameters R_B and C_B into the faradaic parameters R_s and C_s. The plan of attack is laid out in Figure 9.5.3. The operations in each step are equivalent to those in the corresponding steps of the graphical procedure:

(*a*) Since R_Ω is a series element, it can be subtracted directly from R_B. The remaining series combination contains only the faradaic parameters and the double-layer capacitance.

$$R'_B = R_B - R_\Omega \tag{9.5.6}$$

(*b*) This combination is transformed to a parallel combination of R_p and C_p; thus

$$R_p = R'_B\left(\frac{1 + W}{W}\right) \qquad C_p = \frac{C_B}{1 + W} \tag{9.5.7}$$

where $W = (\omega R'_B C_B)^2$. The capacitive element C_p reflects a parallel combination of C_d and a faradaic parallel capacitance C'_p. We can subtract C_d from C_p to give only the faradaic element

$$C'_p = C_p - C_d \tag{9.5.8}$$

(*c*) Now we have a purely faradaic impedance expressed in a parallel equivalent. It is readily rewritten in terms of the usual series combination by (9.5.5):

$$R_s = \frac{R_p}{1 + W_p} \qquad C_s = \frac{C'_p(1 + W_p)}{W_p} \tag{9.5.9}$$

where $W_p = (\omega R_p C'_p)^2$.

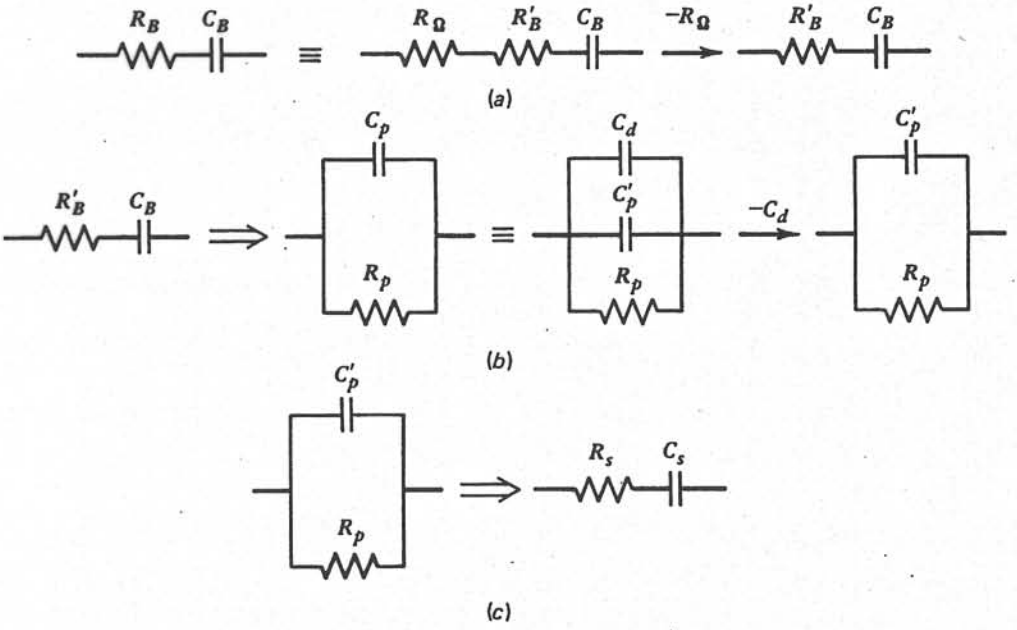

Figure 9.5.3

Extraction of R_s and C_s from R_B and C_B by the analytical method. See the text for an explanation of steps (*a*) to (*c*).